THE STUDY OF THERMOPHYSICAL AND EXCESS THERMODYNAMIC PROPERTIES FOR THE BINARY MIXTURES OF IMIDAZOLIUM-BASED IONIC LIQUIDS WITH POLYETHYLENE GLYCOL 200

By

Tshepo Mahura

B.Sc. Chemistry (Hons)

North West University

Submitted in fulfilment of the academic requirements for the degree of Master of Science in Engineering to the School of Engineering, Discipline of Chemical Engineering, University of KwaZulu-Natal, Durban.

March 2020

Supervisor: Prof Paramespri Naidoo

Co-supervisor: Prof Deresh Ramjugernath

PREFACE

The investigation of study presented in this thesis entitled “THE STUDY OF THERMOPHYSICAL AND EXCESS THERMODYNAMIC PROPERTIES OF MIXTURES OF IMIDAZOLIUM-BASED IONIC LIQUIDS WITH POLYETHYLENE GLYCOL 200” was undertaken in the Thermodynamics Research Unit at the University of KwaZulu-Natal in the School of Engineering, Howard College Campus, Durban, South Africa.

The duration of the study was from April 2017 to September 2019. The study was supervised by Professor Paramespri Naidoo and Professor Deresh Ramjugernath. This thesis has been submitted as the full requirement for the award of the degree of Masters of Science in Chemical Engineering. The study presented in this thesis is my original work unless otherwise stated. The thesis has not previously been submitted for a degree or examination at any other tertiary institute or university.

DECLARATION (PLAGIARISM)

I, Tshepo Mahura, student number 217080101 declare that:

The reported research project is my original research work.

i. This thesis has not been submitted for any degree or examination at any other university before.
ii. All the data such as pictures, graphs or any other information presented in this dissertation, has been acknowledged as being sourced from other persons, except in a case where is my original work.
iii. All the graphs, tables or text copied and pasted from the Internet, has been acknowledged, and the referenced source in this thesis is presented in detail in the References section.
iv. All the other persons' writing in this thesis has been referenced and acknowledged.
    a. Their words have been re-written but the general information attributed to them has been referenced.
    b. Where their exact words have been used, then their writing has been placed in italics and inside quotation marks and referenced.

_____ _____

Mahura T Date

As the candidate's supervisor, I, Prof. Paramespri Naidoo approved this dissertation for submission.

_____

Prof Paramespri Naidoo

As the candidate's co-supervisor, I, Prof. D. Ramjugernath approved this dissertation for submission.

_____

Prof. D. Ramjugernath.

ACKNOWLEDGMENT

Firstly, I would like to express my gratitude to my redeemer and saviour Jesus Christ for giving me the strength to complete my research project. Furthermore, I give thanks and praises to God for granting me the spirit of perseverance, his love and grace is forever available.

I extend my gratitude to my two supervisors Prof Paramespri Naidoo and Prof Deresh Ramjugernath for their non-stop support and direction.

I am also thankful for all the academic support I received from my postgraduate colleagues situated in the chemical engineering department. Special gratitude to Thermodynamics Research Unit (TRU) team as a whole for their support.

Moreover, I express my earnest appreciation to my financial sponsors; NRF Funding and Eddie Pelzer funding scheme on the off chance.

I would like to express my deepest appreciation to my twin brother Tshepiso Mahura, my sister Atlegang Mahura, my mother Mapule Mahura, my grandfather Michael Kegakilwe, my grandmother Tebaco Mahura, my two aunts Keseneilwe Mahura and Nontsisi Thupe for their unconditional support and love. To my friends, I am grateful for the overwhelming support throughout my studies.

Special thanks to the following families, Shomang, Ngcobo, Mogorosi, Pakwe, and Molobye for their love and support.

ABSTRACT

The use of volatile organic compounds in industries has over the years proven to be toxic on the environment along with contributing to unsustainable activity. Ionic liquids (ILs) are classified as green and ecologically friendly solvents. They are regarded as promising choices for replacing harmful volatile organic solvents. Due to the fascinating physicochemical properties of ionic liquids (ILs) and their recyclability, these solvents are gaining momentum as suitable replacements for volatile organic solvents. ILs can be synthesized using countless combinations of cations and anions options, every one of the ions contributing differently towards the overall physicochemical properties of ILs. Application of ILs in different areas, generally require ILs to be mixed with other solvents in order to modify their physicochemical properties. Accurate data of thermophysical and excess thermodynamic properties are required for the configuration process in different process designs and industries.

In this work, density (ρ), speeds of sound (u), viscosity (η) and refractive index (n_D) of the binary mixtures of 1-butyl-3-methylimidazolium hexafluorophosphate ($[\mathrm{BMIM}]^+[\mathrm{PF_6}]^-$), 1-ethyl-3-methylimidazolium tetrafluoroborate ($[\mathrm{EMIM}]^+[\mathrm{BF_4}]^-$) and 1- butyl -3-methylimidazolium tetrafluoroborate ($[\mathrm{BMIM}]^+[\mathrm{BF_4}]^-$) with polyethylene glycol 200 (PEG200), including those of pure liquids, were measured at (293.15, 303.15, 313.15, 323.15 and 333.15) K under atmospheric pressure of p = 0.1 MPa. An Anton Paar DSA 5000M, digital vibrating tube densimeter was used to measure the density and speed of sound, while viscosity measurements were carried out using Lovis 2000 M/ME attachment. Refractive indices were measured using an Atago 7000α. The FT-IR spectra analysis of the pure components and their binary mixtures were also performed using a Shimadzu IR Prestige unit.

Two test systems were measured to confirm the accuracy of the methods, the apparatus used and the calculations of the excess properties. The density (ρ) and excess molar volumes (V^E) for the binary systems of $[\mathrm{BMIM}]^+[\mathrm{Bf_4}]^-$ (1) + methanol (2) was measured and calculated respectively at 298.15 K and p = 0.1 MPa. Similarly, the densities (ρ) and excess thermal expansion coefficient (α_P^E) for the binary system of nicotine (1) + 1-butanol (2) were measured and calculated respectively at 303.15 K and p = 0.1 MPa. The density (ρ) and excess molar volumes (V^E) were used to confirm the calculations for the excess partial molar properties ($\bar{V}_i^E$).

For this work, excess thermodynamic properties were calculated for the new binary systems of selected ILs and PEG200. Excess thermodynamic properties such as excess molar volume (V^E), excess isentropic compressibility (K_S^E), excess viscosity (η^E), excess refractive index (n_D^E), excess thermal

expansion coefficient (α_P^E) were calculated from the thermophysical properties. The excess thermodynamic properties were best correlated using the Redlich-Kister polynomial. Excess partial molar volumes ($\bar{V}_i^E$) and excess partial molar volume at infinite dilution ($\bar{V}_i^{E,\infty}$) were calculated.

Excess thermodynamic properties such as excess molar volume (V^E), excess isentropic compressibility (K_S^E), excess thermal expansion coefficient (α_P^E), excess partial molar volumes ($\bar{V}_i^E$) and excess partial molar volume at infinite dilutions ($\bar{V}_i^{E,\infty}$) all displayed negative deviation throughout the entire composition range for the new systems studied in this work.

The results showed strong ion-dipole interactions between the different molecules in the mixture. Excess thermodynamic properties such as excess viscosity (η^E) and excess refractive index (n_D^E) all exhibited positive deviation also confirming the existence of strong ion-dipole interactions between the two different molecules.

For V^E, the maximum values were observed at ($V^E \approx$ -1.1 $cm^3 \cdot mol^{-1}$ at $x_1 \approx 0.4$), ($V^E \approx$ -1.0 $cm^3 \cdot mol^{-1}$ at $x_1 \approx 0.25$) and ($V^E \approx$ -0.88 $cm^3 \cdot mol^{-1}$ at $x_1 \approx 0.4$) for the 1-butyl-3-methylimidazolium hexafluorophosphate ($[BMIM]^+[Pf_6]^-$), 1-ethyl-3-methylimidazolium tetrafluoroborate ($[EMIM]^+[Bf_4]^-$) and 1- butyl -3-methylimidazolium tetrafluoroborate ($[BMIM]^+[Bf_4]^-$) with polyethylene glycol 200 (PEG200), respectively . For K_S^E, the maximum values were observed at ($K_S^E \approx$ -13 TPa^{-1} at $x_1 \approx 0.30$, $K_S^E \approx$ -15 TPa^{-1} at $x_1 \approx 0.34$ and $K_S^E \approx$ -21 TPa^{-1} at $x_1 \approx 0.38$). For α_P^E, the maximum values were observed at ($\alpha_P^E \approx$ -0.0220 K^{-1} at $x_1 \approx 0.48$, $\alpha_P^E \approx$ -0.010 K^{-1} at $x_1 \approx 0.37$ and $\alpha_P^E \approx$ -0.008 K^{-1} at $x_1 \approx 0.6$). All the binary mixtures follow the order: $[EMIM]^+[BF_4]^-$ > $[BMIM]^+[PF_6]^-$ > $[BMIM]^+[BF_4]^-$.

For η^E, the minimum values were observed at at ($\eta^E \approx$ 1.0 mPa.s at $x_1 \approx 0.57$, 0.9 mPa.s at $x_1 \approx 0.5$ and 0.75 mPa.s at $x_1 \approx 0.58$) for the systems of $[BMIM]^+[Pf_6]^-$, $[EMIM]^+[Bf_4]^-$ and $[BMIM]^+[Bf_4]^-$ with polyethylene glycol 200 (PEG200), respectively. For n_D^E, the maximum values were observed at ($n_D^E \approx 0.004$ at $x_1 \approx 0.35$, $n_D^E \approx 0.0025$ at $x_1 \approx 0.32$ and $n_D^E \approx 0.0022$ at $x_1 \approx 0.35$). All the binary mixtures follow the order: $[EMIM]^+[BF_4]^-$ > $[BMIM]^+[PF_6]^-$ > $[BMIM]^+[BF_4]^-$. Thus, the effect of temperature on the studied binary mixtures showed that the temperature increases with the ion-dipole interactions.

FT-IR spectroscopy was further utilized to confirm the presence of ion-dipole interactions/hydrogen bonding between the molecules of ILs and PEG200. The FT-IR spectra results support the results obtained from calculated excess thermodynamic properties suggesting that there are strong ion-dipole

interactions/hydrogen bonding present between the ions of ILs and molecules of PEG200. The results both from excess thermodynamic calculations and FT-IR spectroscopy analysis confirmed the presence of ion-dipole interactions/hydrogen bonding. The strength of ion-dipole interactions formed between molecules of PEG200 and ions of ILs for all the binary mixtures follows the order: $[EMIM]^+[BF_4]^-$ > $[BMIM]^+[PF_6]^-$ > $[BMIM]^+[BF_4]^-$. This study of the IL + PEG200 binary mixtures contributes to the knowledge and data of thermophysical and excess thermodynamic properties.

TABLE OF CONTENTS

LIST OF TABLES

LIST OF FIGURES

NOMENCLATURE

English letters

A	Fitting parameter
A_i	Polynomial coefficient
B	Fitting parameter
C	Speed of light ($\mathrm{m.s^{-1}}$)
C_P	Molar isobaric heat capacity
D	Capillary inner diameter (m)
f	frequency (Hz)
F	Force (N)
G	Gravity constant (980 $\mathrm{cm.s^{-2}}$)
k	Constant
K_S	Isentropic compressibility ($\mathrm{TPa^{-1}}$)
K_T	Isothermal compressibility ($\mathrm{TPa^{-1}}$)
L	Length of the capillary (m)
L_e	Effective length (m)
M	Mass (g)
M	Molecular weight ($\mathrm{g.mol^{-1}}$)
N	Number of moles (mol)
N	Number of measurements
n_D	Refractive index
p	Pressure
Q_n	Redlich–Kister coefficients
R_2	Radius of the outer cylinder (m)
T	Temperature (K)
T_g	Ideal glass transition temperature (T)
U	Speed of sound ($\mathrm{m.s^{-1}}$)
v	Velocity ($\mathrm{m.s^{-1}}$)
V	Volume ($\mathrm{cm^3}$)
$\bar{V}$	Partial molar volume ($\mathrm{cm^3.mol^{-1}}$)
V_0	Molar volume ($\mathrm{cm^3.mol^{-1}}$)
x_i	Mole fraction
Z	Thermodynamic values (Real property)

Greek letters

α_P	Thermal expansion coefficients (K^{-1})
ρ	Density ($g.\,cm^{-3}$)
ε_r	Relative permittivity ($F.m^{-1}$)
μ_r	Relative permeability ($H.m^{-1}$)
η	Viscosity ($mPa.\,s$)
π	Pi
τ	torque (N.m)
β^2	Ratio of Cylinder radii (m)
ω_2	Rotational speed of the outer cylinder ($m.\,s^{-1}$)
Λ	Wavenumber (cm^{-1})
Φ	Volume fraction
γ	Conductivity
σ_{rel}	Standard relative deviation
T	Period
A	Alpha
$\hbar$	Planck's constant (6.63×10^{-34} J.s)

Subscript

i	i-th component
1	Component 1 (Ionic liquids)
2	Component (Polyethylene glycol 200)

Superscript

E	Excess property
id	Ideal property
∞	Infinite dilution
Exp	Experimental values
Cal	Calculated values

Abbreviations/Acronym

$[BF_4]^-$	Tetrafluoroborate
$[BMIM]^+$	1-butyl-3-methylimidazolium
$[EMIM]^+$	1-ethyl-3-methylimidazolium
$[PF_6]^-$	Hexafluorophosphate
Cal	Calculated
DFT	Density Functional Theorem
Di-EGMME	Di-ethylene glycol monomethyl ether
EGEE	ethylene glycol ethyl ether
EGMEE	Ethylene glycol monoethyl ether
EGMPE	Ethylene glycol monopropyl ether
Exp	Experimental
FT-IR	Fourier-transform infrared
ILs	Ionic liquids
Lit	Literature
PC	Personal computer
PEG200	Polyethylene glycol 200
PEG400	Polyethylene glycol 400
PEGs	Polyethylene glycols
PGMEE	Propylene glycol monoethyl ether
Std	Standard
Tetra-EGDME	Tetra-ethylene glycol dimethyl ether
Tri-EGDME	Tri-ethylene glycol dimethyl ether
Tri-EGMEE	Tri-ethylene glycol monoethyl ether
TRU	Thermodynamics Research Unit
u(x)	Uncertainty
VFT	Vogel-Fulchet-Tammann
WHO	World Health Organization

CHAPTER ONE

INTRODUCTION

Molecular thermodynamic investigations of solute-solvent binary mixtures are increasing owing to its relevance in scientific and engineering applications. There is a continuous necessity for reliable thermodynamic data of mixtures for chemical industries in the design of processes involving chemical separation, heat transfer, mass transfer, and fluid flow.

Intermolecular forces such as ion-dipole interactions, Van der Waals and charge transfer, etc. play an important role in determining the properties of the liquid mixtures. They influence orientation, arrangement, and conformations of molecules in the solutions. Excess thermodynamic calculations are a useful tool for an in-depth understanding of the molecular mechanism of components in mixtures. Thermophysical measurement and their excess parameters provide better insight into the molecular environment of mixtures.

Most certainly, for non-ideal mixtures, direct experiments are performed over the entire composition range. For an efficient and reliable engineering process design, precise and accurate excess thermodynamic data is required for a certain mixture. All the excess thermodynamic properties are derived from thermophysical measurements, thus, thermophysical measurements should be accurate, consistent and reliable (Mirgane, 2011).

The intermolecular interactions of liquid phases are complex in nature. Thus, calculations and correlations of derived thermodynamic parameters is a challenging concept to overcome. Therefore, the characteristic departure from ideal behaviour of physical properties can be established to understand the intermolecular interactions of mixed components (Deenadayalu and Bhujrajh, 2006). Thus, molecular thermodynamic properties depend mainly on the deep understanding of molecular structure and the forces of molecular interactions.

1.1 Blending of polyethylene glycols (PEGs) and ionic liquids (ILs)

Both ILs and PEGs are considered within the framework of green chemistry due to their ‘tunable’ physicochemical properties. Blending ILs with PEGs may bring about a medium that has fascinating and positive physicochemical properties (Rodriguez et al., 2009). Both PEGs and ILs have numerous physicochemical properties such as non-volatility, low melting point, low flammability, good miscibility strength and excellent polarity properties (Zhou et al., 2011, Wasserscheid and Welton, 2008).

Thermophysical properties of ILs such as viscosity (η), density (ρ), conductivity (γ) and polarity can be improved or changed by the addition of co-solvent such as alcohols (Moosavi et al., 2015), polymers (Calado et al., 2013), water (Masaki et al., 2010), ketones (Zhao et al., 2015), and aldehydes (Manoj et al., 2018) . In retrospect, properties of PEGs may likewise be modified by combining PEGs with an IL (Chen et al., 2002). The advantages of blending ILs with PEGs are discussed in detail in chapter 2 section 2.7.

1.2 Recent scientific investigations

Generally, the binary mixtures composed of ILs and volatile organic solvents such as alcohols are the most investigated systems (Krishna et al., 2016, Matkowska and Hofman, 2013, Moosavi et al., 2015). However, thermophysical and thermodynamic data for binary mixtures of alkyl imidazolium-based ILs with polymers such as PEGs has received considerably little attention (Krishna et al., 2016). Thus, the intention of this study is to fully explore and understand the molecular interactions present between the molecules of imidazolium ILs and PEG200. In this study PEG (Mw = 200) was selected on the basis that it is a low weight molecular component. Low molecular weight compounds are liquid at room temperature, making it easy to mix it with ILs (Chen et al., 2005).

The aim of this study was to carry out an extensive investigation into the intermolecular interactions of the binary mixtures composed of alkyl imidazolium-based ionic liquids (ILs) such as (1-butyl-3-methylimidazolium hexafluorophosphate ($[\mathrm{BMIM}]^+[\mathrm{PF_6}]^-$), 1-ethyl-3-methylimidazolium tetrafluoroborate ($[\mathrm{EMIM}]^+[\mathrm{BF_4}]^-$) and 1-butyl-3-methylimidazolium tetrafluoroborate ($[\mathrm{BMIM}]^+[\mathrm{BF_4}]^-$) blended with polyethylene glycol 200 (PEG200) at various concentrations and temperatures. The measured thermophysical properties, derived/calculated thermodynamic properties and FT-IR spectroscopic measurements were used to study the intermolecular interactions occurring in the mixtures.

The objectives of this study were:

i. To measure the thermophysical properties such as density (ρ), speed of sound (u), viscosity (η) and refractive index (n_D) of ionic liquids (ILs) and their binary mixtures with polyethylene glycol (PEG200) at various temperatures and concentrations.
ii. To calculate the excess thermodynamic properties such as excess molar volume (V^E), excess isentropic compressibility (K_S^E), excess viscosity (η^E), excess refractive index (n_D^E), excess

thermal expansion (α_P^E), excess partial molar volume ($\bar{V}_i^E$), partial molar volume at infinite dilution ($\bar{V}_i^{E,\infty}$) for all the binary mixtures at different temperatures.

iii. To correlate and check the accuracy of excess thermodynamic properties using the Redlich-Kister polynomial model.

iv. To investigate the behaviour of molecular interactions present within the studied binary mixtures using both excess thermodynamic properties and FT-IR spectroscopic measurements.

v. To investigate the effect of temperature and concentration upon the binary mixtures.

vi. To investigate the effect of anions and cation of ILs in the molecular interactions with PEG200.

1.3 Outline of this thesis

In this study, extensive investigations of the intermolecular interactions between the imidazolium-based ILs such as 1-butyl-3-methylimidazolium hexafluorophosphate ($[\mathrm{BMIM}]^+[\mathrm{PF_6}]^-$) or 1-ethyl-3-methylimidazolium tetrafluoroborate ($[\mathrm{EMIM}]^+[\mathrm{BF_4}]^-$) or 1- butyl -3-methylimidazolium tetrafluoroborate ($[\mathrm{BMIM}]^+[\mathrm{BF_4}]^-$) with polyethylene glycol 200 (PEG200) were performed. Measurements were carried out at different concentrations, under atmospheric pressure of p = 0.1 MPa and over the temperature range from (293.15 to 333.15) K with 10 K intervals.

Chapter two presents a brief background to ILs, its history, and applications as a substitute for harmful organic solvents. In addition, PEGs are discussed with a focus on PEG200. The advantages of blending PEGs with ILs are also discussed.

Chapter three presents measured thermophysical properties and calculated excess thermodynamic properties selected for this study using both theoretical definition and mathematical definition. Different data correlation techniques used in this study for both binary mixtures and pure components measurements are also discussed in chapter three. The definition, importance, advantage, and disadvantage of FT-IR spectroscopic measurements are also discussed in detail in chapter three.

Chapter four summarises the information presented in the literature on the three selected ILs studied in this work with different polymers. Excess thermodynamic properties of binary mixtures of ILs blended with different polymers are also discussed and summarised in chapter four.

Chapter five presents the experimental procedure for this study. That is, degassing methods for all the chemicals used, calculations used to prepare different concentrations of ILs and PEGs. Methods used to measure all the samples in this study are also presented and discussed in chapter five. The methods

and formulation used to calculate the combined standard uncertainty for the measured thermophysical properties and the mole fraction (x_1) are also presented and discussed in chapter five.

Chapter six presents, the details of chemicals used, and the purity data of chemicals before and after degassing. All the calibration data and test systems performed prior to the main measurements for this study is presented in chapter six. The plotted data for all the measured thermophysical and excess thermodynamic properties of the selected binary mixtures are presented in chapter six. Chapter six also presents the discussion of intermolecular interactions present in the binary mixtures of ILs and PEG200. Parameters obtained using Redlich-Kister polynomial model, the relative standard deviations for excess thermodynamic data are also included. The combined calculated standard uncertainty of mole fraction (x_1) and measured thermophysical data for both test systems and main measurements are well presented in chapter six. Lastly, chapter six also presents the FT-IR spectra analysis of the three studied binary mixtures and the discussion of intermolecular interactions observed from FT-IR spectroscopy.

Lastly, the conclusions and recommendations are provided in Chapters seven and eight respectively.

CHAPTER TWO

LITERATURE REVIEW ON IONIC LIQUIDS (ILs) AND POLYETHYLENE GLYCOLS (PEGs)

This chapter presents a brief background to ILs, its history, and applications as a substitute for harmful organic solvents. In addition, PEGs are discussed with a focus on PEG200. The advantages of blending PEGs with ILs are also discussed.

2.1 Ionic liquids (ILs)

An appropriate definition of an IL, is that it is a salt in the liquid state and is composed of a cation and an anion (González et al., 2007). While common IL are composed entirely of ions, it is a neutral liquid overall. ILs are liquids at ambient temperatures, unlike traditional molecular organic solvents. This includes organic or inorganic molten salts, fused salts, non-aqueous ILs and liquid organic salts (Bahadur et al., 2016). ILs differ from ionic solutions, in a way that ILs contains no free or unattached neutral molecules but only ions, while ionic solutions are composed of both ions and neutral molecules such as salt fused together. Figure 2.1 explains the difference between ionic solutions and ILs.

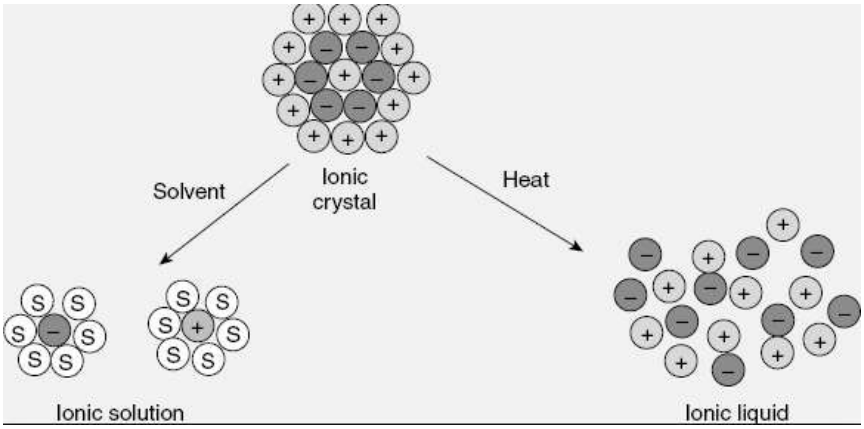

Figure 2.1: Difference between an ionic solution and an ILs (Hess et al., 1995).

ILs generally have lower melting points below or at 100 ^{o}C. Due to its low melting point, ILs remain as liquids within a broad temperature window (Yang and Pan, 2005). The melting point of ILs is mainly affected by the chemical and morphological arrangement of molecules (Keskin et al., 2007). This refers to the low symmetry and the large size of either the cation or the anion in ILs which may also be used to explain the melting point of ILs (Laus et al., 2005).

Ethanol-ammonium nitrate with a melting point of 52 -55 ^{o}C was the first IL to be synthesized (Gabriel and Weiner, 1888). In 1963, Yoke discovered that the mixture of a solid copper chloride with alkyl ammonium chloride formed a liquid at room temperature (Yoke III et al., 1963). In the 1970s, the University of Alabama discovered and characterized a multiple of compounds that were not usual at that time. These components were viewed as liquid clathrates and were made up of more aromatic molecules with an aluminum alkyl compound salt. Presently, they are viewed as ILs, though due to the aromaticity, they are not strictly ILs (Wilkes, 2002).

In the 1970s and 1980s, ILs composed of cations such as imidazolium or pyridinium and anions such as halide or tri-halogen aluminate were originally developed for electrolytes applications in batteries (Chum et al., 1975). A modern era of ILs was first experienced in 1978, after the measurements of physical and chemical properties of 1- butyl pyridinium chloride aluminum chloride mixture [BPC-$AlCl_3$] were published. It was regarded as a modern era because for the first time people started to explore the investigation of ILs and their application (Wilkes, 2002). During the early 90s, Wilkes and Zawarotko synthesized ILs possessing weak coordinating anions such $[BF_4]^-$ and $[PF_6]^-$. These types of ILs allowed a wider range of applications in different areas (Wilkes and Zaworotko, 1992).

For this study, the imidazolium ILs were selected based on their unique polarity property strength. For binary mixtures, imidazolium ILs composed of cation such as C_nMIM and anion such as $[BF_4]^-$ and $[PF_6]^-$ are the most investigated ILs due to their unique polarity property. Polarity of different chemicals is commonly used to classify the solvents. Polarities are generally related to the values of dielectric constant, dipole moments and polarizabilities. Polar solvents are able to dissolve and stabilize dipolar or charged solutes. Thus, ILs are highly polar solvents (Keskin et al., 2007). Since polarity is the simplest indicator of solvent strength, different researchers compared the polarities of different ILs and conventional solvents (Carmichael and Seddon, 2000). (Carmichael and Seddon, 2000) showed that 1-alkyl-3-methylimidazolium ILs made of anions such as $[BF_4]^-$ and $[PF_6]^-$ are within the same polarity range.

ILs having anions such as $[BF_4]^-$ and $[PF_6]^-$ are the most used and investigated ILs. The effects of an anion towards an IL is much more significant and intense as compared to a cation (Keskin et al., 2007). (Chiappe and Pieraccini, 2005) performed an extensive study of cations of the following group of ILs: ammonium, sulfonium, phosphonium, imidazolium, pyridinium, picolinium, pyrrolidinium, thiazolium, oxazolium, and pyrazolium. The conclusion based on the polarity investigations of ILs,

suggested that the imidazolium ILs such as BMIM and EMIM possess a higher degree of polarity. Thus, high polarity implies that imidazolium ILs have a greater ability to form hydrogen bonding with other polar solvents (Chiappe and Pieraccini, 2005). The organic and chemical structure of ILs used in this study are shown in Figure 2.2.

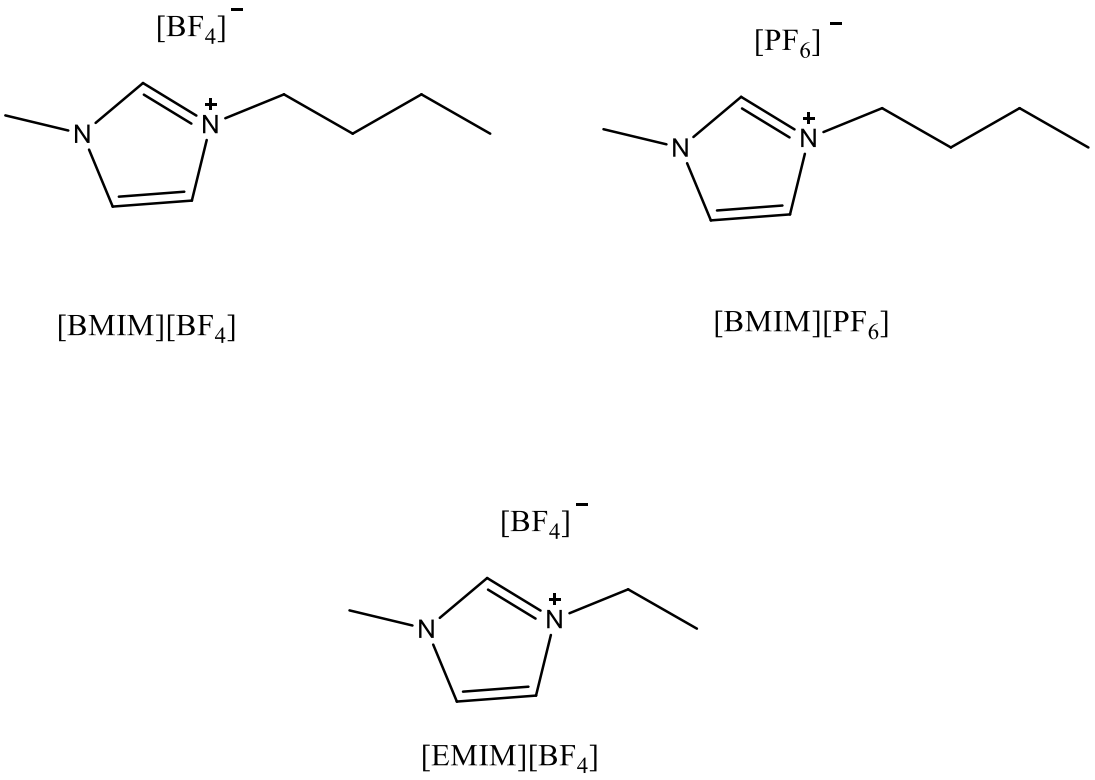

Figure 2.2: Chemical structure of the three selected ILs

2.2 Physicochemical properties of ILs

ILs are advantageous due to their distinctive physicochemical properties. The application of ILs have grown significantly in the last 20 years. The most distinctive physicochemical properties of ILs are listed below.

- Negligible vapour pressure, which makes them environmental-friendly (Welton, 1999)
- High electrical conductivity (Tanaka and Wiley-VCH, 2003)
- High thermal stability (Dupont, 2004)
- ILs have controlled miscibility, which brings about a significant number of workable combinations of cations and anions (Yao et al., 2012).
- Low flammability hazards (Fox et al., 2008).
- Excellent polarity properties for most of organic and inorganic compounds (Plechkova et al., 2010).

- Wide electrochemical window (Schröder et al., 2000)
- Wide liquid range (Huddleston et al., 2001).

ILs have physicochemical properties that might be reasonable for energy devices such as batteries (Bruce et al., 2012). Important physical properties for heat transfer and energy storage applications are melting point, density (ρ), viscosity (η) and conductivity (γ) (Van Valkenburg et al., 2005). In chemical engineering, ρ and η data are needed for calculations concerning chemical separations, fluid flow, mass, and heat transfer (Dávila et al., 2009).

Unlike organic solvents, ILs have reasonably good γ. In view of the way that ILs are made exclusively out of ions, it would be reasonable to conclude that ILs have high γ (Endres and Zein El Abedin, 2006). The γ of ILs is contrarily connected to their η. Subsequently, ILs of higher η exhibit lower γ. As the temperature increases, γ values increases while the η values decrease (Endres and Zein El Abedin, 2006).

Since heat-transfer fluids are generally used in flowing systems, η is an important physical property (Van Valkenburg et al., 2005). Accurate η data is an important transport property needed for industrial applications, as it is needed for the design of process units, such as flow meter devices and pumping systems. One of the special characteristics of ILs is their η, which is frequently larger than those for the volatile organic liquids commonly used in the chemical industry (Gardas and Coutinho, 2008). The η of ILs ranges from 10 mPa·s to around 500 mPa·s at room temperature (Welton, 1999). Most ILs are viscous fluids, with η fairly similar to viscosities of oils, being two to three orders of magnitude larger than those for volatile organic solvents (Marsh et al., 2004). The η of ILs is determined by the type of intermolecular interactions present within the chemical structure of an IL alone. Thus, the different types of electrostatic force play an imperative part towards the η. The stretching of an alkyl chain length leads to an expansion in η (Bonhote et al., 1996). This is due to the dominance of strong van der Waals forces between anion and cation of an IL. A strong van der Waals forces is a result of high energy motion of molecules. For an IL, the strength of the hydrogen bonding is prominent on the anion rather than the cation. The viscosity of the IL is greatly affected by the anion as compared to the cation structure. ILs having fluorinated anions in their molecular structure exhibit hydrogen bonding. This makes the ILs more viscous to ILs with a non-fluorinated anion. Generally, the viscosity (η) of ILs decrease with increasing temperature (Wasserscheid et al., 2002).

Since ILs are known to have a melting point below 100 ^{0}C the melting point of an IL is affected by the combination of anion with cations (Endres and Zein El Abedin, 2006). As the anion increases, the melting point decreases. The melting point of an IL is affected by the size and structure of a cation. Large cations and increased asymmetric substitution results in a melting point reduction (Tanaka and

Wiley-VCH, 2003). Hydrogen bonding strength, the arrangement of particles and the van der Waals interactions are the primary factors that affect the melting point of ILs (Marsh et al., 2004).

The density (ρ) is an important property for sizing of equipment for thermal, heat and energy storage devices and though ρ is not a thermal property but it is needed to calculate other thermally related quantities such as heat storage capacity (Ficke et al., 2010).

ILs, in general, are denser than water with values ranging from 1 to 1.6 g cm^{-3} and their densities decrease with increase in the length of the alkyl chain in the cation (Marsh et al., 2004). The ρ of ILs are also influenced by the character of anions (Endres and Zein El Abedin, 2006).

2.3 Limitation of ILs

The main limitation known to this point based on ILs, is their high viscosity, η (Bates et al., 2002). The η of ILs are reported to be approximately 40 times larger compared to normal organic solvents, and commonly the η of ILs ranges between 20-2000 cP (Anderson et al., 2007). ILs are made of a combination of cations and anions blended together, this combination causes strong coulombic attraction between ions of opposite side. These strong coulombic forces taking place cause ILs to possess high η. Thus, the high η of ILs limits the application of this material in different areas of industry. Thus, in an attempt to decrease the high η of ILs, ILs are mixed/blended together with other organic solvents (Huang et al., 2005). It is reported that the toxicity of most ILs is not well known, as compared to other common organic solvents. In order to fully understand the toxicity of ILs, more research on the effects and application of ILs is needed (Hasib-ur-Rahman et al., 2010).

Fluorinated ILs are found to be much more toxic as compared to the other ILs and have low biodegradability (Muldoon et al., 2007). ILs are considered to be green solvents meaning they are not harmful to the air because they possess low volatility. However, possible release of ILs into the soil or water-courses could become persistent pollutants and pose environmental risks (Hasib-ur-Rahman et al., 2010).

Currently, synthesis of ILs is a challenge, thus not all research institutions have the necessary equipment to carry out the correct synthesis of these fluids. To prepare pure ILs or to execute post-synthesis purification steps are often challenging processes (Mikkola et al., 2007).

2.4 ILs as a replacement for volatile organic compound

The use of volatile organic compounds has proven to be toxic to the environment. Volatile organic compounds are released on a daily basis to the atmosphere through indoor and outdoor activities. Indoor activities include smoking and cooking, and outdoor activities include combustion of fuel, emission

from petrochemical and chemical facilities. The high amount of concentration of volatile organic compounds realized into the atmosphere causes numerous issues such as global warming. According to *WHO*, volatile organic compounds contribute significantly to the formation of cancerous cells in humanity and the animal kingdom (Cohen, 1996).

The use of volatile organic compounds in industry has proven to contribute to global warming due to their toxicity and flammability. ILs serve as an attractive alternative to replace classic volatile organic compounds in green technology, leading to a more sustainable and environmentally friendly chemical industry, especially with respect to air emissions. ILs are able to solubilize many different compounds and this is due to their distinctive properties, especially their negligible vapour pressure, these unique chemical and physical properties are presented in Figure 2.3. The use of ILs in industry could potentially lead to a reduction of harmful emissions caused by volatile organic compounds. The replacement of volatile organic compounds with ILs could be economical due to the fact that ILs are recyclable (Pereiro et al., 2006).

Property	Organic solvents	Ionic liquid
Number of solvent	>1000	>1000 000
Applicability	Single function	Multifunction
Catalytic ability	Rare	Common and tuneable
Chirality	Rare	Common and tuneable
Vapour pressure	Obeys the Clausiu-Clapeyron Equation	Negligible vapour pressure under normal conditions
Flammability	Usually flammable	Usually non-flammable
Solvation	Weakly solvating	Strongly solvating
Polarity	Conventional polarity concepts	Polarity concept questionable
Tuneability	Limited range of solvents available	Virtually unlimited range means "designer solvent"
Cost	Normally cheap	Typically between 2 and 100 times the cost of organic solvents
Recyclability	For environmental imperative	For economic imperative
Viscosity	0.2 – 100 cP	22- 40 000 cP
Density	0.6- 1.7g/cm^3	0.8- 3.3 g/cm^3
Refractive index	1.3- 1.6	1.5- 2.2

Figure 2.3: Comparison between ILs and organic solvents (Plechkova and Seddon, 2008).

2.5 Application of ILs

The application of ILs has grown significantly both in academics and industry in the last decade, with approximately 8000 papers published as reported by (Plechkova and Seddon, 2008). There are approximately one million ILs that can be effectively arranged in the laboratory by combination of various cations and anions and this aggregate is only for the basic primary system. On the off chance that there are one million conceivable basic ILs system, there are one billion possible blends of ILs, and one trillion ternary possible ILs system that can be set up from the combination of anions, cations, and substituents. To date, there are approximately 300 ILs available for commercial use. Thus, a huge gap needs to be filled with knowledge of the synthesis and application of ILs. This growth can be observed in Figure 2.4 which shows the number of publications and citations per year, with the number of publications increasing exponentially.

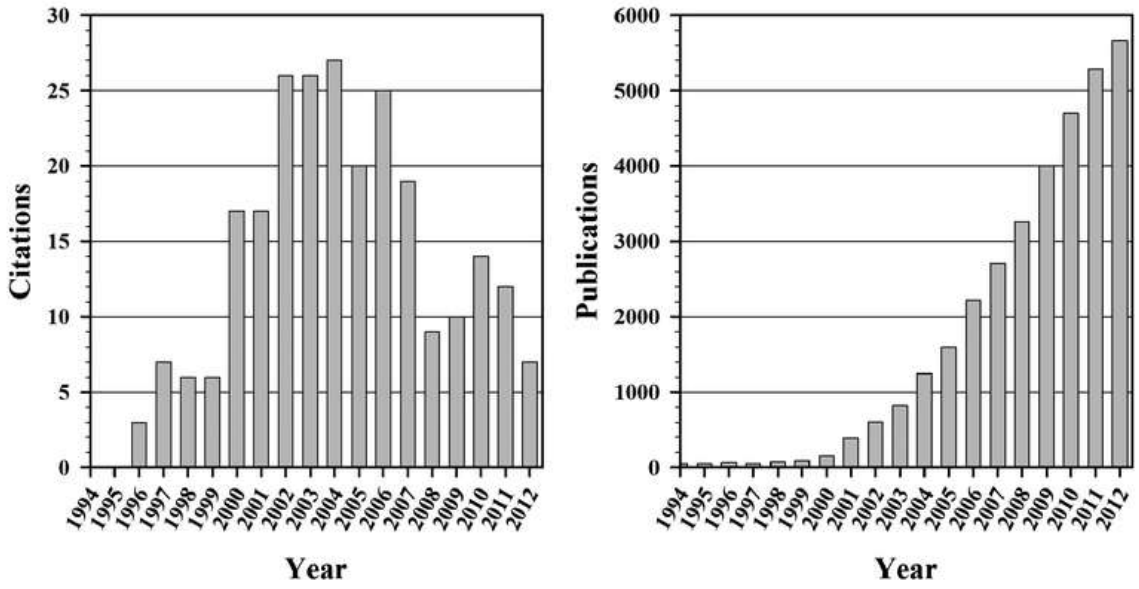

Figure 2.4: The growth of the ILs community as demonstrated through the number of citations (left image) in the figure above and the number of peer-reviewed journal articles (right image) (McCrary and Rogers, 2013)**.**

ILs have drawn massive interest from both academic and industrial applications. They have been applied in different areas in the past, such as bioreactor technology, heat transfer fluids, processing biomass, and as the working fluid to the electrochemical devices such as (Li-ion batteries, dye-sensitized solar cells, double-layer capacitors, Solid-state electrochemical actuators, and fuel cells). Applications of ILs in other areas include the synthesis of nano-particles, areas such as (extraction and separation technology or in catalysis and MALDI matrices) analysis, pharmaceuticals, food, and bio-products (Alvarez et al., 2011). Over a period of 20 years, the application of ILs in different areas has drastically increased. Based on figure 2.5, the number of entries of ILs was over 8000 in 2007. This shows that applications of ILs in different areas have grown significantly.

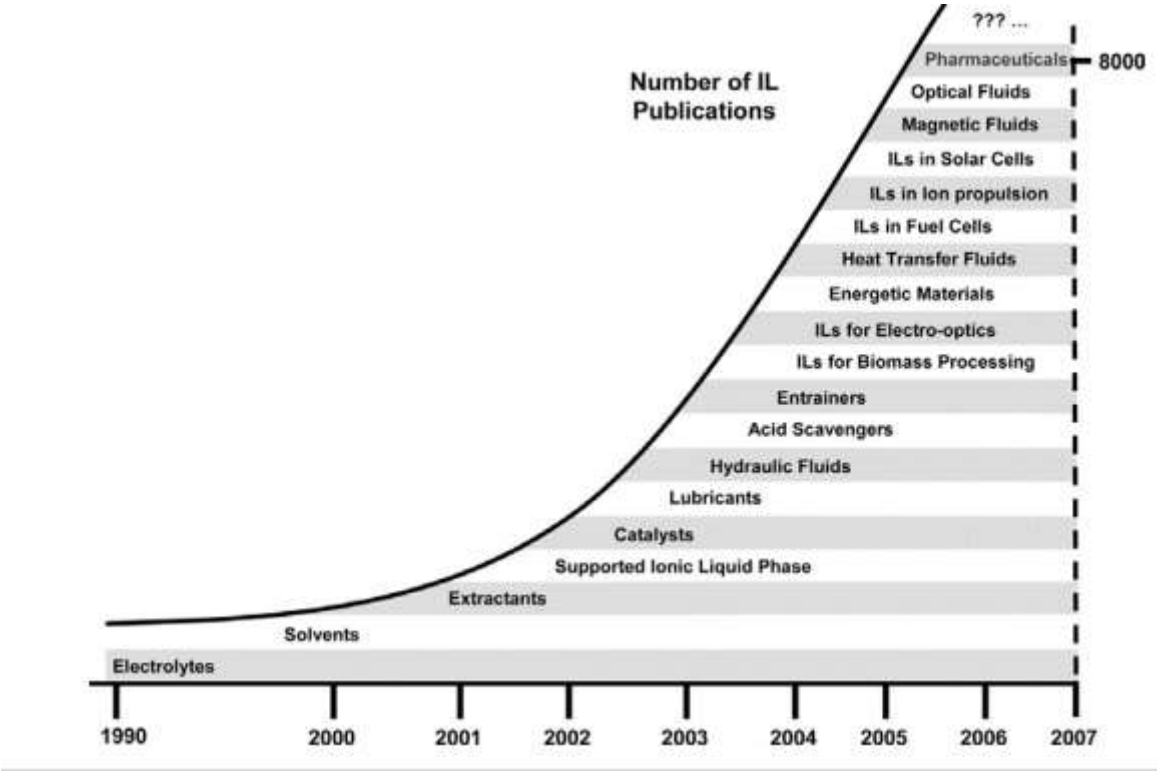

Figure 2.5: Applications of ILs in different areas (Smiglak et al., 2007)**.**

2.6 Application of ILs in different areas.

Research has shown that, electrolytes used in metal air batteries can be replaced with ILs-based electrolytes. The energy supply has become one of the great challenges. As a result, ILs are seen as one of the best alternatives due to their high heat capacity and high stability. ILs are able to evaporate at lower rates than water and organic compound thus, increasing battery life by drying slower (Goodenough and Park, 2013).

Perceiving that roughly half of business pharmaceuticals are organic salts, ILs formed from various pharmaceuticals have been examined. Combining a pharmaceutically active cation with a pharmaceutically active anion leads to a dual dynamic IL in which the activities of two medications are combined (Stoimenovski et al., 2010). In biomedicine, ILs are considered to have the potential to advance formulation science protein-based pharmaceutical arrangements and cellular therapies (Plechkova et al., 2010).

Cellulose is the natural organic compound that is considered as an important bio-renewable compound. The application of cellulose as a bio-renewable feedstock has not be exploited as much due to the fact that a suitable solvent is lacking. In the absence of a suitable solvent, the chemical conversion process of cellulose into useful bio-renewable compound is a challenge. Thus ILs have proven to be suitable

solvents for the conversion process of cellulose into useful bio-renewable compounds (Deetlefs and Seddon, 2003).

ILs have been used to recover uranium and other useful metals from the nuclear fuel and pyrochemical process. This was done by modifying ILs to non-aqueous electrolytes media (Giridhar et al., 2007).

A painting company known as Degussa markets ILs under the name of "TEGO Dispers". These products are added to different types of paints to improve the appearance and the quality of paints (Plechkova et al., 2010).

ILs such as 1-butyl-3-methylimidazolium chloride completely dissolves freeze-dried banana pulp and with an additional 15% DMSO, (dimethyl sulfoxide) lends itself to Carbon-13 NMR analysis. In this manner nutrients such as sucrose, starch, glucose, and fructose can be well monitored during the ripening of a banana (Fort et al., 2006). Extractions of useful compounds from plants for nutritional, pharmaceutical and cosmetic applications are achieved using ILs as an extraction agent (Lapkin et al., 2006).

2.7 Polyethylene glycols (PEGs)

Polyethylene glycols (PEGs) are a group of polymers used in many industrial processes. New toxicity studies on PEG concluded that PEGs are non-toxic, and harmless to the environment (Heldebrant et al., 2006, Herold et al., 1989). PEGs have progressed towards becoming co-solvents of major importance due to their intriguing properties that can be change limitlessly by just fluctuating the average molecular weight and polymeric chain length (Harris and Zalipsky, 1997). Interesting characteristics that make PEGs special are their good biocompatibility and low immunogenicity. PEGs have the ability to amend their chemical structures in accordance with the polarity of the solution (Chen et al., 2002).

For this study, PEG of low molecular weight such as PEG (Mw = 200) was selected. The selection of PEG200 was based on the fact that PEG200 is a liquid at room temperature, making it easy to blend with ILs (Chen et al., 2005). PEG200 possesses a high dielectric constant of $\varepsilon = 20.26$ at 298.15 K (Bonhote et al., 1996), which makes components possessing lesser dielectric constants such ILs to be entirely miscible in it. In a practical sense, this means that all the selected ILs are entirely miscible in PEG200 (Bahadur et al., 2016). The organic and chemical structure of PEG is shown in Figure 2.6.

Figure 2.6: Chemical structure of PEG200.

PEGs have numerous distinctive properties such as non-volatility, low melting point, low flammability and are biodegradable (Zhou et al., 2011). PEGs with shorter chain length such as PEG200 have good miscibility strength (Heisel and Belloni, 1991, Rodriguez et al., 2009).

PEGs compounds are considered as amphiphilic compounds because they contain both alcoholic –OH and partially etheric –O in their structures. PEGs are polar compounds, thus PEGs fluids are both a proton donor and acceptor (Kim et al., 2002). Polar compounds are able to form strong intra and inter-molecular through hydrogen bonding, and also PEGs compounds are able to undergo polymerization process that may differ depending on the chain length, temperature and position of OH group (Visak et al., 2011, Philippova et al., 1985).

2.8 PEGs + ILs

ILs with PEGs when blended may bring about a medium that has fascinating and positive physicochemical properties (Rodriguez et al., 2009). Thermophysical properties of ILs can be improved or changed by the addition of a co-solvent such as alcohols (Moosavi et al., 2015), polymers (Calado et al., 2013), water (Masaki et al., 2010), ketones (Zhao et al., 2015), aldehydes (Manoj et al., 2018) and other hydroxyl compounds In retrospect, properties of PEGs may likewise be modified by combining PEGs with an IL (Chen et al., 2002).

The blending of ionic liquids (ILs) and polyethylene glycols (PEGs) is relatively new and this research has gained momentum recently from both an applied research field and fundamental basis (Rajput et al., 2013, Rodriguez et al., 2009). In the last 10 years, substantial consideration has being given to hybrid-materials or blended solvents, made out of sustainable components such as biodegradable polymers or polymers and ILs (Vuksanovic et al., 2013). Irrespective of the information available on the molecular interactions between ILs and PEGs, the intermolecular interactions data of these mixtures is still insufficient (Daneshvar and Moosavi, 2016).

The blending of ILs and PEGs have been proposed in polymeric electrolytes in batteries (Lodge, 2008, Rodriguez et al., 2009). Due to the efficient ionic conduction of both ILs and PEGs, this material blend can be utilized as electrolytes in different electrochemical devices (Watanabe et al., 1993). The ion transport properties of PEGs containing ILs have been subjected to extensive studies lately, indicating that the synergetic actions between the ILs and the PEGs matrices are crucial for achieving improved transport properties (Simone and Lodge, 2009, Vuksanovic et al., 2013, Calado et al., 2013)

CHAPTER THREE

THEORETICAL FRAMEWORK OF THERMOPHYSICAL PROPERTIES AND EXCESS THERMODYNAMIC PROPERTIES

This chapter presents the theoretical and mathematical background of the selected thermophysical and excess thermodynamic properties for this study. The fundamental thermodynamics expressions are presented before the discussion of the literature data presented for similar systems studied in this work.

Data correlation is of great importance to the scientific field, and the mathematical expressions used for data correlation are presented in this chapter. FT-IR spectroscopy is an important analytical tool used to provide an in-depth analysis of the interaction of both pure components and their mixtures. The definition, the importance, advantage, and disadvantage of FT-IR spectroscopic measurements are also discussed in detail in this chapter.

3.1 Density (ρ)

In engineering, ρ is essential in the development of equations of states which are usually used to correlate two or more parameters. Examples of these parameters are pressure, internal energy, temperature, and volume. The ideal gas law is one of the well-known examples of state functions.

The density (ρ) data of multicomponent solutions play an important role in industrial-scale process design as in vessel sizing, heat and mass transfer. Thermophysical data of ρ is an important concept for developing models and simulations for engineering applications (Vercher et al., 2015).

In the study of ILs ρ is one of the most measured properties and usually, ILs are much denser than water. It was proven that the ρ of imidazolium-based ILs decreases with longer length of alkyl chains in the cations.

Density (ρ) is the quantity of mass (m) to volume (V) in an amount of material. The equation 3.1 represents the mathematical expression of ρ:

$$\rho = \frac{m}{V} \qquad 3.1$$

Thermophysical data of ρ are frequently needed to investigate the thermodynamic properties of binary systems, and ρ data should be accurate in order for the thermodynamic data to be reliable.

3.2 Refractive index (n_D)

The refractive index (n_D) is the thermophysical property defined as the speed of light (c) of a given wavelength in an empty space (vacuum) divided by its velocity (v) in a substance. It can be expressed as:

$$\mathrm{n_D} = \frac{\mathrm{c}}{v} \tag{3.2}$$

The refractive index (n_D) provide data about the conduction of light. At the point when light goes through a substance, the speed diminishes by expanding the refractive index of a substance. These results are due to association or interaction between atoms of parts in substrate and impact of these associations on light. Moreover, in most substrates, the n_D decreases by increasing temperature. The interactions between particles decreases with increasing temperature.

Maxwell introduces the equation relating the permeability and permittivity to the n_D. The relation is known as Maxwell's equation, thus expressed by:

$$\mathrm{n_D} = \pm\sqrt{\varepsilon_r \mu_r} \tag{3.3}$$

Where μ_r and ε_r represent the material of both the relativity of permeability and permittivity, respectively. Mostly, the natural occurrence of material permeability (μ_r) is very close to 1 (Urzhumov, 2007).

Another definition of $\mathrm{n_D}$ is the ratio of the sine of the angle of incidence (medium 1) θ_1 and the angle of refraction of (medium 2) θ_2 and is given by equation 3.4 (Iglesias-Otero et al., 2008).

$$\mathrm{n_D} = \frac{\sin\theta_1}{\sin\theta_2} \tag{3.4}$$

The angles measured are perpendicular to the surface. This definition is based on Snell's law (Iglesias-Otero et al., 2008) and is equivalent to the definition above if the light enters from the reference medium (a vacuum).

Refractive index (n_D) values of liquid mixtures are used to understand the electronic polarizability of the molecule and intermolecular interactions between unlike and similar molecules in the mixture. Industries such as pharmaceutical also uses $\mathrm{n_D}$ to determine the concentration of different samples. The refractive index (n_D) data are also used for the estimation of useful hydrocarbons in the petroleum industry (Koohyar, 2013).

3.3 Viscosity (η)

Viscosity (η) is a transport property that is defined as an internal fluid friction, which can transform kinetic energy of macroscopic motion into heat energy such as the friction between moving solids (Merritt, 1967). In liquid mixture, there is no static friction existing. Nonetheless, there is, instead,

dynamic friction due to random motion of species (i.e. molecules, atoms or ions) in a liquid. The η is essentially caused by the transfer momentum between species and inter-species forces.

The viscosity (η) can be expressed as the shear stress divided by the shear rate (Çengel and Gharaj, 2014).

$$\eta = -\frac{F}{\gamma} \qquad 3.5$$

The shear stress is denoted by F and it represent the drag force of the fluid on the moving plate over the surface of the plate and γ is the shear rate that is the gradient of the velocity of a fluid layer over the distance from the plate to the layer.

The viscosity (η) measurements are needed to understand operations such as mixing, pumping, stirring and diffusion of other molecules through the ILs. The anion and cation of ILs influence the η, viscosity (η) increases with alkyl chain length (cation). Longer alkyl chain length increases the Van der Waals forces between cations, causing the energy of molecules to accelerate rapidly. Generally, ILs possess lower diffusion coefficient because they are held together by strong coulombic forces, thus resulting in higher η.

ILs have higher η and this is one of their disadvantages when compared to the volatile organic solvents. Ongoing research on ILs to replace volatile organic solvent consider this as an important property. Therefore, ILs are usually mixed with other solvents such as alcohol so that they can become easier to handle.

3.4 Speed of sound (*u*)

The speed of sound (*u*) is the distance travelled per unit time by a sound wave as it propagates through an elastic medium. The speed of sound (*u*) can be associated with the first partial derivative of density and accurate data of u can be used to derive equations of states. By measuring *u* (*p, T*), the *u* data can be used to obtain other useful thermophysical properties at an extreme experimental condition such as calorimetric data at high pressure (Barbosa, 2003).

Measurement of u is a helpful source of information i.e., to detect minor changes in gas composition or effect of small concentration change about the thermophysical properties of chemical substances. It is also to understand the intra and intermolecular interactions between liquid mixtures. Measurements of u are a useful tool in process simulation and equipment design (De Azevedo et al., 2004).

Historically, the speed of sound (u) values were used to determine excess property such as isothermal compressibility (K_T). Thus, this excess property was also used to understand interactions between molecules. This is defined as:

$$\mathrm{K_T} = -\frac{1}{\mathrm{V_{0,i}}}\left(\frac{\partial \mathrm{V_{0,i}}}{\partial \mathrm{P}}\right)_{\mathrm{T}} \quad 3.6$$

Where $V_{0,i}$ and P represent molar volume and pressure.

The method for calculating $\mathrm{K_T}$ yielded results which were of low precision and accuracy, as a result, this method was modified to isentropic compressibility(K_s). Presently isentropic compressibility (K_s) values are used to understand the complexity of interactions between the molecules in the liquid mixture. This is defined as:

$$\mathrm{K_s} = -\frac{1}{\mathrm{V_{0,i}}}\left(\frac{\partial \mathrm{V_{0,i}}}{\partial \mathrm{P}}\right)_{\mathrm{S}} = \frac{1}{\rho}\left(\frac{\partial \rho}{\partial \mathrm{P}}\right) \quad 3.7$$

K_s is computed directly from the measured values of u and ρ using the Newton-Laplace equation (Salinas et al., 2015).

$$\mathrm{K_s} = \frac{1}{\rho \mathrm{u}^2} = \frac{\mathrm{V_{0,i}}}{\mathrm{Mu}^2} \quad 3.8$$

For an ideal mixture K_s is considered to be additive in terms of volume fraction. This is considered to be isentropic mainly due to the fact that when the sound wave penetrates the liquid, the temperature and pressure fluctuate with the microscopic volume but the entropy remains constant (Douhéret et al., 2001).

3.5. Excess thermodynamic properties

Excess thermodynamic data derived from thermophysical properties can provide valuable information regarding the behaviour of real mixtures. Molecular excess thermodynamics investigation of the solvent-solute binary system can be useful in different field such as direct application in chemical plant design, in processing and product formation in many industries application, to test theories which attempt to predict binary mixture properties from pure component data and provide data for the evaluation of parameters characterizing interactions between unlike species. The importance and application of blending of ILs with other solvents to make up binary or tertiary system were discussed in chapter two.

Excess property (Z^E) is defined as the difference between the properties of ideal liquid mixtures (Z^{id}) and the real liquid mixtures/measured thermophysical property (Z) (Smith et al., 2005). This is defined mathematically as:

$$Z^{E} = Z - Z^{id} \quad 3.9$$

In this study, Z^E represent excess thermodynamic properties. Equations 3.10 - 3.24 represent different excess thermodynamic properties calculated for this study.

3.5.1 Excess molar volume (V^E)

There are two methods used to determine the excess molar volume (V^E) that is a direct and indirect method. The direct method measures the total volume change upon the mixture. Indirect method calculate V^E from measured ρ values. The reliability of the indirect method for V^E depends greatly on the accuracy and the precision of the method used to measure ρ (Bahadur et al., 2016).

There are three types of indirect methods that are utilized to measure ρ; these include the magnetic float densimeter, mechanical oscillating densitometer and the pycnometry (Handa and Benson, 1979). In this study, the magnetic float densimeter was used to measure density (ρ) and these measurements were used to calculate V^E values. The method used in this study is an indirect method. With adequate precision from ρ measurements, this method is likewise accurate and simple. Equation 3.10 is used to calculate V^E .

$$V^{E} = V_{0,i} - V^{id} \quad 3.10$$

Where

$$V_{0,i} = \frac{\sum_{i=2}^{2} x_i M_i}{\rho_{mixture}} \text{ and } V^{id} = \sum_{i=1}^{2} \frac{x_i M_i}{\rho_i} \quad 3.11$$

V^E and $\rho_{mixture}$ represent excess molar volume and density of the mixture respectively. x_i, M_i and ρ_i represent mole fraction, molecular weight and density of the *i*-th component respectively.

3.5.2 Excess viscosity (η^E)

$$\eta^{E} = \eta - \eta^{id} \quad 3.12$$

Where

$$\eta^{id} = \sum_{i=1}^{2} x_i \eta_i \quad 3.13$$

η represent the viscosity of the mixture. x_i and η_i represent mole fraction and viscosity of the *i*-th component respectively.

3.5.3 Excess refractive index (n_D^E)

$$n_D^E = n_D - n_D^{id} \quad 3.14$$

Where

$$n_D^{id} = \sum_{i=1}^{2} x_i n_{D,i} \quad 3.15$$

n_D represent the refractive index of the mixture. x_i and $n_{D,i}$ represent mole fraction and refractive index of the *i*-th component respectively.

3.5.4 Excess isentropic compressibility (K_s^E)

For this study, the excess isentropic compressibility (K_s^E) is calculated in the manner as suggested by (Benson and Kiyohara, 1976, Srinivasa Rao et al., 2018, Kiyohara et al., 1979).

$$K_S^E = K_S - K_S^{id} \quad 3.16$$

Where

$$K_S = \frac{1}{u^2 \rho_{mixture}} \text{ and } K_S^{id} = \sum_{i=2}^{2} \varphi_i K_{S,i} + T\left[\sum_{i=1}^{2} \frac{\varphi_i V_{0,i} (\alpha_{P,i})^2}{C_{P,i}} - \frac{V^{id} (\alpha_P^{id})^2}{C_P^{id}}\right] \quad 3.17$$

u, $\rho_{mixture}$, and T represents the speed of sound, density and absolute temperature of the mixture respectively. $K_{s,i}$, $C_{P,i}$ and $V_{0,i}$ represent isentropic compressibility, molar isobaric heat capacity and molar volume of the *i*-th component respectively.

The values of φ_i, α_P^{id} and C_P^{id} are calculated using the following equations:

$$\varphi_i = \frac{\frac{x_i M_i}{\rho_i}}{\sum_{i=1}^{2} \frac{x_i M_i}{\rho_i}} \quad 3.18$$

$$\alpha_P^{id} = \sum_{i=1}^{2} \varphi_i \alpha_{P.i} \quad 3.19$$

$$C_P^{id} = \sum_{i=1}^{2} x_i C_{P.i} \quad 3.20$$

φ_i, $\alpha_{P,i}$ and $C_{P,i}$ are the volume fraction, thermal expansion coefficient and molar isobaric heat capacity of *i*-th component respectively.

3.5.5 Excess thermal expansion coefficients (α_P)

A frequently applied derived value for industrial mixtures is the temperature dependence of volume, which is expressed by α_P. It is further used to understand the change in the structure of binary mixture between two components during mixing; α_P are calculated for every mixture composition (Stec et al., 2014). The α_P values of pure components are calculated from the measured ρ by the relation expressed by:

$$\alpha_P = \frac{1}{V_0}\left(\frac{\partial V_{0,i}}{\partial T}\right)_p = -\frac{1}{\rho}\left(\frac{\partial \rho}{\partial T}\right)_p \quad 3.21$$

Differentiation of V_0 with respect to T resulted in the following equation:

$$\left(\frac{\partial V_{0,i}}{\partial T}\right)_p = \left(\frac{\partial V^E}{\partial T}\right)_p + \frac{\partial\left(\sum_1^2 x_i V_{0,i}\right)}{\partial T} \quad 3.22$$

The summation of equation 3.21 and equation 3.22 leads to equation 3.23:

$$\alpha_P = \frac{1}{V_{0,i}}\left[\left(\frac{\partial V^E}{\partial T}\right)_p + \sum_{i=1}^{2} \alpha_i x_i V_{0,i}\right] \quad 3.23$$

Solution thermal expansion coefficients are presented in terms of excess values to emphasize solute-solvent influence on thermal expansion. Equation 3.24 represents the excess thermal expansion coefficient.

$$\alpha_P^E = \alpha_P - \alpha^{id} \quad 3.24$$

3.6 Partial molar volume properties ($\bar{V}_i$)

The partial molar volume ($\bar{V}_i$) is a good indicator to assess the level of interactions between molecules within the binary mixtures. It offers some intuitions about the structural changes during the blending of different components (Mohammadi and Omrani, 2018).

The partial molar volume of each component is expressed by:

$$\bar{V}_i = \left(\frac{\partial V_{0,i}}{\partial n_i}\right)_{T,p,n_i} \quad 3.25$$

By adding Redlich Kister equation to Equation 3.10, this leads to a final equation for partial molar volumes equation ($\bar{V}_i$) (Wood and Battino, 1990). Equation 3.26 and 3.27 represent partial molar volumes for components 1 ($\bar{V}_1$) and components 2 ($\bar{V}_2$). The partial molar volume of component 1 is expressed as:

$$\bar{V}_1 = V^E + V_{0,1} + (1 - x_1)\left(\frac{\partial V^E}{\partial x_1}\right)_{p,T} \quad 3.26$$

The partial molar volume of component 2 is expressed by:

$$\overline{V}_1 = V^E + V_{0,1} + (1 - x_1)\left(\frac{\partial V^E}{\partial x_1}\right)_{p,T} \quad 3.27$$

$V_{0,1}$ and $V_{0,2}$ are the molar volumes of the pure components of ILs and PEG200 respectively.

Simplifying equation 3.26 and 3.27 leads to equations 3.28 and 3.29 for partial molar volumes ($\overline{V}_1$ and $\overline{V}_2$) of components 1 and 2 of any binary mixture respectively.

$$\overline{V}_1 = V^E + V_{0,1} + {x_2}^2 \sum_{i=0}^{4} A_i(2x_1 - 1)^i + 2x_1{x_2}^2 \sum_{i=1}^{4} A_i(2x_1 - 1)^{i-1} \quad 3.28$$

$$\overline{V}_2 = V^E + V_{0,2} + x_1^2 \sum_{i=0}^{4} A_i(2x_1 - 1)^i - 2x_1^2 x_2 \sum_{i=1}^{4} A_i(2x_1 - 1)^{i-1} \quad 3.29$$

The excess partial molar volumes, $\overline{V}_1^E$ and $\overline{V}_2^E$ over the whole composition is calculated using the following expressions:

$$\overline{V}_1^E = \overline{V}_1 - V_{0,1} \quad 3.30$$

$$\overline{V}_2^E = \overline{V}_2 - V_{0,2} \quad 3.31$$

Values of the excess partial molar volumes $\left(\overline{V}_i^E\right)$ of the solute and solvent at infinite dilution $\left(\overline{V}_i^{E,\infty}\right)$ can be calculated from the adjustable parameters of the Legendre polynomials when $x_1 \to 0$ and $x_2 \to 1$. Under such circumstances, the excess partial molar volumes $\left(\overline{V}_i^E\right)$ of the solute and solvent at infinite dilution $\left(\overline{V}_i^{E,\infty}\right)$ is calculated using the following equations:

$$\overline{V}_1^{E,\infty} = V_{0,1} + A_0 - A_1 + A_2 - A_3 + A_4 \quad 3.32$$

$$\overline{V}_2^{E,\infty} = V_{0,2} + A_0 + A_1 + A_2 + A_3 + A_4 \quad 3.33$$

3.7 Data correlation

3.7.1 Pure components

Due to the fact that ILs are composed of a vast number of anions and cations, data correlation by fitting the measured data are needed to check the accuracy of measured values. The R^2-value should be presented to illustrate the fit of the correlation.

Generally, thermophysical properties such as ρ, η, u and n_D usually, tend to decrease with increasing temperature. However, properties are influenced differently by temperature and the relationship with the temperature can vary greatly from property to property.

Thermophysical values are mostly correlated by a linear correlation. This is mostly because of the accuracy of the correlation method. However, sometimes it is more suitable to fit thermophysical values

using higher-order polynomial expression. In this study; ρ, u and n_D data were correlated by means of the polynomial linear fit equation written and compiled in a MATLAB@ program (Gu and Brennecke, 2002). The polynomial linear equation is expressed by:

$$z = \sum_{i=0}^{2} B_i T^i \qquad 3.34$$

z, B_i and T^i represent the thermophysical measured values, polynomial coefficient, and absolute temperature respectively.

In this study, η data were correlated by means of the Vogel–Fulcher–Tammann (VFT) equation written and compiled in a MATLAB@ program. VFT is easy to compute and is also known to correlate η data with high precision (Vogel, 1926). The equation below represents the VFT equation:

$$\eta = Ae^{\frac{B}{T-T_g}} \qquad 3.35$$

A and *B* are fitting parameters, T_g is the 'ideal glass transition temperature' obtained from the literature. The temperature cannot be reached in a finite time experiment, it is therefore replaced by the experimental glass transition temperature (T_g). T_g provides information regarding the nature state (rigidity and flexibility) of an IL at a certain temperature. A and B do not have a clear theoretical meaning but are strongly dependent on T_g (Angell and Sare, 1970).

3.7.2 Binary mixtures

When dealing with the binary mixtures, the impact of the composition on the physicochemical properties is ordinarily studied via analysis of their excess properties.

The Redlich-Kister polynomial model is a very popular model used to correlate excess thermodynamic data and this equation is easy to compute. In this work, the Redlich-Kister polynomial equation was used to correlate the following excess thermodynamic properties; V^E, n_D^E, K_s^E, α_p^E, η^E and n_D^E. The Redlich-Kister polynomial model is used to check the accuracy of the calculated excess thermodynamic properties (Redlich and Kister, 1948). A MATLAB@ program was compiled and used to correlate excess thermodynamic properties using the Redlich-Kister polynomial model. The Redlich-Kister polynomial equation for binary mixtures is expressed as:

$$Z^E = x_i x_j \sum_{i=0}^{4} A_i \left(x_i - x_j\right)^i \qquad 3.36$$

Z^E, x_i, x_j and A_i represent excess thermodynamic properties, mole fraction of the IL, mole fraction of PEG200 and polynomial coefficient for the binary system respectively.

3.7.3 Relative standard deviation

To attain a good correlation of the experimental data for both the pure components and mixtures, the F-test is usually used to determine the appropriate number of parameters. To evaluate the quality fit, the standard relative deviation is used:

$$\sigma_{rel} = \sqrt{\sum_{i}^{N} \frac{\left(\frac{Z^{exp} - Z^{cal}}{Z^{cal}}\right)^2}{N}} \qquad 3.37$$

Z^{exp}, Z^{cal} and N represent the experimental values, calculated values and the number of measurements performed respectively. Deviation of experimental points is presented in the form of the standard relative deviation (σ_{rel}).

3.8 Fourier Transform Infrared (FT-IR) spectroscopy

FT-IR spectroscopy is an analytical technique widely used and applied in science and engineering studies to understand the in-depth molecular mechanism present in different components and mixtures. FT-IR spectroscopy is an important tool for both qualitative and quantitative characterization of liquid material, gas or solid phase. FT-IR spectroscopy is a microscopic instrument that uses light to detect microscopic changes in the ion and dipole moment such as inter and intramolecular interactions in liquids, gases, and solids (Pal et al., 2016).

FT-IR analysis is based on the interplay of electromagnetic radiation with a medium or the measurement of radiation emitted from the medium. Electromagnetic radiation is represented by its energy *E (J).* The relationship is represented below.

$$E = \hbar \cdot f = \frac{\hbar \cdot c}{\lambda} \qquad 3.38$$

ħ, *λ*, and *c* represent Planck's constant (6.63×10^{-34} J.s), wavelength and speed of light respectively. Infrared radiation is electromagnetic radiation which is defined as light in the range of wavelength between 4000 and 400 cm^{-1} (Michelson, 1891).

3.8.1 Advantages and limitations of FT-IR Spectroscopy

Table 3.1 present the limitation and advantages of utilizing FT-IR spectroscopy.

Table 3.1: Advantages and limitations of FT-IR spectroscopy (Torabi, 2001)

Advantage	**Limitation**
FT-IR is a throughput method, implying that all the infrared light passes through the sample at once.	Since FT-IR detects chemical bonds between atoms, it is not practical for the analysis of monatomic materials.
In FT-IR analysis, the detector receives a large amount of light during a short scanning tine.	Other solvents have strong spectral bands, it, therefore, it can be very challenging to characterize chemicals in a low concentration solution.
	FT-IR spectroscopy is sensitive to the background since it cannot make a simultaneous comparison of the background and the sample. Any changes in the background may affect the accuracy of the instrument.

CHAPTER FOUR

LITERATURE REVIEW ON SELECTED IONIC LIQUIDS (ILs) + POLYMERS

This chapter summarises the information presented in literature on the three selected ILs studied in this work with different polymers. Excess thermodynamic properties of the binary mixtures of polymers and ILs are also discussed in this chapter.

4.1 Previously studied binary mixtures

The survey of the open literature indicates that the intermolecular interactions of binary mixtures between polymers and ILs have been given less attention in recent years. No data has been reported for thermophysical property, excess thermodynamic property, and FT-IR spectra analysis of all the binary mixtures selected in this study.

Table 4.1 presents a literature review based on the investigation of intermolecular interactions between the selected ILs and polymers using thermophysical and excess thermodynamic data at atmospheric pressure of p = 0.1 MPa. Due to the lack of thermophysical and thermodynamic data on ILs (1-butyl-3-methylimidazolium hexafluorophosphate ($[\mathrm{BMIM}]^+[\mathrm{PF_6}]^-$), 1-ethyl-3-methylimidazolium tetrafluoroborate ($[\mathrm{EMIM}]^+[\mathrm{BF_4}]^-$) and 1- butyl -3-methylimidazolium tetrafluoroborate ($[\mathrm{BMIM}]^+[\mathrm{BF_4}]^-$)) blended with PEG200, this further strengthens the need for measurements of these combinations.

Table 4. 1: A review of the open literature on the thermophysical and thermodynamic properties for binary mixtures of $[\mathbf{BMIM}]^+[\mathbf{PF_6}]^-$, $[\mathbf{BMIM}]^+[\mathbf{BF_4}]^-$ and $[\mathbf{EMIM}]^+[\mathbf{BF_4}]^-$ + polymers at atmospheric pressure of p = 0.1 MPa.

	$[\mathbf{BMIM}]^+[\mathbf{PF_6}]^-$	$[\mathbf{BMIM}]^+[\mathbf{BF_4}]^-$	$[\mathbf{EMIM}]^+[\mathbf{BF_4}]^-$
Di-EGMME	(Pal et al., 2010)	(Pal and Kumar, 2012)	[-]
PGMEE and PGMME	(Pal et al., 2010)	[-]	[-]
Tri-EGMME	(Pal et al., 2010)	(Pal and Kumar, 2012)	[-]
Tri-EGDME and Tetra-EGDME	(Pal et al., 2010)	[-]	[-]
EGMEE and Tri-EGMEE	(Pal and Kumar, 2011) and (Krishna et al., 2017)	[-]	[-]
PEG200 and PEG400	(Trivedi and Pandey, 2011)	[-]	[-]
EGMPE and EGEE	(Krishna et al., 2016)	[-]	[-]
EGMME	(Krishna et al., 2017)	(Pal and Kumar, 2012)	(Reddy et al., 2016b)

From table 4.1, polymer (EGMME) is the only polymer which has been blended with all the three selected ILs for the investigation of the intermolecular interactions.

The discussion of the intermolecular interactions based on the thermodynamic data for all the binary mixtures presented in table 4.1 is presented in section 4.3.

4.2 Excess thermodynamic properties

The dispersion forces and weak interactions between molecules are denoted by positive deviation of V^E, $\bar{V}_i^E$, $\bar{V}_i^{E,\infty}$, K_S^E and α_P^E, and negative departures of n_D^E and η^E for binary mixtures. The strong specific interaction is represented by negative departures of V^E, $\bar{V}_i^E$, $\bar{V}_i^{E,\infty}$, K_S^E and α_P^E, and positive departures of n_D^E and η^E for binary mixtures (Krestov, 1991, Srinivasa Rao et al., 2018).

4.2.1 Excess molar volume (V^E)

The negative values of V^E are as a result of the following factors (Pandey, 2012):
There are strong chemical interactions between molecules of a solvent and a solute in the mixture and this is known as ion-dipole interactions or also called hydrogen bonding. Negative values of V^E also suggest that there are geometrical fittings between molecules of a solvent and a solute upon the mixture. Molecules possessing smaller volume fit into the free space of molecules having larger volume size, thereby, resulting in contraction of the mixture volume (Pandey, 2012). Thus, due to contraction of the mixture volume, the formation of ion-dipole interactions/hydrogen bonding is dominant. The formation of ion-dipole interactions/hydrogen bonding is between nitrogen atoms of imidazolium cation (Yokozeki et al., 2007b) of ILs and dipolar hydroxyl group –OH of polymer molecules (Krishna et al., 2017).

Positive values of V^E suggest that there are no geometric fitting between molecules of components mixed together. Thus, their molar volume is either the same or the difference is significantly small. This also leads to the expansion of volume between two components. Positive values also imply that there are no specific interactions whether it is dipole-dipole interactions, ion-dipole interactions also known as hydrogen bonding and charge transfer interactions between molecules of components mixed together (Pandey, 2012). Additionally, positive values suggest that the geometric fitting of polymers into the void space of ILs are not favourable, due to the same molar volumes of two components. Thus, there is an expansion of volume upon the mixture. This implies that there are no specific intermolecular interactions between the molecules of polymers and ILs.

4.2.2 Excess isentropic compressibility ($\mathbf{K_S^E}$)

Interpretation of K_S^E data is generally not straightforward and simple because the K_S^E values are affected by both molecular packing and the patterns of molecular aggregation induced by molecular interactions (Papari et al., 2013).

The negative values of K_S^E of ILs with polymers imply that there is volume contraction upon the mixture which leads to the decrease in compressibility. The negative values of K_S^E imply that the molecules in the mixture are more rigid or less compressible than their pure components. In other words, ($V^E < 0$)) (Alavianmehr et al., 2017). Additionally, volume contraction is attributed to the strong attractive interactions between the ions of ILs and molecules of polymers in the mixture. The strong interactions are due to the solvation of ions upon the mixture of different compounds. The strong intermolecular interactions through ion-dipole interactions and interstitial accommodation leads to a more compact structure/or a contraction in volume (Umapathi et al., 2014).

Positive values of K_S^E imply that molecules are not packed together or are not rigid which means more compressibility. There is an expansion of volume ($V^E > 0$) which increases the compressibility ($K_S^E > 0$) of the mixture. Expansion of volume mixture suggests that there are no specific intermolecular interactions. Additionally, the positive values of K_S^E for binary mixtures suggest that there is no solvation of ions in a polymer mixture (Anuradha et al., 2005).

4.2.3 Excess viscosity (η^E)

The negative values of η^E can be attributed to the decrease in the number and strength of hydrogen bonds upon mixing. This suggests that the strong coulombic interactions between the cation and anion are weakened upon mixing with polymers, which leads to a higher mobility of ions and consequently a lower η of the mixtures (Vercher et al., 2015). The viscosities of associates formed between unlike molecules are relatively less than those of the pure component (Roy et al., 2006).

The positive values of η^E suggest that the associates formed between unlike molecules are relatively more than those in the pure components (Kavitha et al., 2012a).

4.2.4 Excess Refractive index (n_D^E)

For n_D^E, the deviation is always opposite to the V^E. Positive values indicate that there are strong interactions involving the formation of ion-dipole interactions/hydrogen bonding between the component molecules of the mixture. Positive n_D^E values denote that there is volume contraction in the mixture, and this causes a decrease in the intermolecular distance. This leads to an increase in n_D due to the enhancement of the dispersion forces (Hirsehfelder et al., 1954).

Negative values of n_D^E indicate weak interactions between the unlike molecules (Kawaizumi et al., 1977). Negative n_D^E values mean that there is an expansion in the volume of the binary mixtures. This expansion of molecules causes the intermolecular distance to increase and causes the refractive index to decrease. The decrease of refractive index causes the reduction of the dispersion forces existing between molecules of two components.

4.2.5 Excess thermal expansion coefficients (α_P^E)

Excess thermal expansion coefficient values (α_P^E) are always connected with the values of V^E function and interactions in the solution (Tamura et al., 1997).

Negative values of α_P^E suggest that the expansivity of the solution is lower than that of pure liquids, thus resulting in the contraction of volumetric thermal expansion between two different compounds

(Shafaati and Almasi, 2017). Negative values of α_P^E reflects the association of components in the mixture are strongly associated in the mixture, meaning there is a breaking of H-bonds followed by specific ion-dipole interactions occurring upon mixing of two different components (Krishna et al., 2016). As a result, the average intermolecular distance between the molecules of polymer and ILs decreases as well leading to the contraction of volume upon the mixture. The decrease in volumetric thermal expansion suggests that there is a specific attraction force involved between the molecules of two components, which results in an increase in volumetric thermal expansion upon mixing which causes the thermal expansivity of the mixture to decrease (Krishna et al., 2016).

The positive values of α_P^E indicate self-association of components in the mixtures, implying that there is no breakage of H-bonds upon mixing the two different components. As a result, no new specific interactions are formed between unknown molecules of two dissimilar components (Alavianmehr et al., 2017). Additionally, positive values of α_P^E suggest that there is an increase in volumetric thermal expansion upon the mixing. This increases in volumetric thermal expansion suggest that there is no specific attraction forces involved between the molecules of two components.
Thus, the average intermolecular distance between the molecules of two different components increases. This implies that there is volume expansion upon the mixture, thus, no specific interactions are formed.

4.2.6 Excess partial molar volume ($\bar{V}_i^E$)

The negative ($\bar{V}_i^E$) values designate the dominance of strong solute-solvent interactions between molecules, whereas the positive ($\bar{V}_i^E$)values indicate the presence of weak solute-solvent interactions (Desnoyers and Perron, 1997).

The excess partial molar volume at infinite dilution ($\bar{V}_i^{E,\infty}$) is calculated from ($\bar{V}_i^E$) values. The ($\bar{V}_i^{E,\infty}$) calculations are of interest because at an infinite dilution it is difficult to study the presences and absence of any molecular interactions. Therefore, the values of partial molar volumes at infinite dilution provide information about solute-solvent interactions that are independent of the composition (Rezaei-Sameti and Rakhshi, 2017).

The negative values of ($\bar{V}_i^{E,\infty}$) suggest that, the self-association of pure components between homogeneous molecules are removed effectively and strong interactions between different molecules are formed (Alavianmehr et al., 2017). This leads to volume contraction and the values of excess partial molar volume at infinite dilution become negative.

Positive values of ($\bar{V}_i^{E,\infty}$) are attributed to self-association of pure components in the mixtures, implying that there is no breakage of any H-bonds upon mixing two different components. As a result, no new specific interactions are formed between unknown molecules of two dissimilar components.

4.3 Excess thermodynamic properties of selected ILs with different polymers (polyethers)

This section discusses the effect of the cation/anion of the three selected ILs towards the molecules (as presented in table 4.1) of EGMME, tri-EGMME and Di-EGMME at 298.15 K under atmospheric pressure of p = 0.1 MPa.

4.3.1 ILs + EGMME

This section discusses the effect of cation/anion of ILs towards EGMME using calculated thermodynamic data.

(Reddy et al., 2016a) reported ρ, u and n_D for $[\mathrm{EMIM}]^+[\mathrm{BF_4}]^-$+ EGMME under atmospheric pressure of p = 0.1 MPa at T = (298.15, 298.15, and 328.15) K. The experimental values were used to calculate the V^E, $\bar{\mathrm{V}}_\mathrm{i}^\mathrm{E}$, $\bar{V}_i^{E,\infty}$, α_P^E, n_D^E and K_s^E. The V^E values are both positive and negative, $\bar{V}_1^E$ values are negative, and $\bar{\mathrm{V}}_2^\mathrm{E}$ values are both negative and positive. The values of α_P^E and K_s^E are all negative and lastly the values of n_D^E are all positive.

(Pal and Kumar, 2012) reported ρ and u for $[\mathrm{BMIM}]^+[\mathrm{BF_4}]^-$+ EGMME under atmospheric pressure of p = 0.1 MPa at T = (298.15, 288.15, and 318.15) K. Experimental values were used to calculate the V^E and K_s^E for the binary mixtures. The binary V^E are negative and K_s^E are also negative.

(Krishna et al., 2017) reported ρ, u and n_D for $[\mathrm{BMIM}]^+[\mathrm{PF_6}]^-$+ EGMME under atmospheric pressure of p = 0.1 MPa at T = (298.15, 298.15, and 323.15) K. Experimental values were used to calculate the V^E, $\bar{V}_i^E$, $\bar{V}_i^{E,\infty}$ and $\mathrm{K_S^E}$ for the binary mixtures. The V^E, $\bar{V}_1^E$, $\bar{V}_2^E$, and K_s^E for the binary mixture, all resulted in negative deviations. The FT-IR spectra were further used to confirm the ion-dipole interactions formed.

The following section discusses the excess thermodynamic properties of the above binary mixtures.

Figure 3.1 presents the variation of V^E, K_s^E and $\bar{V}_i^E$ as a function of mole fraction of ILs. The excess thermodynamic values for all the studied binary systems are negative over the entire ILs composition range.

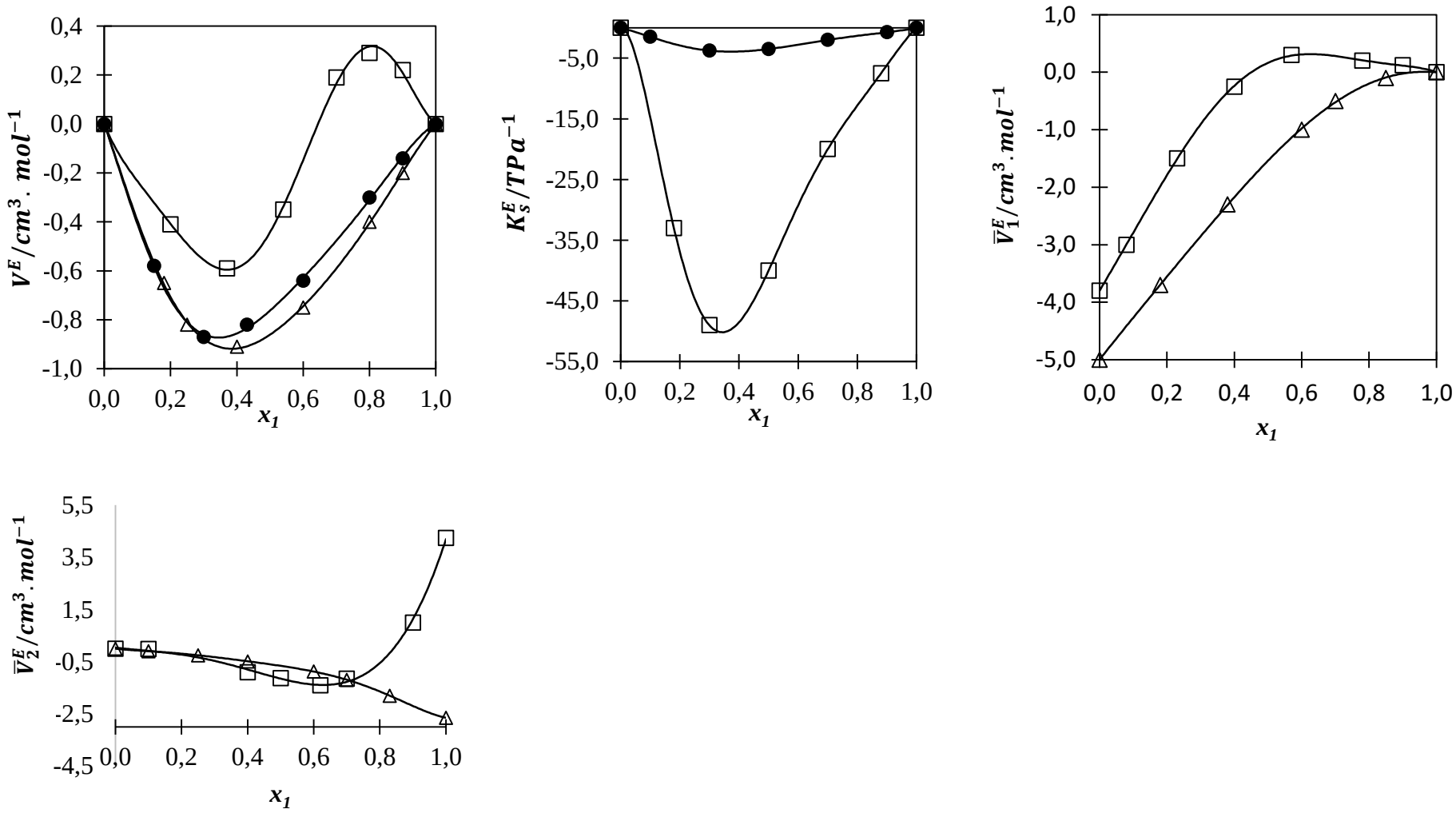

Figure 4.1: Excess thermodynamic for (•) $[\mathbf{BMIM}]^+[\mathbf{BF_4}]^-$ (Pal and Kumar, 2012), (□) $[\mathbf{EMIM}]^+[\mathbf{BF_4}]^-$ (Reddy et al., 2016a) and △$[\mathbf{BMIM}]^+[\mathbf{PF_6}]^-$ (Krishna et al., 2017) + EGMME at T = 298.15 K under atmospheric pressure of p = 0.1 MPa.

For V^E, the $[EMIM]^+[BF_4]^-$ + EGMME system has S-shaped behaviour showing both negative and positive values for V^E. The behaviour at the low mole fraction of IL implies that there are; volume contraction upon the mixture, geometric and packing effect taking place and formation of a strong ion-dipole interactions between ion of IL and dipolar molecules of EGMME The geometric effect of molecules is due to a large difference between the molar volumes of IL and the molar volume of EGMME. This means that EGMME tends to fill the free space of $[EMIM]^+[BF_4]^-$ much better at a low mole fraction of $[EMIM]^+[BF_4]^-$ due to the formation of hydrogen bonding.

Positive values of V^E occur at a high mole fraction of IL implying that there is no packing effect between the large molecules of ILs and the small molecules of EGMME. As a result, there is volume expansion upon mixing. Thus, the intermolecular forces between the ions of IL and dipole molecules of EGMME are weak to form any specific interactions also known as the dissociation of hydrogen bonding.

Negative values of V^E for $[BMIM]^+[BF_4]^-$ and $[BMIM]^+[PF_6]^-$ + EGMME imply that there is volume contraction upon the mixture, geometric and packing effect taking place and formation of a strong ion-dipole interactions between ion of IL and dipolar molecules of EGMME. From the results the magnitude of V^E values for EGMME with ILs follow the order; $[BMIM]^+[PF_6]^-$ > $[BMIM]^+[BF_4]^-$ > $[EMIM]^+[BF_4]^-$.

Comparing the effect of the anion of $[BMIM]^+[PF_6]^-$ and $[BMIM]^+[BF_4]^-$, the magnitude of V^E follow the order $[PF_6]^-$ > $[BF_4]^-$. The minimum negative value of $[PF_6]^-$ anion reached is greater than the V^E negative value of $[BF_4]^-$ anion. This implies that the $[PF_6]^-$ anion has much more ability to form stronger intermolecular interactions/hydrogen bonding with EGMME than with the $[BF_4]^-$ anion. It is clear that the chemical structure of an anion is strongly affected the V^E values.

Comparing the effect of the cation of $[BMIM]^+[PF_6]^-$ and $[BMIM]^+[BF_4]^-$, the magnitude of V^E follows the order $[BMIM]^+$ > $[EMIM]^+$. The V^E values of binary system of $[BMIM]^+$ cation are more negative than that of $[EMIM]^+$. It is clear that the shorter butyl cation has a greater ability to form stronger interactions/hydrogen bonding with EGMME than the longer ethyl cation chain of IL.

The negative values of K_S^E, imply that the mixture is rigid (less compressible) than the corresponding ideal mixture. With the mixture being more rigid (with lower compressibility ($K_S^E < 0$)), the molecules are more packed together implying that there is a contraction of volume present. Negative values

suggest that there is a geometric fitting between solute and a solvent leading to a more compact/rigid structure. The rigidity of the mixture means that there are strong ion-dipole interactions. Additionally, negative values are due to the solvation of the ions in the solution, indicating that there are ion-dipole interactions/hydrogen bonding (Umapathi et al., 2017). The solvation of EGMME molecules in the mixture increases as the concentration of IL increases. Thus, the compressibility (contraction) of the mixture decreases, causing the mixture to be more compact. The values of K_s^E for ILs with EGMME follow in this order: $[BMIM]^+[BF_4]^-$ > $[EMIM]^+[BF_4]^-$.

The negative values of K_s^E is consistent with negative values of V^E. This suggests that the binary mixtures of all the binary mixtures are less compressible than the corresponding ideal mixture indicating the presence of ion-dipole interactions.

Thus, it is clear that the alkyl chain of cation affects the strength of molecular interactions and hydrogen bonds. The magnitude of K_s^E values for EGMME with ILs follow the order; $[BMIM]^+[BF_4]^-$ > $[EMIM]^+[BF_4]^-$. The longer the alkyl chain of a cation the greater the solvation of ion.

For $\bar{V}_i^E$, negative deviation is observed for binary mixture of $[BMIM]^+[PF_6]^-$ and $[EMIM]^+[BF_4]^-$+ EGMME. In general, the negative of $\bar{V}_1^E$ and $\bar{V}_2^E$ values suggest that there is a strong solute-solvent interactions between ion of ILs and dipolar molecules of EGMME molecules.

The values of $\bar{V}_1^E$ and $\bar{V}_2^E$ for ILs with EGMME follow in the order: $[BMIM]^+[PF_6]^-$ > $[EMIM]^+[BF_4]^-$. Thus, it is clear that the alkyl chain of cation and the molecular weight of an anion affects the strength of the molecular interactions.

Figure 4.2 presents the FT-IR spectra for the $[BMIM]^+[PF_6]^-$ + EGMME.

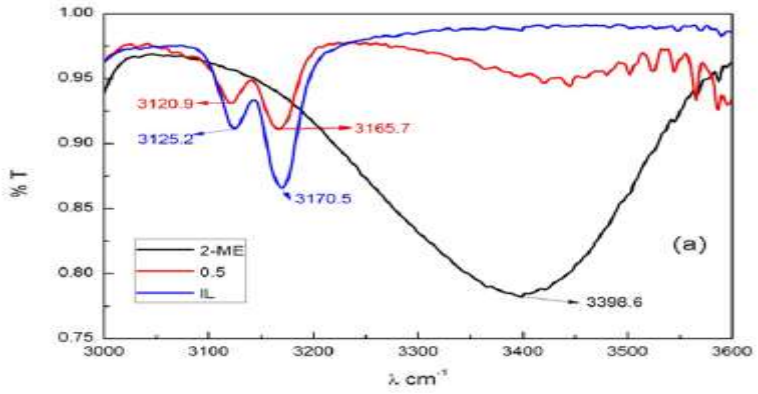

Figure 4.2: Normalized FT-IR spectra of pure (■) $[\mathbf{BMIM}]^+[\mathbf{PF_6}]^-$, (■) $[\mathbf{BMIM}]^+[\mathbf{PF_6}]^-$ + EGMME mole fraction of ($\boldsymbol{x_1 = 0.5}$) and (■) EGMME at temperature T = 298.15 K under atmospheric pressure of p = 0.1 MPa (Krishna et al., 2017).

The frequency region of 3100 – 3200 cm^{-1} represents the C-H bonds predominantly originating from the aromatic imidazolium ring of the ILs (Dhumal et al., 2011). The two broad bands are observed in the region (3100 – 3200 cm^{-1}), these two broad bands rings may exist in two different environments, e.g in dissociated ions and ion pairs (Pandey et al., 2013).

On addition of EGMME, these two different peaks representing (C-H stretching mode) shifts towards lower frequencies. This shift is due to ion-dipole interactions/hydrogen bonding between nitrogen molecules of imidazolium cation of ILs (Yokozeki et al., 2007b) and dipolar hydroxyl (–OH) group of EGMME molecules.

All the calculated excess thermodynamic data and FT-IR spectra are in good agreement with each other, implying that the results are reliable and consistent. From all the results, it is clear that the intermolecular investigation can be conducted using both excess thermodynamic properties and FT-IR spectra analysis. From FT-IR spectra analysis, the strong ion-dipole interactions arise from the hydroxyl (OH) group of the dipolar EGMME molecules and nitrogen molecules of alkyl imidazolium ILs. Excess thermodynamic indicates that the strength of ion-dipole interactions formed in these binary systems follow the order: $[\mathrm{BMIM}]^+[\mathrm{PF_6}]^-$ > $[\mathrm{BMIM}]^+[\mathrm{BF_4}]^-$ > $[\mathrm{EMIM}]^+[\mathrm{BF_4}]^-$.

4.3.2 ILs + Di-EGMME

This section discusses the effect of the cation/anion of ILs towards Di-EGMME using calculated thermodynamic data.

(Pal et al., 2010) reported ρ, u and n_D for $[\mathrm{BMIM}]^+[\mathrm{PF_6}]^-$+ Di-EGMME under atmospheric pressure of p = 0.1 MPa at T = (288.15, 298.15, and 308.15) K. Experimental values were used to calculate the V^E, n_D^E and K_S^E for the binary mixtures. The binary V^E are negative, n_D^E are positive and K_S^E are negative.

(Pal and Kumar, 2012) reported ρ and u for $[\mathrm{BMIM}]^+[\mathrm{BF_4}]^-$+ Di-EGMME under atmospheric pressure of p = 0.1 MPa at T = (288.15, 293.15, 298.15, 303.15, 308.15, 313.15 and 318.15) K. Experimental values were used to calculate the V^E and K_S^E for the binary mixtures. The binary V^E and K_S^E are all negative.

The following section discusses the excess thermodynamic properties of the above binary mixture.

Figure 4.3 presents the variation of V^E and K_S^E as a function of mole fraction of ILs. The excess thermodynamic values for all the studied binary systems are negative over the entire ILs composition range.

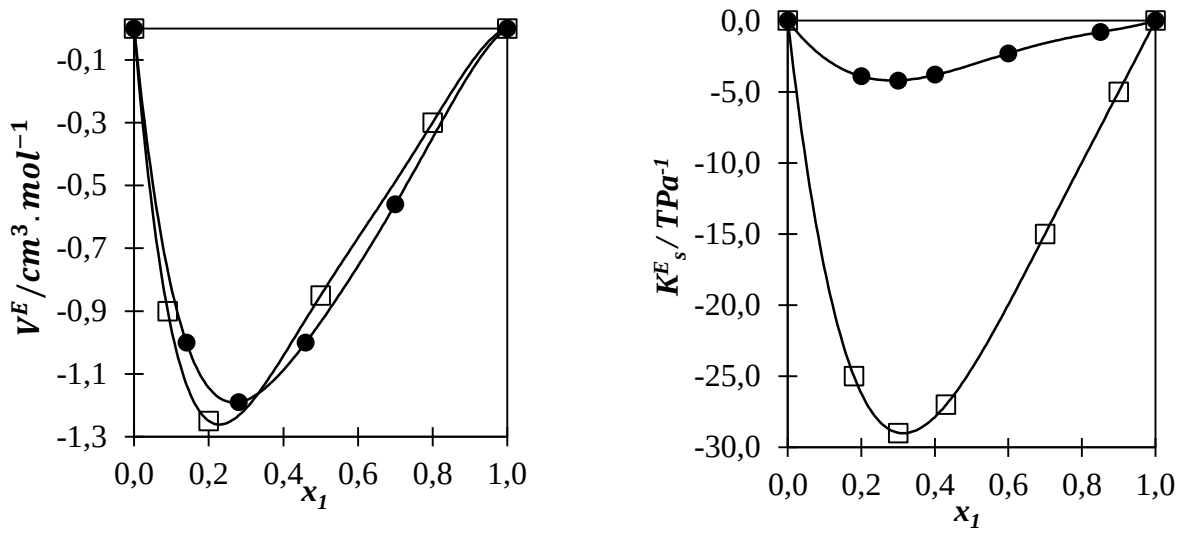

Figure 4.3: Excess thermodynamic for Excess thermodynamic for (•)[**BMIM**]$^+$[**BF$_4$**]$^-$ (Pal et al., 2010, Pal and Kumar, 2012) and (□)[**BMIM**]$^+$[**PF$_6$**]$^-$ (Pal et al., 2010) + Di-EGMME at T = 298.15 K under atmospheric pressure of p = 0.1 MPa.

The negative values of V^E of $[BMIM]^+[PF_6]^-$and $[BMIM]^+[BF_4]^-$ + Di-EGMME suggests that there is volume contraction upon the mixture. This is due to the geometric and packing effect between the molecules of ILs and Di-EGMME. This results in strong ion-dipole interactions/hydrogen bonds between the molecules of ILs and Di-EGMME. From the results the magnitude of V^E values for Di-EGMME with ILs follow the order: $[BMIM]^+[PF_6]^-$ > $[BMIM]^+[BF_4]^-$.

Comparing the effect of the anion, the magnitude of V^E follow the order $[PF_6]^-$ > $[BF_4]^-$ and thus there is a strong packing effect by associations between ILs and Di-EGMME molecules through hydrogen bonding. Thus, the ability of $[BMIM]^+[PF_6]^-$ to accommodate molecules of Di-EGMME into its free space is much greater than that of $[BMIM]^+[BF_4]^-$. It is clear that the size of anion affects the formation of hydrogen bonds, the larger the anion the greater the interactions and vice versa.

The negative values of K_S^E, imply that the binary mixture is less compressible than the corresponding ideal mixture. The strong intermolecular interactions through interstitial accommodation (volume contraction) and orientational ordering leads to a more rigid structure. Thus the strong intermolecular interactions are due to the solvation of ions in the solution (Umapathi et al., 2017). The solvation of Di-EGMME molecules into the mixture increases as the concentration of IL increases. Thus, the compressibility (contraction) of the mixture decreases, causing the mixture to be more compact.

The magnitude of K_S^E values follow the order: $[\mathrm{BMIM}]^+[\mathrm{PF_6}]^-$ > $[\mathrm{BMIM}]^+[\mathrm{BF_4}]^-$. Comparing the effect of the anion of $[\mathrm{BMIM}]^+[\mathrm{PF_6}]^-$ and $[\mathrm{BMIM}]^+[\mathrm{BF_4}]^-$, the magnitude of K_S^E follow the order $[\mathrm{PF_6}]^-$> $[\mathrm{BF_4}]^-$. Thus, it is clear that the size of the anion affects the formation of hydrogen bonding. Hence the larger the anion the stronger the interactions. The results of K_S^E are consistent with the V^E results.

4.3.3 ILs + Tri-EGMME

This section discusses the effect of the cation/anion of ILs towards Tri-EGMME using calculated thermodynamic data.

(Pal and Kumar, 2011) reported ρ and u for $[\mathrm{BMIM}]^+[\mathrm{PF_6}]^-$+ Tri-EGMME under atmospheric pressure of p = 0.1 MPa at T = (288.15- 318.15) K with 5 K interval. Experimental values were used to calculate the V^E and K_S^E for the binary mixtures. The binary V^E and K_S^E are all negative across the composition range.

(Pal and Kumar, 2012) reported ρ and u for $[\mathrm{BMIM}]^+[\mathrm{BF_4}]^-$ + Tri-EGMME under atmospheric pressure of p = 0.1 MPa at T = (288.15 – 318.15) K with 5 K interval. Experimental values were used to calculate the V^E for the binary mixtures. The binary $\mathrm{V^E}$ are all negative across the composition range.

The following section discusses the excess thermodynamic properties of the above binary mixture.

Figure 4.4 presents the variation of V^E as a function of mole fraction of ILs. The excess thermodynamic values for all the studied binary systems are negative over the entire ILs composition range.

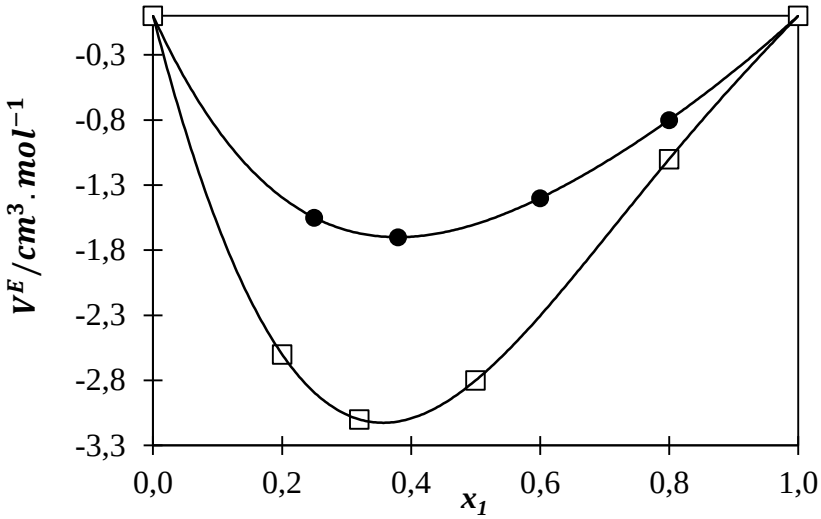

Figure 4.4: Excess thermodynamics for the binary mixtures of (□)$[BMIM]^+[BF_4]^-$ (Pal and Kumar, 2012) and (●)$[BMIM]^+[PF_6]^-$ (Pal et al., 2010) + Tri-EGMME at 298.15 K under atmospheric pressure of p = 0.1 MPa.

The negative values of V^E for the following binary system; ILs + Tri-EGMME suggest that there is volume contraction upon mixing. Volume contraction is due to interstitial accommodation and orientational ordering leading to a more compact structure which contributes to negative values of V^E. Thus volume contraction leads to strong ion-dipole interactions/ hydrogen bonding between the dipolar hydroxyl –OH molecules of Tri-EGMME and nitrogen atoms of imidazolium cation (Yokozeki et al., 2007b). The magnitude of V^E values for Tri-EGMME with ILs follow the order; $[BMIM]^+[BF_4]^-$ > $[BMIM]^+[PF_6]^-$.

Comparing the effect of the anion, the magnitude of V^E follows the order $[PF_6]^-$ > $[BF_4]^-$. The ability of $[BMIM]^+[PF_6]$ to accommodate molecules of Tri-EGMME into its free space is greater than that of $[BMIM]^+[BF_4]^-$. Thus, there is interstitial accommodation between the molecules of ILs and Tri-EGMME. The geometric accommodation suggests that there is volume contraction upon the binary mixture. Volume contraction is also due to strong ion-dipole interactions between the molecules of Tri-EGMME and ILs. Thus, it is clear that the size of anion affects the formation of hydrogen bonds. Hence the larger the anion the greater the interactions and vice versa.

CHAPTER FIVE

EXPERIMENTAL METHODS

This chapter presents the experimental procedures used in this study. The first section of this chapter presents the details of the methods used to dry the ILs used in this study. The second section presents the calculations used to prepare different concentrations of mixtures for measurements. The third section presents the details of the instruments used to measure all thermophysical properties investigated in this study. This is followed by the fourth section which presents the details of the FT-IR spectroscopy instrument used to investigate the intermolecular interactions present upon mixing.

5.1 Analysis of the water content

ILs are said to be hygroscopic in nature, thus an excess amount of water available in ILs may influence the measurements and results. It is vital to know the water content of ILs and the water content should be kept at a low value (Kallidanthiyil Chellappan, 2012).

Besides the water content present in compounds, halides are also said to affect the thermophysical data of ILs. However, the halide content could not be determined since compounds used were purchased and not synthesized in the laboratory. Furthermore, determination of the amount of halides is only possible if compounds used were synthesized in the laboratories.

ILs used in this study were dried using the vacuum degassing method (ultrasonic bath filled with oil and vacuum pump). The chemicals were placed under vacuum pressure at T = 343.15 K for at least 72 hours prior to measurements in order to reduce the water content. After the degassing method, the chemicals were then stored under room temperature and atmospheric pressure in a desiccator filled with molecular sieves to reduce and avoid moisture. In this study, the Karl Fisher titration method was used to measure water content in all ILs used.

The Karl Fisher titration method is accepted globally to measure water content in different industries such as pharmaceuticals, food, oil and chemicals (Neukermans, 2015). In this study, the Karl-Fischer Moisture Titrator (MKS-500) purchased from Trilab was used. The titrant hydranal-composite 5 was

purchased from Sigma-Aldrich. Hydranal-composite 5 is one component which contains all reactants such as sulphur dioxide, iodine, and one or more bases.

5.2 Sample preparation

The mole fraction of components (x_i) in the mixture were prepared to cover the entire composition range. Binary samples were prepared by starting with the pure component being PEG as a first sample and continuing with sample two. This was done by mixing different masses of ILs and PEG200, thus the number of moles (n_i) was obtained. Equation 5.1 represents the number of moles obtained.

$$\mathrm{n_i} = \frac{\mathrm{m_i}}{\mathrm{M_i}} \tag{5.1}$$

m_i and M_i represent the mass and molecular weight of the *i*-th component respectively. The summation of the total number of moles (n_i) for both components is important. Equation 5.2 represent the total number of moles (n_i) for component 1 and 2.

$$\sum_{i=1}^{2} \mathrm{n_i} = \mathrm{n_1} + \mathrm{n_2} \tag{5.2}$$

n_i is the number of molecules for the i-th component and $\sum_{i=1}^{2} n_i$ is the sum of the number of moles for the two *i*-th components.

The mole fraction of components (x_i) in the mixture were calculated by dividing equation 5.1 with equation 5.2. Thus equation 5.3 present the overall mole fraction of components (x_i)

$$\mathrm{x_i} = \frac{\mathrm{n_i}}{\sum_{i=1}^{2} \mathrm{n_i}} \tag{5.3}$$

Air-tight Stoppard glass vials were filled with different mass ratios and weighed on the analytical mass balance (Ohaus) having an accuracy of ± 0.0001 g. The binary mixtures were shaken to ensure complete homogeneity of the ILs and PEG200 mixture.

A medical syringe was used to withdraw the sample from the glass vial. The homogeneous samples were then injected into the different instruments used to measure the thermophysical properties. The injection process via the medical syringe was slow as this was done to avoid the formation of bubbles inside the measuring instrument.

5.3 Thermophysical measurements

5.3.1 Density (ρ), speed of sound (u) and viscosity (η) measurements

The Anton Paar DSA 5000 is known to have high precision and accuracy and this instrument is mainly designed to measure the density (ρ) and speed of sound (u) simultaneously. The Lovis 2000 M/ME is designed to measure viscosity (η). This viscometer used in this study is directly connected to Anton Paar DSA 5000. Thus, all the measurements of ρ, u and η were measured simultaneously using the

Anton Paar DSA 5000 combined with Lovis 2000 M/ME. Prior to each experimental run, the accuracy of both the Anton Paar DSA 5000 and Lovis 2000 M/ME were first verified using standard calibration solutions as obtained from the manufacturer. After the calibration, deionized water (liquid 1) was used to clean the instrument followed by acetone (liquid 2). The unit was then dried with dehumidified air at atmospheric pressure. The measurements were repeated four times for ρ, u and η. This was done to ensure the consistency of results.

5.3.1.a Density (ρ) measurements

The measurement of ρ for both the pure compounds and their binary mixtures were carried out using the digital vibrating tube densimeter (Anton Paar DSA 5000M) with an accuracy of T = ±0.02 K. The instrument is designed to measure both u and ρ simultaneously. The instrument capacity to measure ρ is within the range of (0 to 3) g. cm^{-3} and a temperature range of T = (0 - 70) °C with pressure variation from p = (0 to 0.3) MPa. The accuracy, repeatability, and reproducibility of the digital vibrating tube densimeter is (± 7 × 10^{-6}, ± 1 × 10^{-6} and ± 5 × 10^{-6}) g. cm^{-3} respectively (Anton Paar, 2017a).

The vibrating tube for measuring ρ consists of a U-shaped thin-walled glass tube that is held in a large body that separates it from external mechanical perturbations. This tube is filled with the liquid sample mixture and ρ can be derived starting from the equation for the period (τ) of a vibrator oscillating at its resonance frequency in the fundamental harmonic mode:

$$\tau = 2\pi \sqrt{\frac{m_{tube} + \rho \times V_{tube}}{C}} \quad 5.4$$

With m_{tube} and V_{tube}, the mass and volume of the tube, respectively, and C being a constant depending on the size and shape of the tube (proportional to Young's modulus). The ρ of the fluid can be described as:

$$\rho = A + B\tau^2 \quad 5.5$$

A and B represent constants for the instrument for every individual oscillator. Mathematical expressions for constants A and B are shown in equations 5.6 and 5.7, respectively.

$$A(T,p) = \frac{c(T,p)}{4\pi^2 V_{tube}(T,p)} \quad 5.6$$

$$B(T,p) = \frac{m_{tube}}{V_{tube}(T,p)} \quad 5.7$$

5.3.1.b Speed of sound (u) measurements

The measurement of u for both pure compounds and their binary mixtures were carried out using the speed of sound analyzer cell (Anton Paar DSA 5000M) with an accuracy of T = ± 0.02. The instrument capacity to measure u is within the range of (1000 to 2000) m. s^{-1}, a temperature ranges of T = (0 - 70)

°C with pressure variation from p = (0 to 0.3) MPa. The accuracy, repeatability, and reproducibility of the speed of sound analyzer are ($\pm 2 \times 10^{-1}$, $\pm 1 \times 10^{-1}$ and $\pm 5 \times 10^{-1}$) m. s^{-1}, respectively (Anton Paar, 2017a).

Speed of sound (u) measurements were conducted in a cell with piezoelectric transducers in opposing walls. This technique is known as the propagation time technique (De Azevedo et al., 2004). The sample passes through the piezoelectric ultrasound transmitter, which is made up of two transducers. The first transducer is responsible for the emission of sound waves that pass through the sample and the second transducer acts as a receiver for sound waves emitted by the first transducer (Fortin et al., 2013). Thus, u is determined by the ratio between the known distance of the transmitters and the receiver. This is achieved by the propagation time of the sound waves (De Azevedo et al., 2004). The temperature is kept constant in the same manner as the ρ measurement.

5.3.1.c Viscosity (η) measurements

The η measurements for this study were determined using Lovis 2000 M/ME with an accuracy of T = ± 0.02 K. The instrument capacity to measure viscosity is within the range of (0.3 - 10 000) mPa.s in temperature range of T = (5 - 100) °C with pressure variation from p = (0 to 0.3) MPa. The accuracy, reproducibility, and repeatability of the viscometer are ($\pm 2 \times 10^{-3}$, $\pm 1 \times 10^{-3}$ and $\pm 2 \times 10^{-3}$) mPa.s respectively (Anton Paar, 2017b).

The Lovis 2000 M/ME is a rolling-ball viscometer and the process follows the Hoeppler's falling ball principle. According to this principle, the viscosity (η) is determined by measuring the time it takes for the ball to pass through the liquid. The Hoeppler's principle defines a falling angle of 70°. A liquid bath thermostat is responsible for the temperature control. Results are given as kinematic, intrinsic or dynamic η. In order for the Lovis 2000 M/ME to measure η accurately, a capillary should be inserted inside the viscometer cell.

Three capillaries were available from the manufacturer which had the following diameters (1.6, 1.8 and 3.0) mm, and ball diameters of (1.5, 1.5 and 1.8) mm with η ranges respectively (0.3-10, 2.5-70 and 20-230) mPa.s. All three capillaries were tested and the capillary having 1.8 mm diameter gave valid results while the other two capillaries having a diameter of 1.5 mm yielded invalid results. Erroneous results are due to the ball getting stuck inside the capillary during viscosity measurements. Generally, ILs mixtures are very viscous, thus a capillary with a larger diameter is needed. A capillary having a diameter of 1.8 mm was used and the viscosity data were reproducible with each other implying that the ball was able to pass through the mixture during the measuring process. When the set temperature was reached, these capillaries were placed at angles of 70° and -70° to measure the time it takes for the

ball to move from one detector to another through the mixture. The falling and rolling ball η is calculated by:

$$\eta = k \times (\rho_{ball} - \rho_{mixture}) \times t \quad 5.8$$

k is the constant that depends upon the type of capillary used, the distance and the angle between two detectors. ρ_{ball} is the density of the falling ball and t is the time needed for the ball to move from the first detector to the second.

5.3.2 Refractive index (n_D) measurements

In the study, the n_D measurements were determined using an Atago 7000α with an accuracy of T = ±0.03 K. Prior to each experimental run, the instrument was firstly cleaned with deionized water and dried with acetone. The measurements were repeated four times for n_D measurements. This was done to ensure the consistency of the results. The instrument capacity to measure the refractive index is within the range of (1.32700 - 1.58000) in temperature range of T = (5 - 70) °C. The accuracy, repeatability, and reproducibility of the refractometer are ($\pm 4 \times 10^{-5}$, $\pm 2 \times 10^{-5}$ and $\pm 4 \times 10^{-5}$) respectively (ATAGO U.S.A., 2017).

The Atago 7000α refractometer is equipped with a microflow cell and an integrated Peltier thermostat ensuring accurate and automatic temperature control. The refractometer contains an optical lens and requires approximately 1 ml of each sample to cover the lens. A conical design ensures even distribution of the sample over the lens. A base plate covers the sample to avoid contact with the external environment or any dust particles from invalidating the measurement. The refractometer has an LCD display and the measurement time is 10 seconds for each sample. Refractive indices are recorded with a resolution of $\pm 1 \times 10^{-6}$.

5.4 Fourier transform infrared (FT-IR) spectroscopy

FT-IR spectra analysis of both the pure components and the binary mixture were performed at room temperature. The FT-IR analysis of the binary mixture (ILs + PEG200) were performed at equimolar sample (x_1 = 0.5). This was done for all the binary mixtures studied for this work. All the spectroscopic analyses for this study were carried using FT-IR spectrometer (Shimadzu IR Prestige –21). Prior to the measurements the instrument was cleaned with deionized water and dried with acetone. This was to remove impurities. FT-IR spectra is very sensitive, thus air scanning was done to remove any CO_2 absorption in the background. Samples were placed upon the pellet disc for the analysis. The scanning range of the pellet disks used were from (400 – 4000) cm^{-1} with 4.0 cm^{-1} resolution. The analyses were performed to investigate the presence of ion-dipole interactions/hydrogen bonding and the strength of molecular association in these mixtures. The IR data from the instrument was initially saved as an Ascii

file then as an Excel document by using the PC connected to the instrument. The data analysis was done using Excel software.

5.5 Uncertainties of the measured thermophysical quantities

5.5.1 Combined standard uncertainty for ρ, u, n_D and η

The description and equations for the uncertainties of the measured variables for this study are explained clearly in Appendix G.1. The combined uncertainty *u(x)* of the measured thermophysical properties is calculated from the uncertainty which arises from any of the two categories of uncertainty type A or type B. Type A refers to evaluation of data based on the statistical approach in which the mean is taken to represent the true value (Taylor and Kuyatt, 1994). To evaluate type A uncertainty both mean and standard deviation should be calculated. The uncertainty of the composition measurements of type A is expressed as:

$$\mathrm{u(x_i)} = \frac{\mathrm{s(x_i)}}{\sqrt{\mathrm{n}}} \tag{5.9}$$

Where x_i, n and $s(x_i)$ represent each thermophysical measured value, number of all the measured values and standard deviation (variance of measured values).

Type B uncertainty is evaluated by several methods and information related to the measurements. The uncertainty type B is evaluated by other means (not purely statistical) such as literature and information provided by the manufacturer (accuracy, repeatability, and reproducibility). The overall standard uncertainty is represented by:

$$\mathrm{u(x_i)} = \frac{\Delta \mathrm{a}}{\sqrt{3}} \tag{5.10}$$

where Δa is the half the width of the interval. The rectangular distribution model is the default model in the absence of any other information (Taylor and Kuyatt, 1994). Thus, the combined standard uncertainty for measured thermophysical properties is given by:

$$\mathrm{u(x)} = \pm\sqrt{\mathrm{u_a(x)^2 + u_{rep}(x)^2 + u_b(x)^2}} \tag{5.11}$$

Where *x* represents thermophysical properties such as ρ, η, u and $\mathrm{n_D}$. $u_{rep}(x)$ is the measurement repeatability values for thermophysical properties, u_a and u_b are the accuracy and reproducibility of the instrument respectively.

5.5.2 Combined standard uncertainty in the mixture composition

The accuracy of the overall standard uncertainty of the measured properties is dependent upon the standard uncertainty of the mole fractions of two components used in this study i.e, x_1 for IL and x_2 for PEG200. For a homogeneous mixture composition mole fraction (x_1) is constant throughout irrespective of the change in temperature and pressure. The equation that is used to compute the standard

uncertainty for mole fraction (x_1) is derived from the mass of the two components (m_1) and (m_2) representing ILs and PEG200 respectively, as mass is the only measured quantity that is used to determine mole fraction (Mohammed, 2016). The standard uncertainty $u(x_1)$ is given in terms of the relative standard uncertainties $u_r(m_1)$ and $u_r(m_2)$ of the two mass measurements as follows:

$$u(x_1) = (1 - x_1)[u_r^2(m_1) + u_r^2(m_2)]^{1/2} \qquad 5.12$$

The derivation of equation 5.12 is presented in Appendix G.2

CHAPTER SIX

RESULTS AND DISCUSSIONS

The results of the thermophysical property measurement of ρ, u, η and n_D and calculations of the excess properties are detailed in this chapter. The results are presented in five sections, with section one presenting the information such as the supplier details and purity of all chemicals used in this study. Section two presents the calibrations performed prior to the main measurements. Section three presents the results of the two test systems measured. Section four presents the thermophysical property measurements and excess thermodynamics associated plots for all the binary mixture of PEG200 + ILs, followed by the discussion of the intermolecular interactions between the molecules of PEG200 and ILs. Section four also presents the excess thermodynamic parameters fitted using the Redlich-Kister polynomial equation and calculated combined standard uncertainties for both selected measured thermophysical properties and mole fractions (x_1). Section five presents the FT-IR spectra of the studied binary mixtures and analysis of the intermolecular interactions.

6.1 Details of the chemicals used in this study

The solvent used in the present study, polyethylene glycol 200) (CAS No: 25 322-68-3) was purchased from Sigma-Aldrich. Imidazolium based ILs used in the present study, namely 1-butyl-3-methylimidazolium tetrafluoroborate $[\mathrm{BMIM}]^+[\mathrm{BF_4}]^-$ (CAS No: 174501-64-5), 1-butyl-3-methylimidazoilum hexafluorophosphate $[\mathrm{BMIM}]^+[\mathrm{PF_6}]^-$ (CAS No: 174501-64-5) and 1-ethyl-3-methylimidazolium tetrafluoroborate $[\mathrm{EMIM}]^+[\mathrm{BF_4}]^-$- (CAS No: 43314-16-3) were purchased from Ionic Liquids Technologies Inc. The details of pure components are presented in table 6.1.

The vacuum degassing method used in this study was effective, thus there was a significant change in water content before and after degassing. The water content present in the chemicals before and after degassing are presented in table 6.1.

Table 6.1: List of chemicals used and supplier details.

Component	Supplier	% Purity (wt)[a]	Initial water content (ppm)	Final water content (ppm)
PEG200	Sigma-Aldrich	99	550	350
$[\mathbf{BMIM}]^+[\mathbf{BF_4}]^-$	Ionic Liquids Technologies Inc	99	310	210
$[\mathbf{BMIM}]^+[\mathbf{PF_6}]^-$	Liquids Technologies Inc	99	360	220
$[\mathbf{EMIM}]^+[\mathbf{BF_4}]^-$	Ionic Liquids Technologies Inc	98	400	240

- [a] As stated by the supplier.
- Karl Fisher analysis was used to measure water content.
- Vacuum degassing method (using ultrasonic bath, rotary evaporator and vacuum pump at high pressure) was used to purify and dry the chemicals.

6.2 Combined standard uncertainty

6.2.1 Combined standard uncertainty for thermophysical properties

In any experimental work, it is important to maintain high precision and accuracy of results. This is to ensure the credibility of results. To ensure this, experimental procedure, cleaning and calibration of the instruments were performed and handled with high caution. The calibrations were done to ensure that the measuring instrument and reported values were the true and correct readings.

For the experimental values and results to be reliable, the numerical value of the measured values should be accompanied by the calculated uncertainty. In computing, the uncertainty of measurements, the repeatability uncertainty, the accuracy uncertainty and reproducibility uncertainty of the instrument were incorporated. Equation 6.1 was used to compute the uncertainty of the measured values.

$$\mathrm{u(x)} = \pm\sqrt{\mathrm{u_a(x)^2 + u_{rep}(x)^2 + u_b(x)^2}} \qquad 6.1$$

Where *x* represents the thermophysical property such as ρ, η, u and n_D. The repeatability of the measured value is represented by u_{rep}, with u_a and u_b representing the accuracy and reproducibility

of the instrument used, respectively. The formulation and methods for computing the uncertainty are presented and discussed in Appendix G.1.

6.2.2 Combined standard uncertainty for the binary mixture composition

The accuracy of the overall standard uncertainty of the measured properties is dependent upon the combined standard uncertainty of the mole fractions of two components used in this study, that is, x_1 for IL and x_2 for PEG200. Equation 6.2 was used to compute the standard uncertainty of the binary mixture composisition.

The standard uncertainty $u(x_1)$ is given in terms of the relative standard uncertainties $u_r(m_1)$ and $u_r(m_2)$ of the two mass readings as follows:

$$u(x_1) = (1 - x_1)[u_r^2(m_1) + u_r^2(m_2)]^{1/2} \quad 6.2$$

Thus, the methods and formula for calculating uncertainty of the mixture composition are explained in detail in Appendix G.2.

6.3 Calibrations

In any experimental work, calibration prior to main measurements is very important as it is used to maintain accuracy and reliability of results. In this work, calibrations were performed for density (ρ), viscosity (η), and refractive index (n_D). All the calibration data and associated graphs are presented in appendix A.

The calibration of the devices used in this study were explained in section 5.5. Table 6.2 presents the combined standard uncertainties for all the calibration data.

Table 6.2: Combined standard uncertainties of the calibration values**.**

$\boldsymbol{\rho/g.cm^{-3}}$	$\boldsymbol{\eta/mPa.s}$	$\boldsymbol{n_D}$
± 0.00002	$\pm$0.002	$\pm$0.00005

Temperature standard uncertainties for calibration of density (ρ), viscosity (η) and refractive index (n_D) is *u (T)* = ± 0.01 K, *u (T)* = ± 0.01 K and 0.05 K respectively.

6.4 Test systems

Two test systems were measured before experiments on the PEG200 + ILs systems could be performed. This was necessary to check the accuracy of the instrument used for ρ measurements. This also helped to understand the methods and techniques needed for this study. The test systems were selected based on the availability of data in the literature. The excess thermodynamic data for V^E, $\bar{V}_1^E$ and $\bar{V}_2^E$ and α_P^E for the test systems are presented in appendices B.1 – B.3 respectively. V^E and α_P^E were correlated by means of the Redlich-Kister polynomial model using a MATLAB@ program compiled and written for this study.

For test systems, (V^E and α_P^E) were correlated using the Redlich-Kister polynomial equation. Equation 6.3 represents a Redlich-Kister polynomial equation which was used for the correlation of test systems as discussed in details in section 4.6.2.

$$Z^E = x_i x_j \sum_{i=0}^{4} A_i \left(x_i - x_j\right)^i \qquad 6.3$$

Z^E, x_i, x_j and A_i represent excess thermodynamic properties, mole fraction of component i, mole fraction of component j and polynomial coefficient for the binary system, respectively.

6.4.1 Excess molar volume (V^E)

Density (ρ) measurements for $[BMIM]^+[Bf_4]^-(1)$ + methanol (2) were performed at 298.15 K and p = 0.1 MPa. The measured data compared well with literature (Vercher et al., 2015) as shown in Figure 6.1.

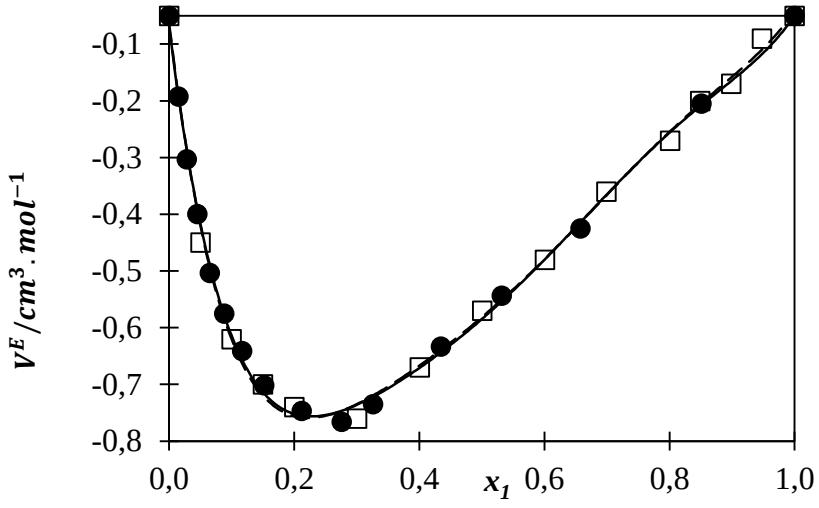

Figure 6.1: Plot of V^E versus liquid mole fraction for the system of $[BMIM]^+[BF_4]^-(1)$ + methanol (2) at T = 298.15 K and p = 0.1 MPa. V^E (●−), calculated values (This work); V^E(□ − −) literature values (Vercher et al., 2015). Solid and dotted lines represent the Redlich-Kister model.

Table 6.3: The Redlich Kister fitting parameters and standard deviation values for the literature system of $\boldsymbol{V^E}$, for the system $[\mathbf{BMIM}]^+[\mathbf{BF_4}]^-(\mathbf{1})$ + methanol (2) at T = 298.15 K.

Z^E	T/K	A_0	A_1	A_2	A_3	A_4	σ
V^E (lit)	298.15	-2.127	1.842	-1.258	2.158	-2.053	0.01925
V^E(cal)	298.15	-0.0021	0.0021	-0.0006	0.0012	-0.0036	1.74×10^{-5}

Lit: Vercher et al. (2015)

The V^E values for the binary test system are negative over the entire $[\mathrm{BMIM}]^+[\mathrm{BF_4}]^-$ composition range. There were calculated using the measured density (ρ) data of $[\mathrm{BMIM}]^+[\mathrm{BF_4}]^-(1)$ + methanol (2) system at 298.15 K and p = 0.1 MPa. The results calculated compared well to those reported in literature (Vercher et al., 2015). The solid and dotted line represent the Redlich Kister polynomial fit. A standard deviation value of the literature data is higher than that of calculated values (test system) which are 0.01925 and 0.0000174 respectively. The high standard deviation value of the literature data is mostly likely due to the inconsistent of data point at the liquid mole fraction of nicotine of 0.3. Thus, based on the comparison between the calculated values and the literature values, it can therefore be concluded that the method performed in measuring the test system was handled with care and caution as compared to the literature data. Thus, making the test system more accurate and reliable than the literature values.

6.4.2 Excess thermal expansion coefficient (α_P^E)

Figure 6.2 presents the test system of α_P^E, for the binary mixture of nicotine (1) + 1-butanol (2) at T = 303.15 K and p = 0.1 MPa.

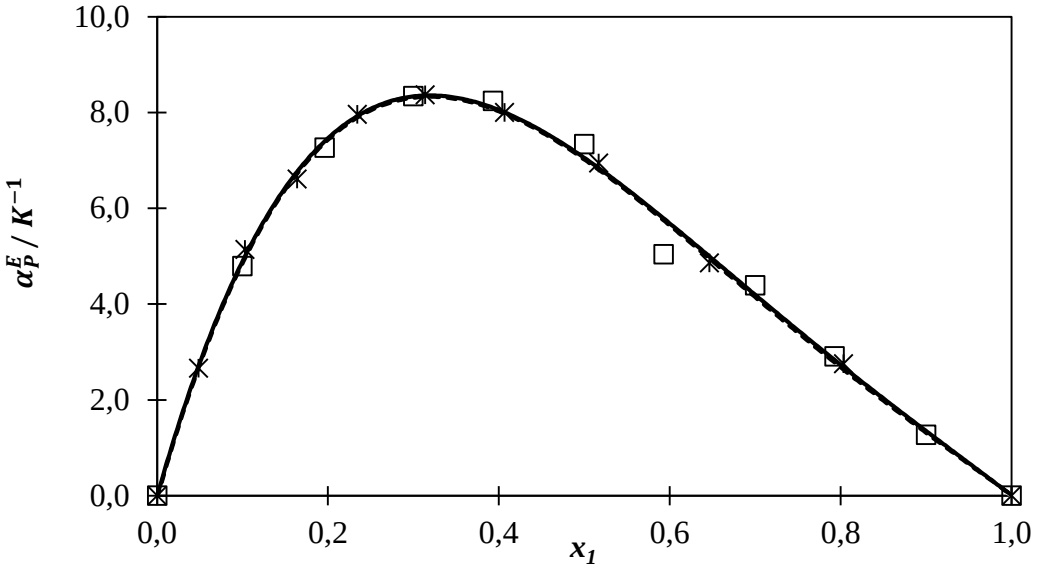

Figure 6.2: Thermal expansion coefficients,$\boldsymbol{\alpha_P^E}$, versus liquid mole fraction for the system of nicotine (1) + 1-butanol (2) at T = 303.15 K and p = 0.1 MPa. $\boldsymbol{\alpha_P^E}$ (∗), Calculated values (This work); $\boldsymbol{\alpha_P^E}$ (□)literature values (Soldatovic et al., 2016) Solid and dotted lines represent the Redlich-Kister model.

Table 6.4: The Redlich Kister fitting parameters and standard deviation values for the literature system of $\boldsymbol{\alpha_P^E}$, for nicotine (1) + 1-butanol (2) binary system at T = 303.15 K and p = 0.1 MPa.

Z^E	T/K	A_0	A_1	A_2	A_3	A_4	σ
α_P^E (lit)	303.15	27.89	-26.63	13.42	5.791	-6.862	0.32980
α_P^E (cal)	303.15	28.36	-26.29	5.961	6.031	10.61	0.09792

Lit: Soldatović et al. (2016)

The α_P^E values for the binary test systems are all positive over the entire composition range. Using the measured density (ρ) values of nicotine (1) + 1-butanol (2) system at 303.15 K and p = 0.1 MPa, the thermal expansion coefficients were determined. The calculated results compare well to those reported in literature (Soldatovic et al., 2016). The solid and dotted lines represent the Redlich Kister polynomial fit. The standard deviation value from literature is higher than that of calculated values (test system) which are 0.3298 and 0.09792 respectively. The high standard deviation of literature is mostly likely due to the inconsistent data point at the liquid mole fraction of nicotine between 0.5 and 0.6 mole

fraction. Thus, based on the comparison between the calculated data and the literature data, it can therefore be concluded that the test system method was handled with care and caution as compared to the literature. Thus, confirming the test system method to be more accurate and reliable than the literature data.

6.4.3 Excess partial molar volumes ($\bar{V}_1^E$ and $\bar{V}_2^E$)

Density (ρ) measurements for nicotine (1) + 1-butanol (2) were performed at 303.15 K and p = 0.1 MPa. Figure 6.3 presents the test system of ($\bar{V}_1^E$ and $\bar{V}_2^E$) as a function of volume fraction of nicotine. The ($\bar{V}_1^E$ and $\bar{V}_2^E$) values for the binary test systems are positive over the entire nicotine composition range. The measured data compared well with literature (Soldatovic et al., 2016). Since there were no reported excess properties for the $[BMIM]^+[BF_4]^-(1)$ + methanol (2) system, it was necessary to validate the calculation methods of the excess properties. Hence, the nicotine + 1-butanol system was measured and studied.

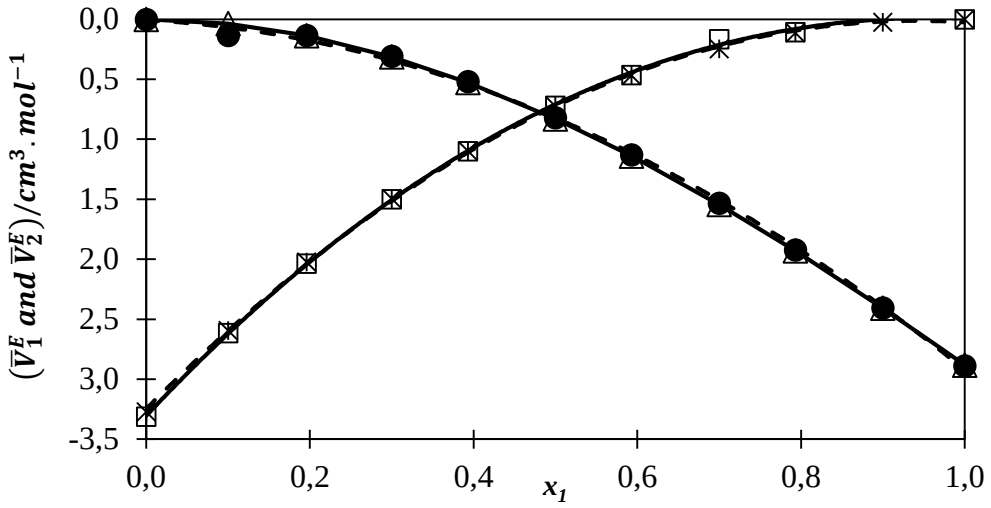

Figure 6.3: Plot of $\bar{V}_1^E$ **and** $\bar{V}_2^E$ versus liquid mole fraction for the system of nicotine (1) + 1-butanol (2) at T = 303.15 K and *p* = 0.1 MPa. $\bar{V}_1^E$ ($\square -$) and $\bar{V}_2^E$ ($\triangle -$) , calculated values (This work); ; $\bar{V}_1^E$ ($* - -$) and $\bar{V}_2^E$ ($\bullet - -$), literature values (Soldatovic et al., 2016). The solid and dotted line represents the trendline.

6.4.4. Calculated combined standard uncertainty for the test systems

Table 6.5 presents the calculated combined standard uncertainties for density (ρ) and speed of sound (u) measurements.

Table 6. 5: Combined standard uncertainties for the test systmes.

Binary mixtures	x_1	$\rho/g.cm^{-3}$	$u/m.s^{-1}$
$[\mathbf{BMIM}]^+[\mathbf{BF_4}]^-(\mathbf{1})$ + methanol and of nicotine (1) + 1-butanol (2)	$\pm$0.0004	± 0.00002	$\pm$0.02

Temperature standard uncertainties for Anton Paar: *u(T)* = ± 0.01.

6.5 Comparison of the experimental values and literature values for validation of reliable results

A comparison of the experimental values of density ($\boldsymbol{\rho}$), refractive index ($\boldsymbol{n_D}$) and molar isobaric heat capacity ($\boldsymbol{C_P}$) of pure liquids with the corresponding literature values at different temperatures and at *p* = 0.1 MPa are discussed. The purity of the chemicals were further assessed by comparison of the experimental $\boldsymbol{\rho}$, u and $\boldsymbol{n_D}$values with literature values as shown in the table 6.6.

Table 6.6: Comparison of the experimental values of $\boldsymbol{\rho}$, $\boldsymbol{n_D}$ and $\boldsymbol{C_P}$ of pure liquids with the corresponding literature values at different temperatures and at *p* = 0.1 MPa.

Component	*T/K*	$\rho^{lit,a}$	ρ^{exp}	$n_D^{lit,b}$	n_D^{exp}	$C_p^{lit,c}$	C_p^{cal}
		$(\mathbf{g.cm^{-3}})$				$(\mathbf{J.mol^{-1}.K^{-1}})$	
PEG200	293.15	1.1248[1]	1.1249	1.4600[1]	1.4607	413.5[4]	-
	303.15	1.1164[1]	1.1169	1.4575[3]	1.4575	417.2[4]	-
	313.15	1.1090[1]	1.1089	1.4532[1]	1.4538	422.0[4]	-
	323.15	1.1082[2]	1.1081	1.4497[1]	1.4504	426.8[4]	-
	333.15	1.0931[1]	1.0929	1.4463[1]	1.4470	-	432.9[d]
$[\mathbf{BMIM}]^+[\mathbf{BF_4}]^-$	**293.15**	**1.2044[5]**	**1.2046**	**1.4232[9]**	**1.4230**	**362.5[13]**	**-**
	303.15	**1.1974[5]**	**1.1974**	**1.4206[10]**	**1.4205**	**367.2[13]**	**-**
	313.15	**1.1908[6]**	**1.1903**	**1.4179[11]**	**1.4179**	**371.9[13]**	**-**
	323.15	**1.1830[7]**	**1.1833**	**1.4153[11]**	**1.4154**	**376.6[13]**	**-**
	333.15	**1.1763[8]**	**1.1763**	**1.4125[12]**	**1.4129**	**381.4[13]**	**-**

Table 6.7: cont.

Component	*T/K*	$\rho^{lit,a}$	ρ^{exp}	$n_D^{lit,b}$	n_D^{exp}	${C_p}^{lit,c}$	${C_p}^{cal}$
		$(\mathbf{g.cm^{-3}})$				$(\mathbf{J.mol^{-1}.K^{-1}})$	
$[\mathbf{BMIM}]^+[\mathbf{PF_6}]^-$	293.15	1.3712[14]	1.3710	1.4110[14]	1.4108	405.0[19]	-
	303.15	1.3624[15]	1.3624	1.4073[18]-	1.4074	410.3[19]	-
	313.15	1.3543[16]	1.3540	1.4050[18]	1.4058	416.0[19]	-
	323.15	1.3459[17]	1.3457	1.4030[18]	1.4032	421.9[19]	-
	333.15	1.3376[16]	1.3375	1.4000[14]	1.4005	430.2[20]	-
					-		
$[\mathbf{EMIM}]^+[\mathbf{BF_4}]^-$	293.15	1.2826[14]	1.2822	1.4140[14]	1.4142	306.5[13]	-
	303.15	1.2750[14]	1.2750	1.4111[20]	1.4119	309.8[13]	-
	313.15	1.2674[14]	1.2670	1.4090[14]	1.4092	313.2[13]	-
	323.15	1.2600[14]	1.2595	1.4060[21]	1.4066	316.8[13]	-
	333.15	1.2525[14]	1.2521	1.4034[21]	1.4039	320.6[13]	-

[a]Density, [b]refractive index literature values and [c]molar isobaric heat capacity literature values at T = (293.15 – 323.15) K with an interval of 10 K at p = 0.1 MPa. [d]Molar isobaric heat capacity value obtained using the least square method (Appendix C).

[1](Živković et al., 2013)
[2](Wu et al., 2013)
[3](Ali et al., 2013)
[4](Francesconi et al., 2007)
[5](Ciocirlan et al., 2011)
[6](Wu et al., 2015)
[7](Gardas et al., 2007)
[8](Montalban et al., 2015)
[9](Vakili-Nezhaad et al., 2012)
[10](Iglesias-Otero et al., 2007)
[11] (Ciocirlan et al., 2014)
[12](Tariq et al., 2009)
[13] (Waliszewski et al., 2005)
[14] (Bahadur et al., 2016)
[15] (Zafarani-Moattar and Shekaari, 2005)
[16](Huo et al., 2007)
[17](Krishna et al., 2017)
[18](Soriano et al., 2009)
[19](Troncoso et al., 2006)
[20](Ciocirlan et al., 2014)
[21](Carissimi et al., 2019)

6.6 Measurements of thermophysical properties for pure ILs

The thermophysical data measured are presented in tabular format in Appendix D. The associated graphs for ρ, η, u and n_D are presented in Figure 6.4.

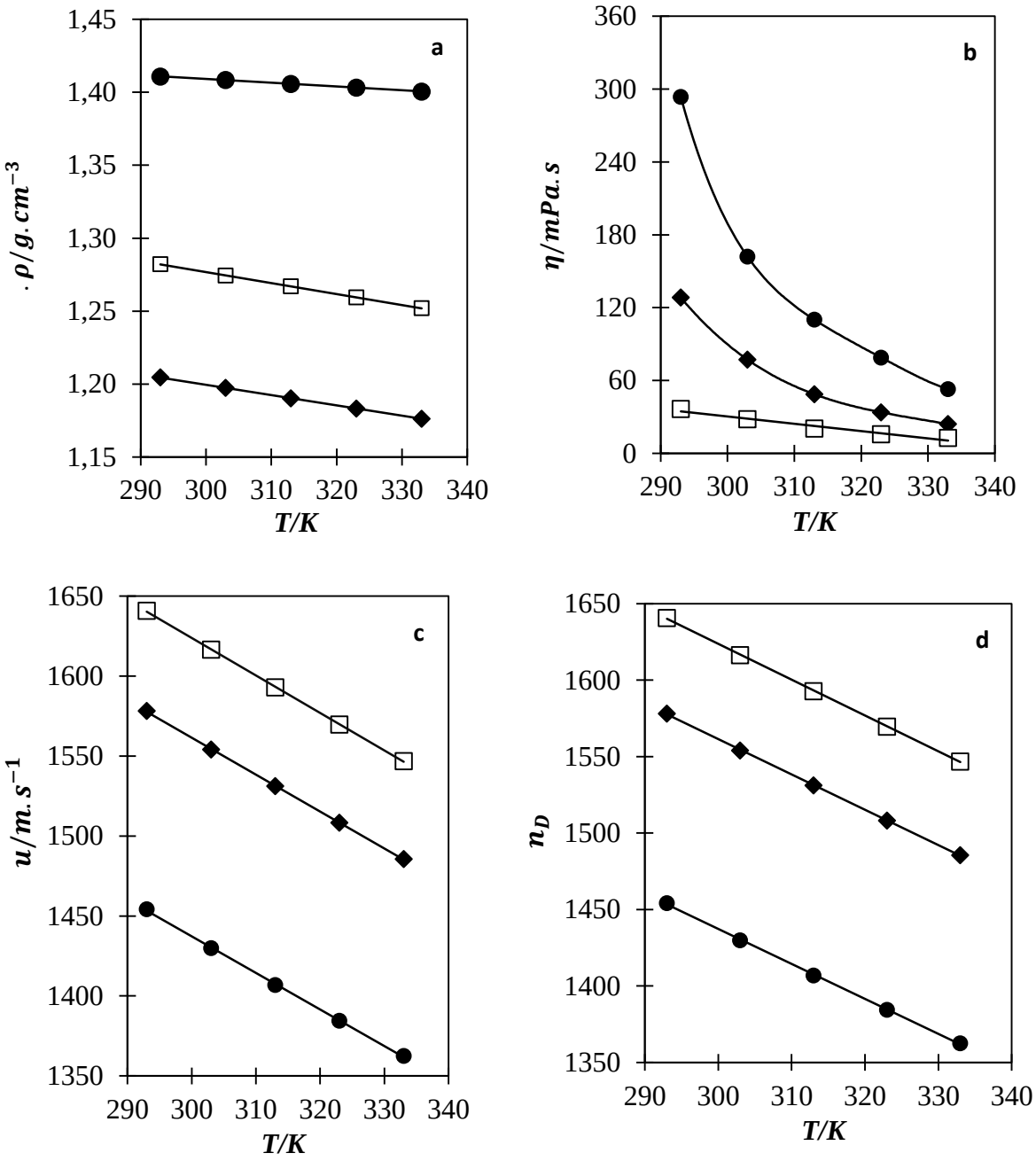

Figure 6.4: Plot of the thermophysical properties for pure components (♦) $[\mathbf{BMIM}]^+[\mathbf{BF_4}]^-$, (●)$[\mathbf{BMIM}]^+[\mathbf{PF_6}]^-$and (□) $[\mathbf{EMIM}]^+[\mathbf{BF_4}]^-$ at p = 0.1 MPa.

The ρ, η, u and $\boldsymbol{n_D}$ plots are represented by a, b, c, and d respectively. The solid lines for ρ, u and $\boldsymbol{n_D}$ were correlated using the least-squares model and the solid line for η was correlated using the Vogel–Fulcher–Tammann (VFT) model.

The thermophysical data such as ρ, u and n_D were correlated using a linear least square equation as shown in Equation 6.3 and discussed in section 3.7.1.

$$z = \sum_{i=0}^{2} B_i T^i \qquad 6.3$$

where z, B and T^i represent the thermophysical measured values, polynomial coefficient, and absolute temperature, respectively.

Table 6.7 presents the calculated least-square fitting parameters and standard deviation for measured values such as density (ρ), speed of sound (u) and refractive index (n_D).

Table 6.8: Least square fitting parameters for pure $\boldsymbol{\rho}$, u and $\boldsymbol{n_D}$ of ILs from (293.15 to 333.15) K at p = 0.1 MPa.

Z	*ILs*	B_0	B_1	B_2	σ
$\boldsymbol{\rho}$	$[BMIM]^+[BF_4]^-$	1.452	-0.0009667	4.140×10^{-7}	1.859×10^{-5}
	$[EMIM]^+[BF_4]^-$	1.529	-0.0009184	2.642×10^{-7}	2.731×10^{-5}
	$[BMIM]^+[PF_6]^-$	1.425	0.0001382	-6.317×10^{-7}	7.804×10^{-5}
$\boldsymbol{u}$	$[BMIM]^+[BF_4]^-$	2456	-3.597	0.002057	0.2594
	$[EMIM]^+[BF_4]^-$	2564	-3.858	0.002414	.08629
	$[BMIM]^+[PF_6]^-$	2513	-4.777	0.003971	0.2086
$\boldsymbol{n_D}$	$[BMIM]^+[BF_4]^-$	1.494	-0.0002304	-3.685×10^{-8}	4.057×10^{-5}
	$[EMIM]^+[BF_4]^-$	1.452	- 0.0000151	-3.866×10^{-7}	9.751×10^{-5}
	$[BMIM]^+[PF_6]^-$	1.447	-0.0000058	-4.001×10^{-7}	4.195×10^{-5}

The viscosity (η) data was correlated using a Vogel–Fulcher–Tammann (VFT) equation. Equation 6.4 represents the expression used.

$$\eta = Ae^{\frac{B}{T-T_g}} \qquad 6.4$$

Where A and B are fitting parameters, T_g is the 'ideal glass transition temperature' obtained from the literature. The VFT model used for correlation of η was discussed in section 3.7.1.

Table 6.8 presents the calculated VFT fitting parameters and standard deviation for measured values such as viscosity (η).

Table 6.9: Vogel–Fulcher–Tammann (VFT) fitting parameters for pure η of ILs from (293.15 to 333.15) K at p = 0.1 MPa.

ILs	*A*	*B*	T_g/K	σ
$[\mathbf{BMIM}]^+[\mathbf{BF_4}]^-$	0.7548	0.5709	176.24[a]	0.09
$[\mathbf{EMIM}]^+[\mathbf{BF_4}]^-$	0.03235	0.3387	187[b]	0.10
$[\mathbf{BMIM}]^+[\mathbf{PF_6}]^-$	0.5566	0.3616	190.6[c]	0.07

[a] (Vila et al., 2006); [b] (Hayamizu et al., 2004); [c] (Zhang et al., 2006).

6.6.1 Density (ρ)

The values of ρ for the three pure ILs as a function of temperature are shown in Figure 6.4.a. The ρ of all the 1-alkyl-3-methylimidazolium-based ILs decreases linearly with temperature. This linear behavior is common to ILs in general. The ρ of all three ILs follow the order $[\mathrm{BMIM}]^+[\mathrm{PF_6}]^- > [\mathrm{EMIM}]^+[\mathrm{BF_4}]^- > [\mathrm{BMIM}]^+[\mathrm{BF_4}]^-$.

For ILs such as $[\mathrm{BMIM}]^+ [\mathrm{BF_4}]^-$ and $[\mathrm{BMIM}]^+ [\mathrm{PF_6}]^-$, the density for these ILs follow the trend: $[\mathrm{PF_6}]^- > [\mathrm{BF_4}]^-$. For these pure ILs, the ρ values increases as the molecular weight of an anion increases. The ρ values for the IL with the $[\mathrm{PF_6}]^-$ anion is much greater than the ρ values for the IL with the $[\mathrm{BF_4}]^-$ anion. According to (Fröba et al., 2008) a large anion has much more ability to accommodate itself closer to the relatively large cation as compared to a small anion.

For ILs such as $[\mathrm{BMIM}]^+[\mathrm{BF_4}]^-$ and $[\mathrm{EMIM}]^+ [\mathrm{BF_4}]^-$, the densities of these ILs follow the trend: [EMIM] > [BMIM]. The ILs with shorter cation chain length are much denser than ILs with a longer cation chain length. The dispersive interactions of ILs are known to be affected by the alkyl chain length of imidazolium cation. From the order above, the dispersive interactions within the ILs increase with alkyl chain length, causing a *nanostructural organization* in polar and non-polar regions. The cation alkyl chain of an IL make up the non-polar region whereas the anion makes up both the non-polar and polar region (Kolbeck et al., 2010).

As observed in Figure 6.4.a the ρ values decrease with an increase in temperature, which is caused by the thermal agitation of the molecules. As the temperature increases, the kinetic energy of the molecules also increases causing the molecules to accelerate and to spread apart. This is termed thermal agitation, which causes the molecules to take up more volume hence a decrease in ρ. A change in ρ values of anions and cations clearly shows that the ρ of ILs is affected by the molecular weight and structural arrangement of ions.

6.6.2 Viscosity (η)

The viscosity (η) for the three pure ILs as a function of temperature are shown in Figure 6.4.b. The η of all the 1-alkyl-3-methylimidazolium-based ILs decreases exponentially with temperature in the range (293.15 to 333.15) K. All three ILs possess high values of η at the low temperature. The η of all three ILs follow the order: $[BMIM]^+[PF_6]^-$ > $[BMIM]^+[BF_4]^-$ > $[EMIM]^+[BF_4]^-$.

For ILs such as $[BMIM]^+$ $[BF_4]^-$ and $[BMIM]^+$ $[PF_6]^-$, the viscosity of the ILs follow the order: $[PF_6]^- > [BF_4]^-$. It is clear that the $[PF_6]^-$ anion possesses higher values of η and the $[BF_4]^-$ anion possesses lower values of η. Anions having greater molecular weight tend to be much more viscous than anions having small molecular weight. The explanation for the rise of η values for $[BMIM]^+[Bf_4]^-$ and $[BMIM]^+[Pf_6]^-$ is that the size of the anion is large enough to facilitate the interactions between the anion and cation (Kavitha et al., 2012a).

For ILs such as $[BMIM]^+[BF_4]^-$ and $[EMIM]^+$ $[BF_4]^-$, the viscosity of the ILs follows the order: $[BMIM]^+$ > $[EMIM]^+$. The $[EMIM]^+$ cation possesses lower values of η and the $[BMIM]^+$ cation possesses the highest values of η. For cations, the shorter the alkyl chain, the lower the η of the IL and vice versa for longer alkyl chains. According to (Bonhô, 1996), van der Waals (Debye forces) interactions increase with increasing cation alkyl chain length, thus leading to higher viscosities. The values of η decreases with an increase in temperature. This is due to an increase in the Brownian motion of the constituent molecules of the IL (Capelo et al., 2012). The viscosity trends of the ILs studied is in good agreement with the study done by (Navia et al., 2008) using the same ILs.

6.6.3 Speed of sound (u) and refractive index (n_D)

It is observed that u and n_D behave in a similar manner. The values of n_D and u for the three pure ILs as a function of temperature are shown in figure 6.6.c for u and figure 6.6.d for n_D. The u and n_D of all the 1-alkyl-3-methylimidazolium-based ILs decreases linearly with temperature in the range (293.15 to 333.15) K. This is the usual trend observed for pure ILs (Gusain et al., 2018). All three ILs possess high values of u and n_D at a low temperature. The values of u and n_D for all three ILs follow the order $[EMIM]^+[BF_4]^-$ > $[BMIM]^+[BF_4]^-$ > $[BMIM]^+[PF_6]^-$.

For the $[BMIM]^+$ $[BF_4]^-$ and $[BMIM]^+$ $[PF_6]^-$ ILs, the u and n_D follow the order:$[BF_4]^-$ > $[PF_6]^-$. It is observed that the $[BF_4]^-$ anion possesses higher values of u and n_D, while the $[PF_6]^-$ anion possesses lower values of n_D and u. The anion having more fluorine molecules and possessing greater molecular weight tend to have lower values of u and n_D than an anion of lower molecular weight and less fluorine molecules.

For ILs such as $[BMIM]^+[BF_4]^-$ and $[EMIM]^+ [BF_4]^-$, the speed of sound and refractive indices follow the order: $[EMIM]^+ > [BMIM]^+$. The IL with the$[BMIM]^+$ cation possess the lowest values of u and n_D, while the $[EMIM]^+$ cation possess the highest values of n_D and u. Cations behave in a similar manner to anions, i.e., the smaller the molecular weight the higher the u and n_D and the larger the molecular weight the lower the n_D and u. The shorter the alkyl chain, the higher the u and n_D of the IL and vice versa for longer alkyl chains. From the results the values of u and n_D decreases with an increase in temperature. The conclusion is that the size and structural arrangement of ions affect the overall thermophysical property.

6.7 Thermophysical properties for binary mixtures

The measured thermophysical data of the binary mixtures of $[BMIM]^+[BF_4]^-$, $[BMIM]^+[PF_6]^-$ and $[EMIM]^+[BF_4]^-$ with PEG200 are presented in appendices D.1– D.3 respectively. Only the graphical plots are presented in this section.

6.7.1 Density (ρ)

Figure 6.5 presents the variation of ρ as a function of mole fraction of ILs. The ρ values for all the studied binary systems are positive over the entire ILs composition range.

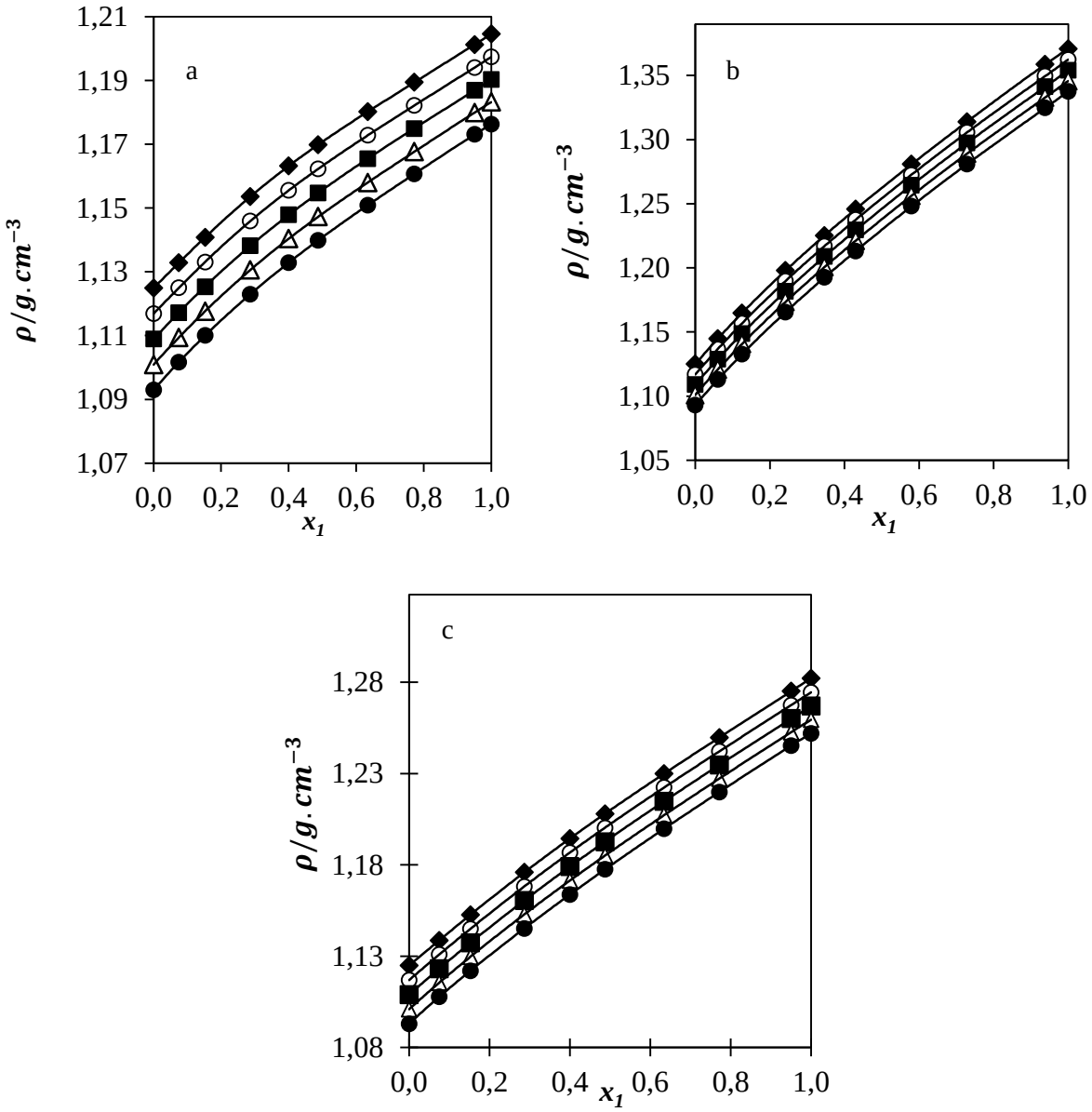

Figure 6.5: Plot of ρ versus the IL (x_1) for the IL + PEG systems. (a) $[\mathbf{BMIM}]^+[\mathbf{BF_4}]^-$, (b) $[\mathbf{BMIM}]^+[\mathbf{PF_6}]^-$ and (c) $[\mathbf{EMIM}]^+[\mathbf{BF_4}]^-$.Exp data from this work: (♦)293.15 K, (○)303.15 K, (■)313.15 K, (△)323.15 K, (●)333.15 K at p = 0.1 MPa. The solid line is the trendline.

Figure 6.5 shows the measured values of ρ for alkyl imidazolium-based ILs with PEG200 at T= (293.15, 303.15, 313.15, 323.15 and 333.15) K over the entire composition range plotted against the mole fraction of the IL. It is observed that the ρ values increase as the concentration of the ILs in the mixture increases. The ρ values decreases as the temperature increases for all imidazolium-based ILs systems under atmospheric pressure. Generally, ILs are completely miscible with medium to high dielectric liquids and immiscible with components that possess low dielectric constant (Domanska and Krolikowska, 2010).

PEG200 possesses a high dielectric constant of $\varepsilon = 20.26$ at 298.15 K (Bonhote et al., 1996), making ILs to be entirely miscible in PEG200. In a practical sense, this means that all the selected ILs are entirely miscible in PEG200 (Bahadur et al., 2016). The increase in ρ values for binary mixtures (ILs + PEG200) is possibly due to the increase in the solute-solvent interactions between the IL and PEG200 (Jamal et al., 2016). The ρ values of imidazolium-based ILs with PEG200 follow the order: $[\mathrm{BMIM}]^+[\mathrm{PF_6}]^- > [\mathrm{EMIM}]^+[\mathrm{BF_4}]^- > [\mathrm{BMIM}]^+[\mathrm{BF_4}]^-$.

Comparing the effect of the anion of $[\mathrm{BMIM}]^+[\mathrm{PF_6}]^-$ and $[\mathrm{BMIM}]^+[\mathrm{BF_4}]^-$, the ρ follow the order $[\mathrm{PF_6}]^- > [\mathrm{BF_4}]^-$. The binary mixture containing the $[\mathrm{BF_4}]^-$ anion possesses much lower ρ values as compared to the binary mixture with the $[\mathrm{Pf_6}]^-$ anion at the same condition. Due to lower ρ values of $[\mathrm{BF_4}]^-$ binary mixture, $[\mathrm{BMIM}]^+[\mathrm{BF_4}]^-$ + PEG200 possess weaker interaction than binary mixture composed of $[\mathrm{BMIM}]^+[\mathrm{PF_6}]^-$. Therefore, the highest ρ values for mixtures with $[\mathrm{PF_6}]^-$ is due to the increased size of the anion with the same cation.

Comparing the effect of the cation of $[\mathrm{BMIM}]^+[\mathrm{PF_6}]^-$ and $[\mathrm{BMIM}]^+[\mathrm{BF_4}]^-$, the ρ follow the order $[\mathrm{EMIM}]^+ > [\mathrm{BMIM}]^+$. This cation order indicates that the lower alkyl chain length is much denser than longer alkyl chain length. This is due to the ion-ion pair interactions decreasing with increasing size of cation alkyl chain length, resulting in a *nano-structural organization* in polar and non-polar regions. Polar group region possesses the cationic head groups and the anions while the non-polar regions are composed of alkyl chains. When the chain length of the cation is enhanced, the non-polar region increases and takes up more space, as a result the IL with of greater cation alkyl chain experiences lower ρ (Umapathi et al., 2014). From the order, the highest values of ρ are due to the decreased length of the cation with the same anion and vice versa. The results obtained give a clear indication that the ρ of the binary mixtures is affected by two factors: the size of the anion and the length of the alkyl group of cation.

6.7.2 Viscosity (η)

Figure 6.6 presents the variation of η as a function of mole fraction of ILs. The η values for all the studied binary systems are positive over the entire ILs composition range.

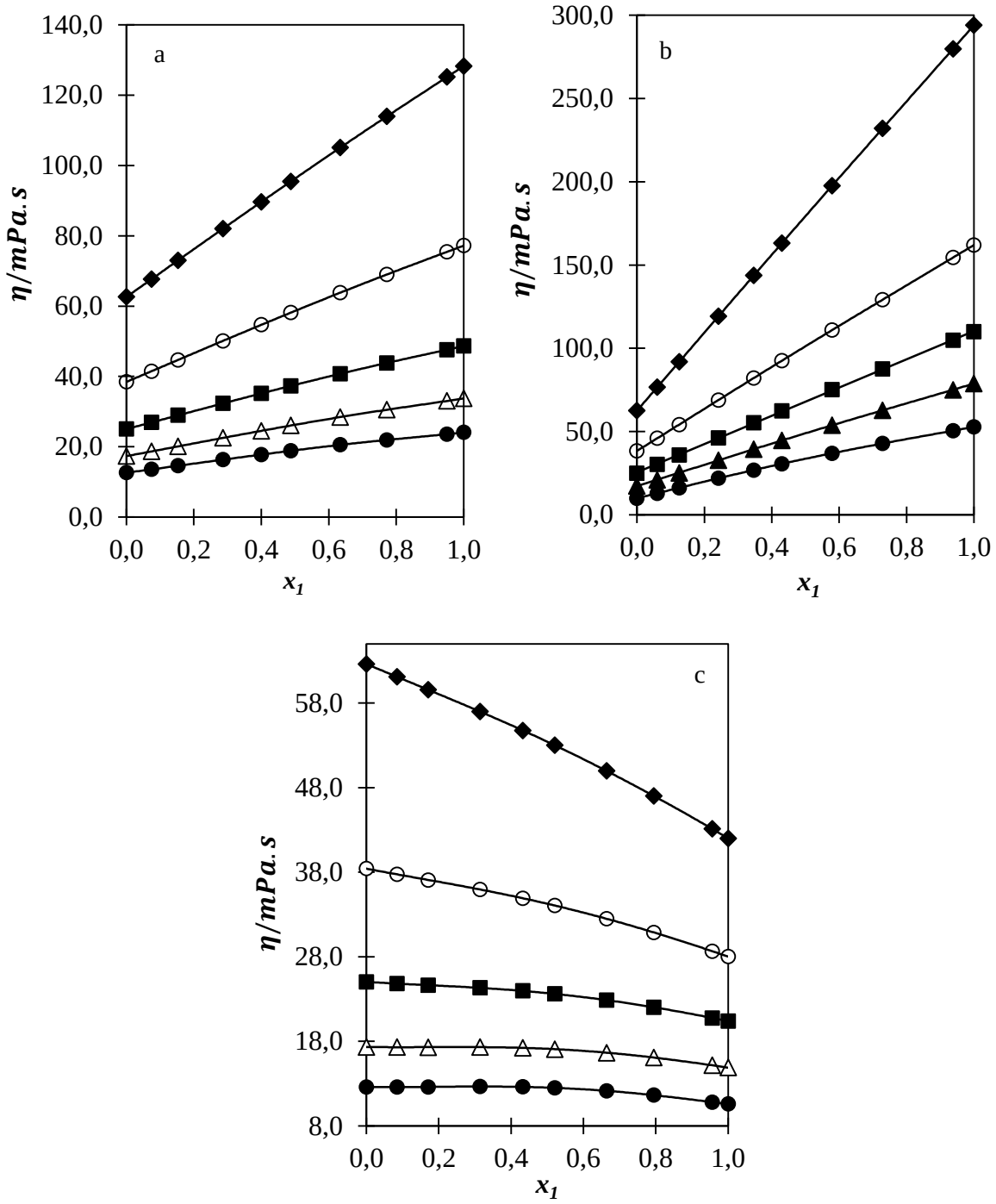

Figure 6.6: Plot of η versus the IL (x_1) for the IL + PEG200 systems. (a) $[\mathbf{BMIM}]^+[\mathbf{BF_4}]^-$, (b) $[\mathbf{BMIM}]^+[\mathbf{PF_6}]^-$ and (c) $[\mathbf{EMIM}]^+[\mathbf{BF_4}]^-$. Exp data from this work: (♦)293.15 K, (○)303.15 K, (■)313.15 K, (△)323.15 K, (●)333.15 K at p = 0.1 MPa. The solid line represents the trendline.

Figure 6.6 shows the measured values of η for alkyl imidazolium-based ILs with PEG200 at T = (293.15, 303.15, 313.15, 323.15 and 333.15) K over the entire composition range plotted against the mole fraction of the IL. The thermophysical properties of ILs are dependent upon the length of the alkyl chain and molecular structure of the anion. The η values of the alkyl imidazolium-based ILs with PEG200 follow the order: $[\mathrm{BMIM}]^+[\mathrm{PF_6}]^-$ > $[\mathrm{BMIM}]^+[\mathrm{BF_4}]^-$ > $[\mathrm{EMIM}]^+[\mathrm{BF_4}]^-$. It is also observed that the η values decreases as the temperature increases for all the binary systems at atmospheric pressure. This may be due to the increase in the Brownian motion of the constituents molecules of ILs (Capelo et al., 2012).

Binary mixtures of $[\mathrm{BMIM}]^+[\mathrm{BF_4}]^-$+ PEG200 and $[\mathrm{BMIM}]^+[\mathrm{PF_6}]^-$+ PEG200 behave similarly; the value of η increases with a mole fraction of ILs at all temperatures investigated. This behavior implies that there are strong molecular interactions between the ions of IL and PEG200 molecules. An increase is observed and this suggests that the coulombic interactions are strengthened as the concentration of ILs increases, leading to lower mobility of ions (Govinda et al., 2013).

The opposite behavior is observed for $[\mathrm{EMIM}]^+[\mathrm{BF_4}]^-$ with PEG200, in which the η values decreases as the concentration of the ILs increases. This behavior implies that intermolecular interactions between the ions of IL and molecules of PEG200 are weak, suggesting that van der Waals forces are dominant. These interactions lead to much lower η values as compared to the IL with the BMIM^+ cation.

The reason for the low η values is that, the size of the cation $[\mathrm{EMIM}]^+$ is not large enough to facilitate the interactions between anion IL and PEG200 (Govinda et al., 2013). Additionally this low value of η of IL $[\mathrm{EMIM}]^+$ is also due to charge delocalization in the anion, leading to any dissociation of bond formation (Kavitha et al., 2012b). Due to a large gap in size between $[\mathrm{EMIM}]^+$ and $[\mathrm{BF_4}]^-$, the interactions are not sufficient to enhance the η values. The results might imply that the greater motions of ions is responsible for the lower η values of $[\mathrm{EMIM}]^+[\mathrm{Bf_4}]^-$with PEG200.

For the two ILs composed of the same cation $[\mathrm{BMIM}]^+$ with the two different anions combinations $[\mathrm{BF_4}]^-$ and $[\mathrm{PF_6}]^-$, the η values follow the order: $[\mathrm{PF_6}]^-$ > $[\mathrm{BF_4}]^-$. It is clear that the η values of the binary mixture is affected by the size of the anion, indicating that the greater the molecular weight, the high the η values for the binary mixture. $[\mathrm{PF_6}]^-$ is able to facilitate strong intermolecular interactions with $[\mathrm{BMIM}]^+$ and PEG200 molecules much stronger than the $[\mathrm{BF_4}]^-$anion.

Comparing the effect of the cation of $[\mathrm{BMIM}]^+[\mathrm{BF_4}]^-$ and $[\mathrm{EMIM}]^+[\mathrm{BF_4}]^-$, the η values yielded opposite results. For the $[\mathrm{BMIM}]^+$ mixture, the coulombic interactions increases as the concentration of

ILs increases. For the $[EMIM]^+$ mixture, the van der Waals forces increases as the concentration of IL increases.

From the results, it is clear that the η values of the binary mixture is affected by the size and the molecular structure of both anion and cation.

6.7.3 Speed of sound (u)

Figure 6.7 presents the variation of u as a function of mole fraction of ILs. The u values for all the studied binary systems are positive over the entire ILs composition range.

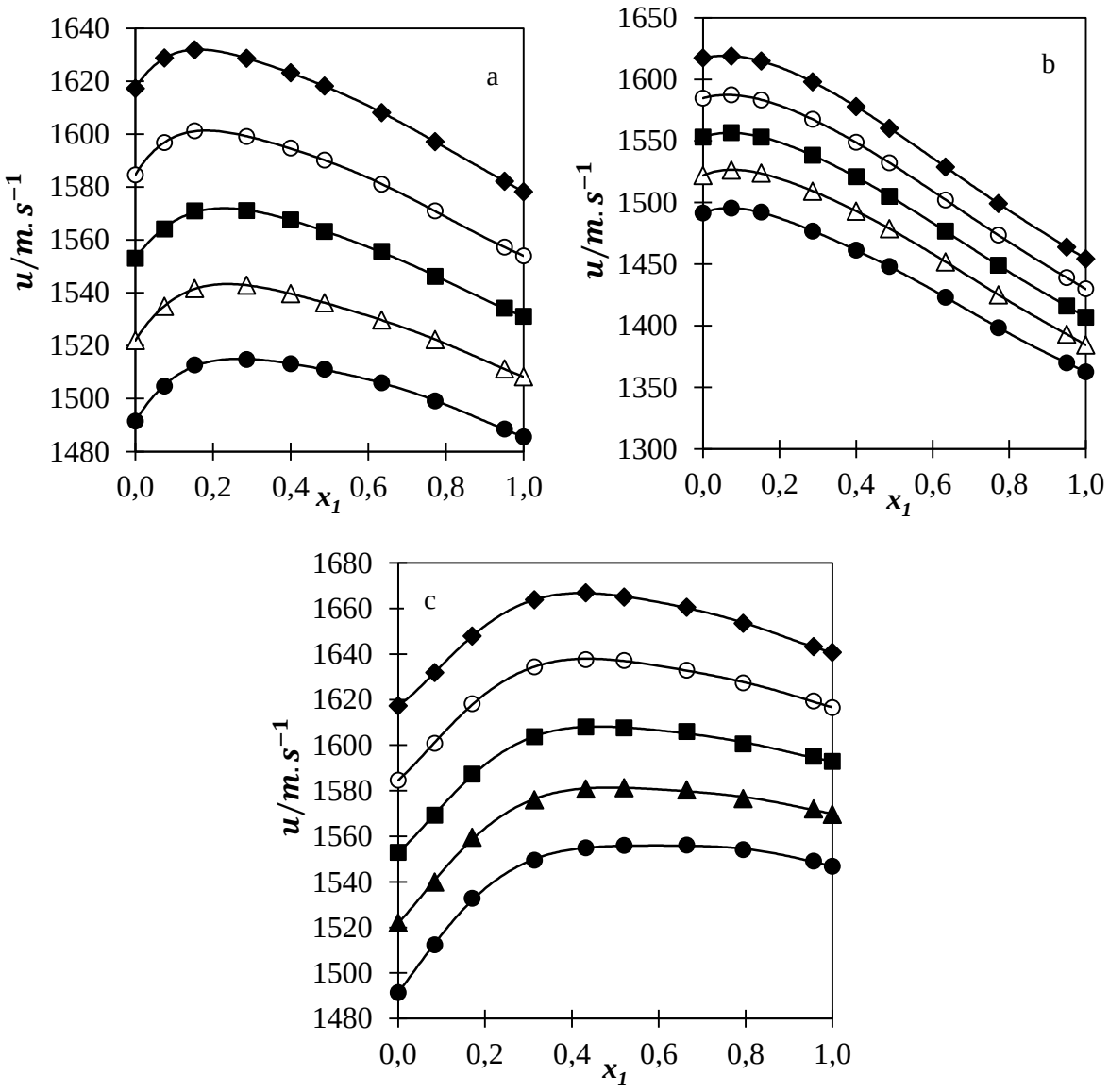

Figure 6.7: Plot of u versus the IL (x_1) for the IL + PEG systems. (a) $[\mathbf{BMIM}]^+[\mathbf{BF_4}]^-$, (b) $[\mathbf{BMIM}]^+[\mathbf{PF_6}]^-$ and (c) $[\mathbf{EMIM}]^+[\mathbf{BF_4}]^-$. Exp data from this work: (♦)293.15 K, (○)303.15 K, (■)313.15 K, (△)323.15 K, (●)333.15 K at p = 0.1 MPa. The solid line is the trendline.

Figure 6.7 shows the measured values of *u* for alkyl imidazolium-based ILs with PEG200 at T= (293.15, 303.15, 313.15, 323.15 and 333.15) K over the entire composition range plotted against the mole fraction of the IL. The values of *u* are one of the essential thermophysical properties, which can be used to understand the molecular interactions between liquids. The knowledge of the ultrasonic studies of imidazolium-based ILs and their mixtures are vital in several industrial processes (Govinda et al., 2016).

The thermophysical properties of ILs are dependent on the alkyl chain of the cation and nature of the structure of anion. The *u* values of the alkyl imidazolium-based ILs with PEG200 follow the order: $[EMIM]^+[BF_4]^-$ > $[BMIM]^+[BF_4]^-$ > $[BMIM]^+[PF_6]^-$and *u* values of all three selected binary mixture of ILs with PEG200 decreases with increasing temperature.

For binary mixtures of $[BMIM]^+[BF_4]^-$, $[BMIM]^+[PF_6]^-$ and $[EMIM]^+[BF_4]^-$ with PEG200, the values of *u* initially increase as the concentration of ILs increases up to $x_1 \approx 0.16$, $x_1 \approx 0.058$ and $x_1 \approx 0.38$ respectively. This increase implies that there are self-interactions occurring between the ions of ILs and the molecules of PEG200 (Kavitha et al., 2014).

Thereafter, the *u* of $[BMIM]^+[BF_4]^-$, $[BMIM]^+[PF_6]^-$ and $[EMIM]^+[BF_4]^-$ with PEG200 drastically decreases with increasing mole fraction of ILs at x_1 > 0.16, x_1 > 0.058 and x_1 > 0.38 respectively at all studied temperatures. This inconsistent behavior of *u* may be due to diminished ion-ion interactions between ILs and PEG200 as the concentration of ILs increases (Kumar et al., 2016).

Figure 6.7 presents the *u* for two ILs composed of the same $[BMIM]^+$ cation and two different anions $[BF_4]^-$and $[PF_6]^-$. Comparing the effect of the anion, the *u* follow the order $[BF_4]^-$ > $[PF_6]^-$. This order indicates that the interaction of smaller sized anion $[Bf_4]^-$ with PEG200 is stronger than the interactions of ILs having smaller molecular weight $[PF_6]^-$ (Govinda et al., 2015). The *u* values for the binary mixture with the $[PF_6]^-$ anion decreases much more rapidly than the binary mixture with the $[BF_4]^-$ anion. Thus, the $[PF_6]^-$ anion possesses much lower *u* values as compared to the system with the $[BF_4]^-$ anion. This is due to the diminished ion-ion interactions.

Figures 6.7.a and 6.7.c show the *u* values for the two binary mixtures of ILs composed of the same $[BF_4]^-$ anion and two different cations combinations $[BMIM]^+$and $[EMIM]^+$. The *u* results follow the order: $[EMIM]^+$ > $[BMIM]^+$. This order indicates that the self-interaction of the lower alkyl cation chain length cation is much stronger than the larger alkyl cation chain length (López and Illas, 1998). The order follows the same behavior for ion-ion molecular interactions. Therefore, the differences in the speed of sound results for the ILs with PEG200 are mainly due to the sizes of anion and varying alkyl chain length of the cation.

6.7.4 Refractive index (n_D)

Figure 6.8 presents the variation of n_D as a function of mole fraction of ILs.

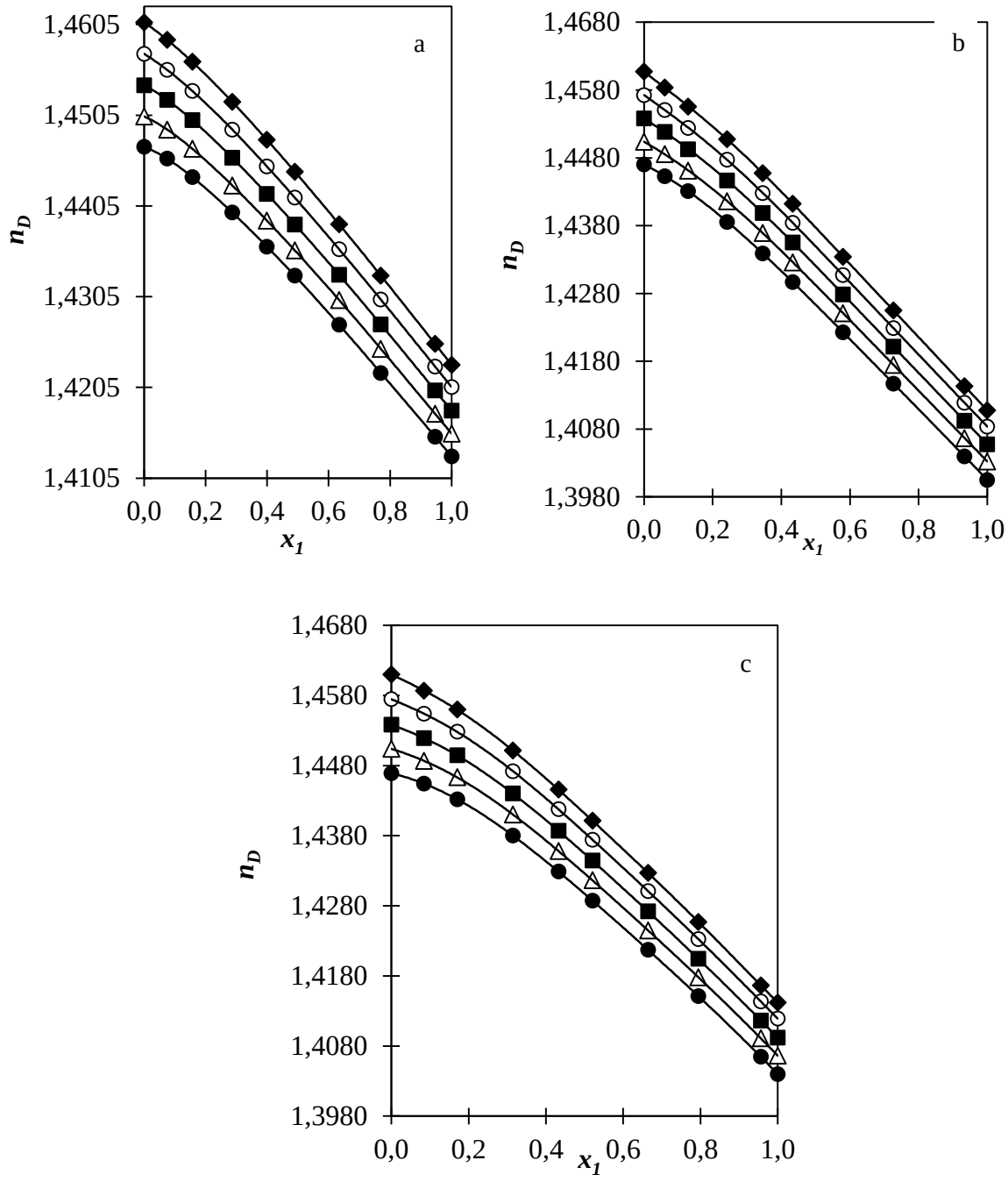

Figure 6.8: Plot of n_D versus the IL (x_1) for the IL + PEG systems. (a) $[\mathbf{BMIM}]^+[\mathbf{BF_4}]^-$, (b) $[\mathbf{BMIM}]^+[\mathbf{PF_6}]^-$ and (c) $[\mathbf{EMIM}]^+[\mathbf{BF_4}]^-$. Exp data from this work: (♦)293.15 K, (○)303.15 K, (■)313.15 K, (△)323.15 K, (●)333.15 K at p = 0.1 MPa. The solid line is the trendline.

Figure 6.8 shows the measured values of n_D for alkyl imidazolium-based ILs with PEG200 at T = (293.15, 303.15, 313.15, 323.15 and 333.15) K over the entire composition range plotted against the mole fraction of the IL. The n_D can be used as a measure of the electronic polarizability of a molecule and can also provide useful information about the interactions between molecules (Govinda et al., 2016). The values of n_D decreases with increasing concentration and temperature of ILs in the mixture. This trend is mainly due to weakened ion-ion pair interactions between the IL and molecules of PEG200 and self-interaction between the ions of ILs (Govinda et al., 2015). The n_D values of the alkyl imidazolium-based ILs with PEG200 follow the order: $[\mathrm{BMIM}]^+[\mathrm{BF_4}]^-$ > $[\mathrm{EMIM}]^+[\mathrm{BF_4}]^-$ > $[\mathrm{BMIM}]^+[\mathrm{PF_6}]^-$.

Comparing the effect of the anion of $[\mathrm{BMIM}]^+[\mathrm{PF_6}]^-$ and $[\mathrm{BMIM}]^+[\mathrm{BF_4}]^-$, the n_D follow the order $[\mathrm{BF_4}]^-$ > $[\mathrm{PF_6}]^-$. For ILs with the same cation that is $[\mathrm{BMIM}]^+$ with different anions of various molecular size, the n_D values decreases as the molecular weight of the anion increases. It is observed that the mixtures with $[\mathrm{PF_6}]^-$ possesses lower values of n_D while mixtures with $[\mathrm{BF_4}]^-$possess higher values of n_D. The ion-ion interactions of ILs with PEG200 decreases with increasing molecular size of the anion. This implies that the smaller anions have a greater ability to form stronger interactions with the molecules of PEG200 as compared to the ILs with larger anions.

Comparing the effect of the cation of $[\mathrm{BMIM}]^+[\mathrm{BF_4}]^-$ and $[\mathrm{EMIM}]^+[\mathrm{BF_4}]^-$, the n_D follow the order $[\mathrm{BMIM}]^+$ > $[\mathrm{EMIM}]^+$.This implies that the ion-ion interaction between ILs and PEG200 decreases with decreasing size of alkyl cation chain length. Thus, the cation size affects the overall values of n_D.

6.8 Excess thermodynamic properties of binary mixtures

The excess thermodynamic data of the binary mixtures of $[BMIM]^+[BF_4]^-$, $[BMIM]^+[PF_6]^-$ and $[EMIM]^+[BF_4]^-$ with PEG200 are presented in appendices E.1 – E.3, respectively. The graphical plots are presented in this section.

6.8.1 Excess molar volume (V^E)

Figure 6.9 presents the variation of V^E as a function of mole fraction of ILs. The V^E values for all the studied binary systems are negative over the entire ILs composition range.

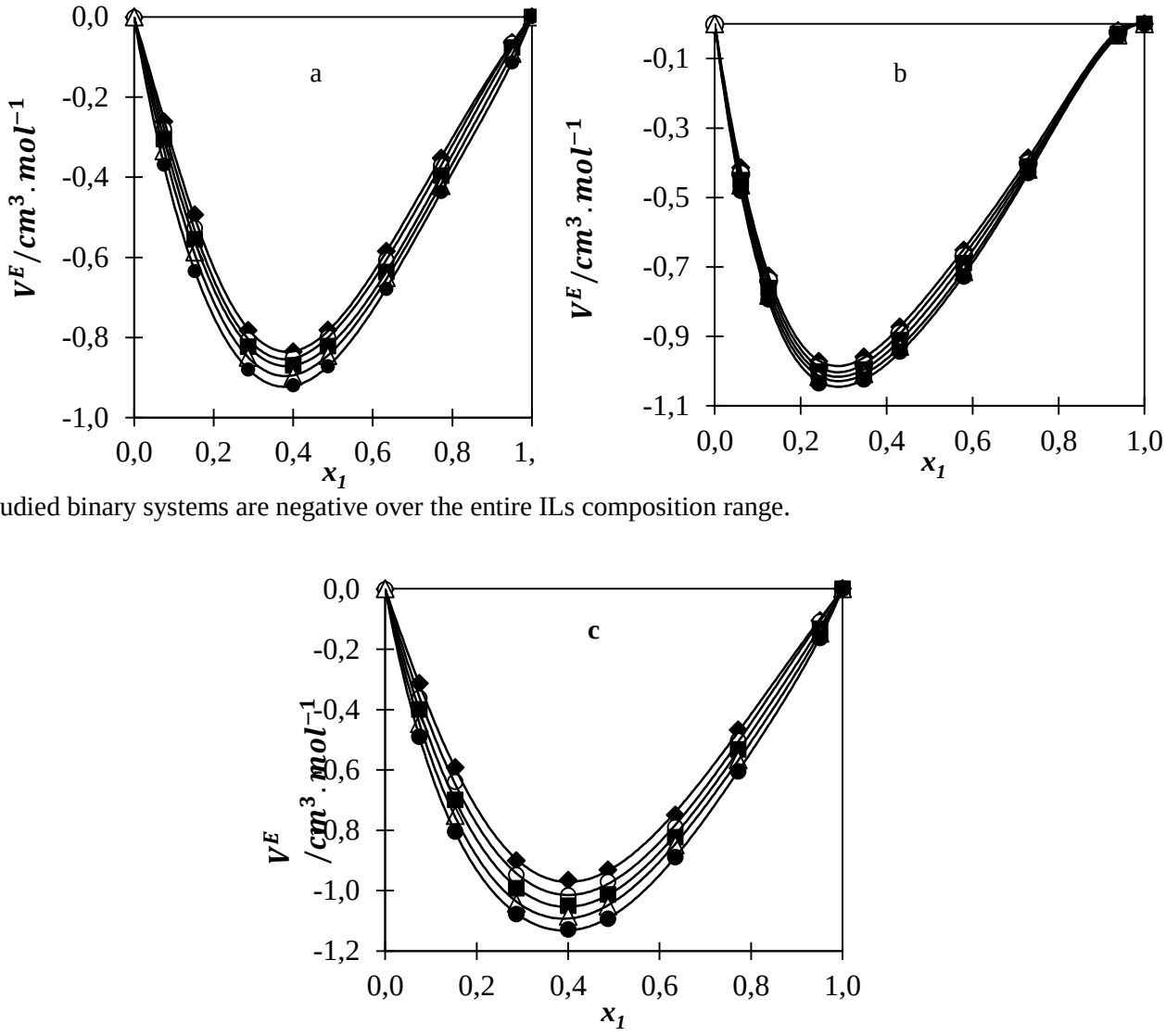

Figure 6.9: Plot of V^E versus the IL (x_1) for the IL + PEG systems. (a) $[BMIM]^+[BF_4]^-$, (b) $[BMIM]^+[PF_6]^-$ and (c) $[EMIM]^+[BF_4]^-$. Exp data from this work: (♦)293.15 K, (○)303.15 K, (■)313.15 K, (△)323.15 K, (●)333.15 K at p = 0.1 MPa. The solid lines represent the correlation obtained with the Redlich-Kister polynomial equation.

The V^E values for all the studied binary systems are negative throughout the entire ILs composition and temperature range. The negative values of V^E arise from the chemical contributions that compromise of specific interactions such as hydrogen bonding or ion-dipole interactions and charge transfer (donor-acceptor) complexes (Krishna et al., 2016).

The structural and geometric contribution is also known to contribute to the sign inversion of V^E for binary systems. Structural contributions are due to the geometrical fitting of the molecules of different molecular sizes into one another structure/s resulting in either negative or positive departure from ideal behaviour (Ali and Nain, 2002). The ILs exists as a 3-D network and is bulkier than the polymers, so it easily accommodates the smaller sized polymer molecules into the interstices upon mixing. This leads to volume contraction upon mixing (Zafarani-Moattar and Shekaari, 2006).

All the studied binary mixtures resulted in negative deviation from ideal behaviour. This implies that there exists strong hydrogen bonding between PEG200 and the alkyl imidazolium ILs. Hydrogen bonds between PEG200 and ILs are formed (i) by proton donation of the acidic protons (mainly C2-H) from the imidazolium cation to the hydroxyl -OH from PEG200 monomer unit, (ii) through proton acceptance, proton acceptance is due to hydrogen bond basicity of ILs anion accepting the protons from the PEG200 terminal –OH groups (Rodriguez et al., 2009). The negative V^E of the studied binary mixtures, is due to the large difference in molar volume between ILs and PEG200. This implies that it is possible for the small PEG200 molecules to fit into the interstices of ILs upon mixing at all investigated temperatures.

The results revealed that the values of V^E becomes more negative or decreases when the temperatures increase from 293.15 K to 333.15 K. The strength of the hydrogen bonding is dependent upon the temperature, since as the temperatures increases the kinetic energy of molecules increases, causing the ion-dipole interactions to intensify (Bahadur et al., 2016). Therefore, the ion-dipole interactions (ions from ILs and dipole of PEG200 molecules) become more significant due to the availability of greater number of PEG200 dipoles, leading to a decrease in mixture volume (Wang et al., 2005). Furthermore, the expansion in free volume due to an increase in temperature seems to be dominated by more favourable fitting of smaller PEG200 molecules into the larger voids created by the larger IL molecules at high temperatures, leading to a contraction in volume.

The magnitude of V^E varies from low concentrations to higher concentration of ILs. From the results, it is observed that the magnitude of the negative sign decreases as the mole fraction of ILs increases. It is clear that the more efficient parking is due to the different sizes and shapes of IL cation and anion combinations.

All the V^E curves are asymmetric and negative in the entire composition range, indicating negative deviation from ideal behaviour. The magnitude of the V^E of all the binary mixtures follow the order: $[EMIM]^+[BF_4]^-$ > $[BMIM]^+[PF_6]^-$ > $[BMIM]^+[BF_4]^-$, having maximum values at ($V^E \approx$ -1.1 $cm^3 \cdot mol^{-1}$ at $x_1 \approx 0.4$), ($V^E \approx$ -1.0 $cm^3 \cdot mol^{-1}$ at $x_1 \approx 0.25$) and ($V^E \approx$ -0.88 $cm^3 \cdot mol^{-1}$ at $x_1 \approx 0.4$), respectively.

Comparing the effect of the anion of $[BMIM]^+[PF_6]^-$ and $[BMIM]^+[BF_4]^-$, the magnitude of V^E follow the order $[PF_6]^-$ > $[BF_4]^-$. The net value of V^E for $[BMIM]^+[PF_6]^-$ mixture is greater than the V^E of $[BMIM]^+[BF_4]^-$. From the results, it is clear that the chemical structure of the anion in the imidazolium based ILs strongly affects the V^E. The mixture with the $[PF_6]^-$ anion possesses a greater negative value than the $[BF_4]^-$ anion.

The hydrogen bonding between the ILs and polymers mainly depend on the size and the basicity of the anion of the ILs (Kavitha et al., 2012c). The high V^E negative values in $[PF_6]^-$ based IL systems may be due to the basicity of the $[PF_6]^-$ anion being stronger than that of the $[BF_4]^-$ anion, which leads to the strength of the hydrogen bonds and ion-dipole interactions to increase rapidly.

Similarly, the ability of $[BMIM]^+[PF_6]^-$ interstices to accommodate PEG200 is much greater than that of $[BMIM]^+[BF_4]^-$, which makes the strength of the ion-dipole interactions between the molecules of $[BMIM]^+[PF_6]^-$+ PEG200 to be stronger than that of $[BMIM]^+[BF_4]^-$ + PEG200.

Comparing the effect of the cation of $[BMIM]^+[BF_4]^-$ and $[EMIM]^+[BF_4]^-$, magnitude of V^E follow the order $[EMIM]^+$ > $[BMIM]^+$. The results show that the values of V^E is much more negative for shorter alkyl cation chain length under the same experimental conditions. The more negative value of V^E serves as evidence of the ion-dipole interactions and enhanced packing effect with the IL possessing shorter alkyl cation chain. Clearly, moderate steric hindrance is expected from the alkyl chain of $[BMIM]^+$. Therefore, it is vital to note that the strength of ion interactions between the molecules of ILs and PEG200 is highly dependent on the nature of the cation.

6.8.2 Excess viscosity (η^E)

Figure 6.10 presents the variation of η^E as a function of mole fraction of ILs. The η^E values for all the studied binary systems are positive over the entire composition range.

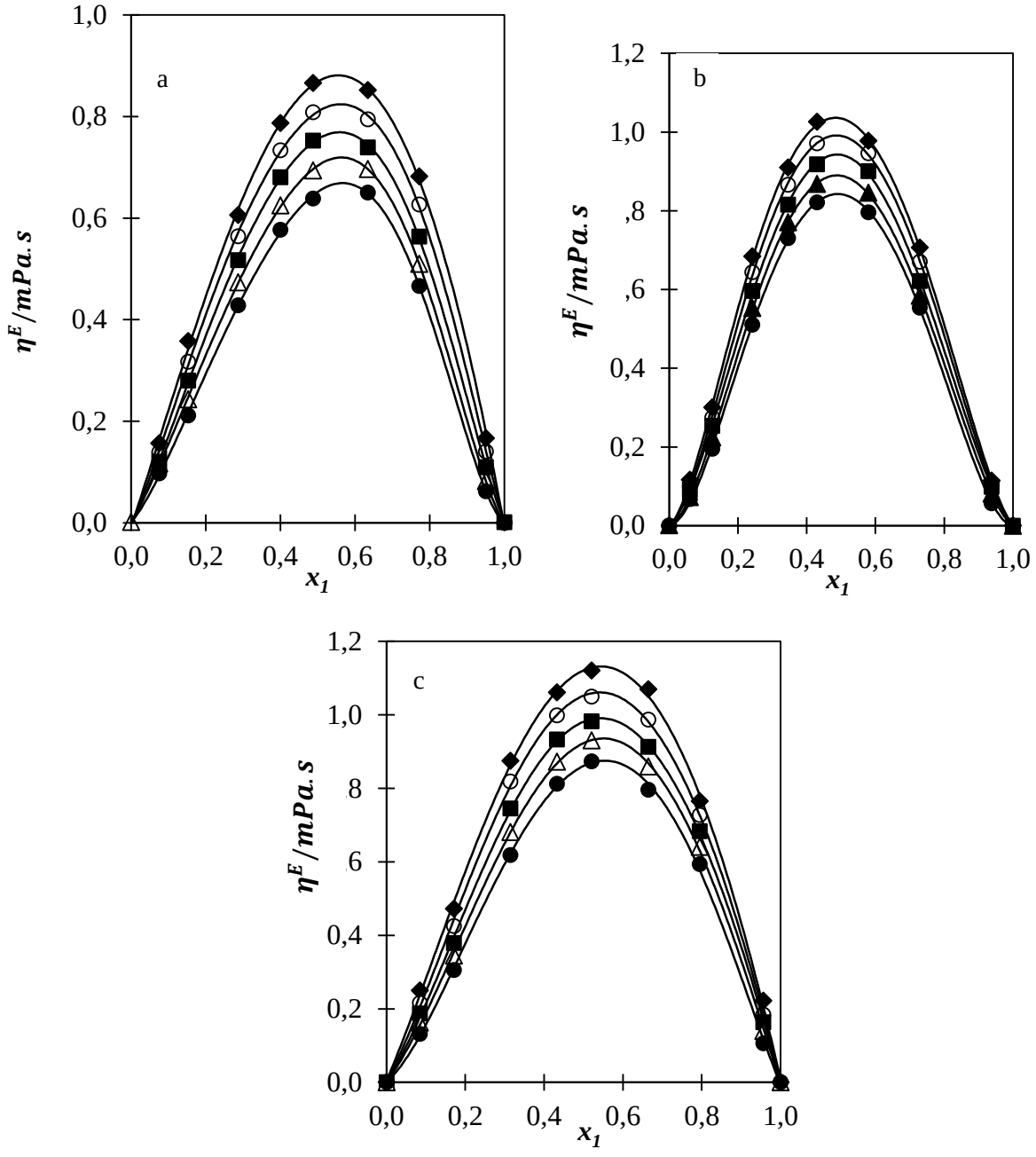

Figure 6.10: Plot of η^E versus the IL (x_1) for the IL + PEG systems. (a) $[\mathbf{BMIM}]^+[\mathbf{BF_4}]^-$, (b) $[\mathbf{BMIM}]^+[\mathbf{PF_6}]^-$ and (c) $[\mathbf{EMIM}]^+[\mathbf{BF_4}]^-$. Exp data from this work: (♦)293.15 K, (○)303.15 K, (■)313.15 K, (△)323.15 K, (●)333.15 K at p = 0.1 MPa. The solid lines represent the correlation obtained with the Redlich-Kister polynomial equation.

Figure 6.10 shows the η^E graphs of the binary mixtures of ILs and PEG200. The η^E trends are positive throughout the entire composition range. All the binary mixtures are asymmetric and the magnitude of η^E follows this order: $[EMIM]^+[BF_4]^-$ > $[BMIM]^+[PF_6]^-$ > $[BMIM]^+[BF_4]^-$. The maximum η^E point for $[EMIM]^+[BF_4]^-$, $[BMIM]^+[PF_6]^-$ and $[BMIM]^+[BF_4]^-$ binary systems are observed at ($\eta^E \approx 1.0$ mPa.s at $x_1 \approx 0.57$, 0.9 mPa.s at $x_1 \approx 0.5$ and 0.75 mPa.s at $x_1 \approx 0.58$), respectively.

The maximum and positive values of η^E suggest that the association formed between unlike molecules are relatively more than those in the pure components (Kavitha et al., 2012a). For a positive deviation of the binary mixture of ILs with PEG200, η^E values decrease with increasing temperature as shown in figure 6.10. As the temperature increases, the interactions become acutely reduced because of the dissociation of the IL ion pair (Kavitha et al., 2012b).

The positive values of η^E suggest that there is high capacity packing occurring between the ions of ILs and molecules of PEG200, which implies that there is volume contraction upon mixing. This high packing effect (contraction of volume) suggests that there are strong ion-dipole interaction forces also known as hydrogen bonding between the ions of ILs and molecules of PEG200.

Comparing the effect of the anion of $[BMIM]^+[PF_6]^-$ and $[BMIM]^+[BF_4]^-$, the magnitude of η^E follow the order $[PF_6]^-$ > $[BF_4]^-$.The η^E values decreases with decreasing molecular weight of anion, which suggests that the strength of the interaction decreases from $[PF_6]^-$ to $[BF_4]^-$ with PEG200.

Comparing the effect of the cation of $[BMIM]^+[BF_4]^-$ and $[EMIM]^+[BF_4]^-$, magnitude of η^E follow the order $[EMIM]^+$ > $[BMIM]^+$. The results explicitly elucidates that the η^E values decrease with an increase in cation alkyl chain length. Thus, the coulombic interactions between the molecules of PEG200 and ions of ILs decreases as the cation alkyl chain length increases. It is clear from the above discussion that the nature and structure of both the cation and anion greatly influences the η^E values.

The η^E values are found to be opposite to the sign of V^E for all three binary mixtures, which is in agreement with the view proposed by (Roy et al., 2010). A relationship between the sign of η^E and V^E has been observed for a number of binary systems (Roy et al., 2011), i.e., η^E is positive when V^E is negative and vice-versa.

6.8.3 Excess isentropic compressibility (K_S^E)

Figure 6.11 present the variation of K_S^E as a function of mole fraction of ILs. The K_S^E values for all the studied binary systems are negative over the entire ILs composition range. The C_P values are needed to calculate K_S^E. Table 6.8 presents C_P values for all three ILs and PEG200 at different temperature. The C_P value of PEG200 at 333.15 K was not available in the literature, thus it was calculated. The estimated fitting parameters for C_P which are C_0, C_1 and C_3 were calculated using linear equation 4334. From the linear equation, the C_p value for 333.15 K was estimated and calculated using an extrapolation method. The estimated and calculated C_P value at 333.15 K for PEG200 is 432.9 $\mathrm{J.mol^{-1}.K^{-1}}$. These details can be found in Appendix C.

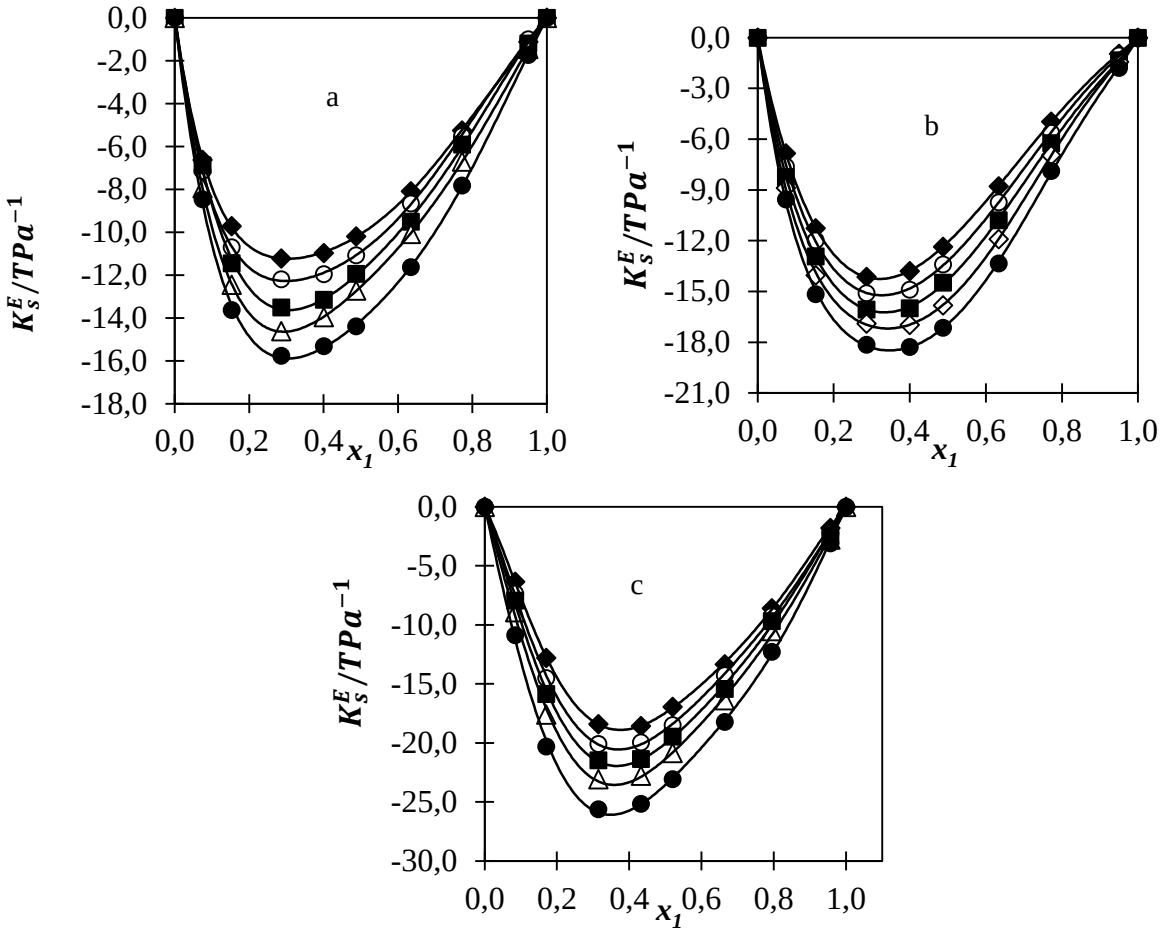

Figure 6.11: Plot of K_S^E versus the IL (x_1) for the IL + PEG systems. (a) $[\mathbf{BMIM}]^+[\mathbf{BF_4}]^-$, (b) $[\mathbf{BMIM}]^+[\mathbf{PF_6}]^-$ and (c) $[\mathbf{EMIM}]^+[\mathbf{BF_4}]^-$. Exp data from this work: (♦)293.15 K, (○)303.15 K, (■)313.15 K, (△)323.15 K, (●)333.15 K at p = 0.1 MPa. The solid lines represent the correlation obtained with the Redlich-Kister polynomial equation.

In figure 6.11, the negative K_S^E values indicate strong ion-dipole interactions between the molecules of PEG200 and ions of ILs. Mixing of ILs with PEG200 induces the dissociation of PEG200, thus during the mixing process, the molecules of PEG200 will solvate in the interstitial accommodation of ILs. This will lead to a decrease in the intermolecular free space and formation of closer molecular aggregates. A strong intermolecular interaction through ion-dipole interactions, charge transfer, interstitial accommodation, and orientational ordering leads to a more compact, rigid structure which contributes to the negative deviation of K_S^E (Sharrna et al., 2010).

The fitting curves for binary systems of ($[BMIM]^+, [BMIM]^+[PF_6]^-$ or $[EMIM]^+[BF_4]^-$ + PEG200) are all symmetric and present the minimum values in the ILs mole fraction at ($K_S^E \approx$ -13 TPa^{-1} at $x_1 \approx 0.30$, $K_S^E \approx$ -15 TPa^{-1} at $x_1 \approx 0.34$ and $K_S^E \approx$ -21 TPa^{-1} at $x_1 \approx 0.38$), respectively.

The negative values of K_S^E for ILs with PEG200 imply that the solvent molecules around the solute are less compressible than the solvent moleculesF in the bulk solutions. As PEG200 is added to ILs, there is a decrease depicted in the compressibility graph at all temperature ranges. The decrease in compressibility is due to volume contraction upon the mixtures. Therefore, at high temperatures the mixture becomes more rigid (with less compressibility ($K_S^E < 0$)) thus, there is volume contraction (molecules are more packed ($V^E < 0$)) (Alavianmehr et al., 2017). Additionally, contraction of volume implies that there are strong ion-dipole interactions in the mixture. The strong interactions are due to the solvation of the ions in the solution. The magnitude of K_S^E values follow the order: $[EMIM]^+[BF_4]^-$ > $[BMIM]^+[PF_6]^-$ > $[BMIM]^+[BF_4]^-$.

Comparing the effect of the anion of $[BMIM]^+[PF_6]^-$ and $[BMIM]^+[BF_4]^-$, the magnitude of K_S^E follow the order $[PF_6]^-$ > $[BF_4]^-$. This means that the mixture composed of large size of anion $[Pf_6]^-$ is much more rigid (less compressibility) and compact than with a mixture with anion composed of smaller molecular weight $[BF_4]^-$ anion. Rigidity of a mixture means there is a volume contraction upon the mixture, which is attributed to strong ion-dipole interactions. Therefore, the solvation of ions in the solution is much greater for ILs with the $[PF_6]^-$ anion than $[BF_4]^-$ anion.

Comparing the effect of the cation of $[BMIM]^+[BF_4]^-$ and $[EMIM]^+[BF_4]^-$, magnitude of K_S^E follow the order $[EMIM]^+$ > $[BMIM]^+$. Results depicted that the K_S^E values for binary system with the $[EMIM]^+$ cation are more negative than that of $[BMIM]^+$. The more negative K_S^E values for mixtures with $[EMIM]^+$ serves as further evidence that the mixture is more rigid (less compressibility and more volume contraction)

for the smaller ethyl cation chain length ($[EMIM]^+$) of IL as compared to a longer butyl cation chain length ($[BMIM]^+$) of IL mixture.

The rigidity of a mixture means there is a volume contraction upon the mixture, which is attributed to strong ion-dipole interactions. Therefore, the solvation of ions in the solution is much greater for $[EMIM]^+$ cation as compared to $[BMIM]^+$ cation. Thus, it clear that the strength of the intermolecular interactions between ions of ILs and molecules of PEG200 depends upon the chain length of the alkyl group and the size of the anion of ILs.

Figure 6.11 depicts negative values of K_S^E over the entire composition range at all temperatures. From the results, the effect of temperature is more obvious for K_S^E as compared to V^E, and this behavior is observed for all the binary systems. As a consequence of increasing temperature, the K_S^E values become more negative. The K_S^E values decrease much more with increasing temperature, with the temperature increase due to the kinetic energy of the molecules increasing resulting in free PEG200 molecules being available in the mixture which causes a hydrogen bonding. The formation of hydrogen bonding is a result of individual breaking of hydrogen bonds between individual unknown molecules. This behavior suggests that there are strong interactions between free PEG200 dipolar molecules and the ions of ILs. The interactions indicate complete solvation of free PEG200 molecules. Also, there is structural fitting taking place between the molecules of PEG200 and free space created by ILs. This behavior causes volume contraction (Rao et al., 2004).

6.8.4 Excess Refractive index (n_D^E)

Figure 6.12 presents the variation of n_D^E as a function of mole fraction of ILs. The n_D^E values for all the studied binary systems are positive over the entire ILs composition range.

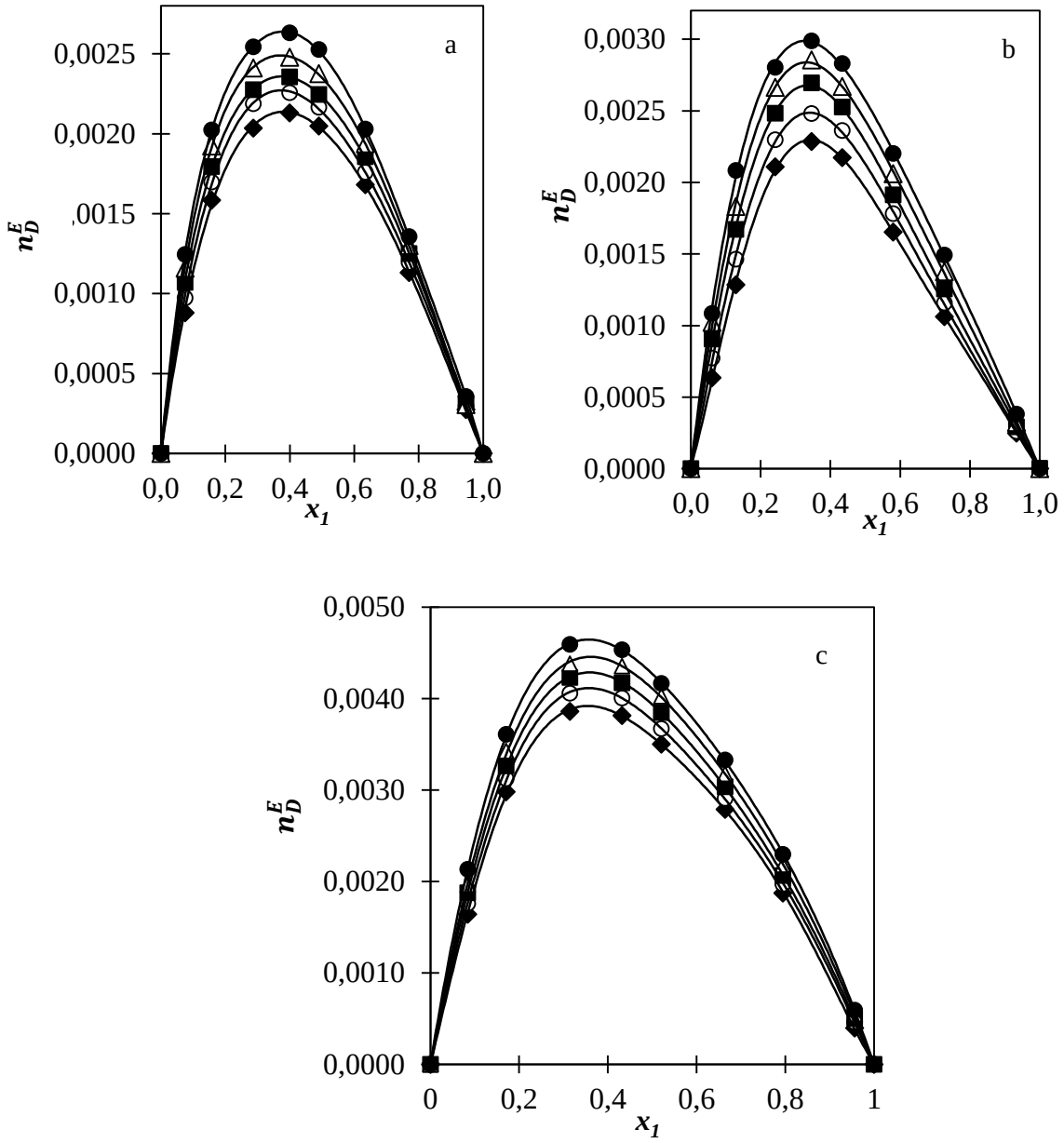

Figure 6.12: Plot of n_D^E versus the IL (x_1) for the IL + PEG systems. (a) $[\mathbf{BMIM}]^+[\mathbf{BF_4}]^-$, (b) $[\mathbf{BMIM}]^+[\mathbf{PF_6}]^-$ and (c) $[\mathbf{EMIM}]^+[\mathbf{BF_4}]^-$. Exp data from this work: (♦)293.15 K, (○)303.15 K, (■)313.15 K, (△)323.15 K, (●)333.15 K at p = 0.1 MPa. The solid lines represent the correlation obtained with the Redlich-Kister polynomial equation.

All the n_D^E curves are asymmetric and follow the order: $[EMIM]^+[BF_4]^-$ > $[BMIM]^+[PF_6]^-$ > $[BMIM]^+[BF_4]^-$, having the maximum values at ($n_D^E \approx 0.004$ at $x_1 \approx 0.35$, $n_D^E \approx 0.0025$ at $x_1 \approx 0.32$ and $n_D^E \approx 0.0022$ at $x_1 \approx 0.35$), respectively.

The positive value of n_D^E for all the studied ILs binary systems increases as the temperature increases, indicating that the light propagates at lower velocity when temperature increases (Mrad et al., 2016). Positive n_D^E values are attributed to the ion-dipole interactions/ hydrogen bonding between the molecules of PEG200 and ions of ILs (Mrad et al., 2016). Positive n_D^E values mean that there is contraction in volume of the binary mixtures, and this contraction will cause a decrease in intermolecular distance which will results in ions of ILs and dipole molecules of PEG200 coming close together, causing a strong ion-dipole interactions. This, therefore, forces the refractive index to increase. The decrease in intermolecular distance is due to enhancement of London dispersion forces which leads to strong intermolecular interactions such as hydrogen bonding/ion-dipole interactions (Reis et al., 2010). It is worth mentioning that the values of n_D^E is always opposite to the values of V^E (Akbar and Murugesan, 2012) .

Positive deviations of n_D^E always correspond to negative deviations of V^E, with the minimum and maximum of both values existing at the corresponding mole fraction of IL (Brocos et al., 2003). The positive deviation of n_D^E is mainly due to the fact that there are less free volume available. As a result, photons are likely to interact with molecules causing contraction of volume upon the mixture (Iglesias-Otero et al., 2008).

Comparing the effect of the anion of $[BMIM]^+[PF_6]^-$ and $[BMIM]^+[BF_4]^-$, the magnitude of n_D^E follows the order $[PF_6]^-$ > $[BF_4]^-$.This implies that, the large size of anion $[PF_6]^-$ may form strong intermolecular interactions with PEG200 molecules as compared to the smaller sized anion $[BF_4]^-$. Therefore, the volume contraction upon mixing is much greater for $[PF_6]^-$ anion than $[BF_4]^-$ anion.

Comparing the effect of the cation of $[BMIM]^+[BF_4]^-$ and $[EMIM]^+[BF_4]^-$, magnitude of n_D^E follows the order $[EMIM]^+$ > $[BMIM]^+$. The more positive n_D^E values for the ethyl cation of IL serves as further evidence that the interactions between small sizes of ethyl cation IL with PEG200 are stronger than in the higher butyl chain IL.

These results show that the strength of the intermolecular interactions between ions of ILs and molecules of PEG200 depends on the chain length of the alkyl group and the size of the anion of ILs

6.8.5 Excess thermal expansion coefficients (α_P^E)

Figure 6.13 presents the variation of α_P^E as a function of mole fraction of ILs. The α_P^E values for all the studied binary systems are negative over the entire ILs composition range.

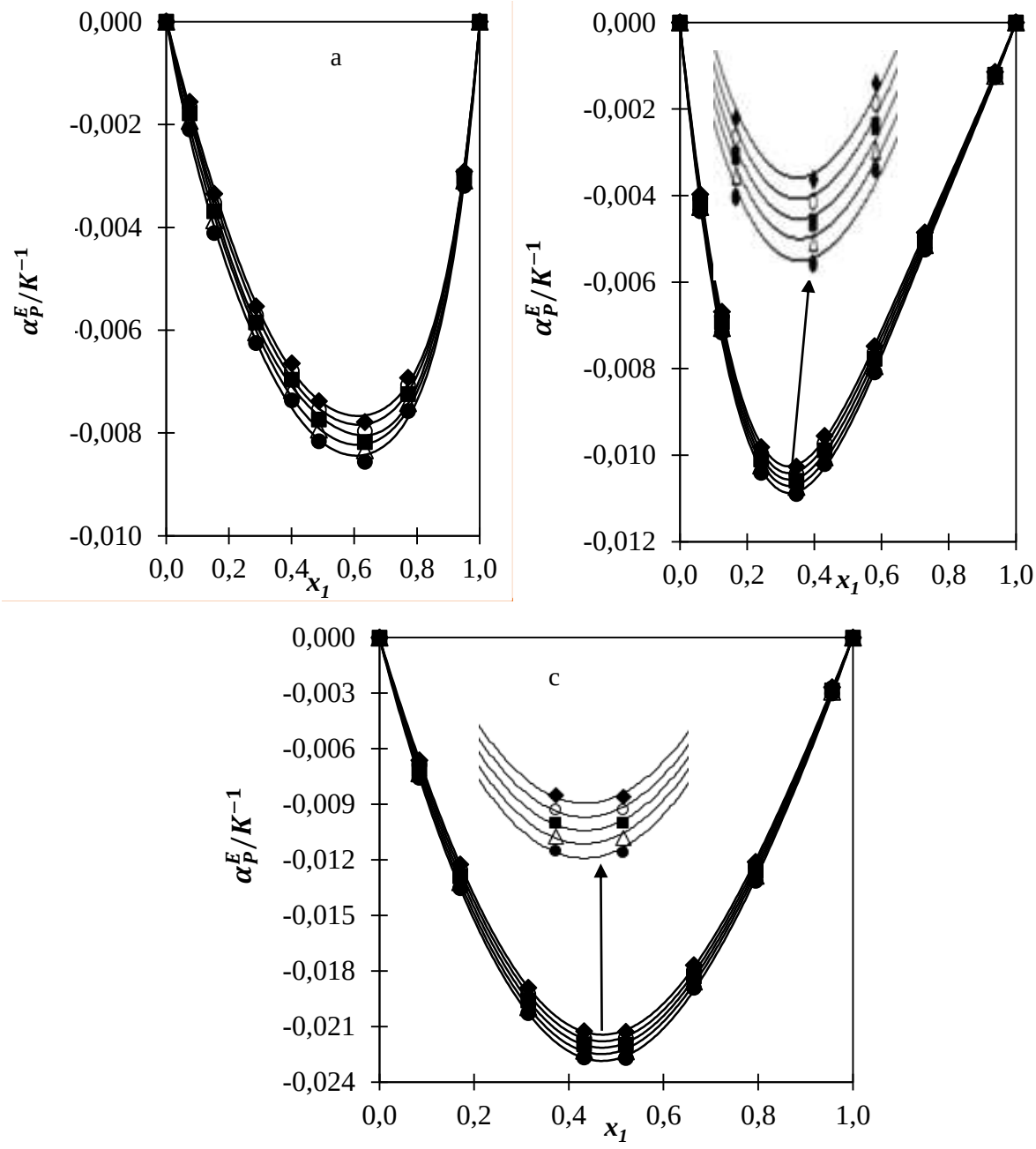

Figure 6.13: Plot of $\boldsymbol{\alpha_P^E/K^{-1}}$ versus the IL ($\boldsymbol{x_1}$) for the IL + PEG systems. (a) $[\mathbf{BMIM}]^+[\mathbf{BF_4}]^-$, (b) $[\mathbf{BMIM}]^+[\mathbf{PF_6}]^-$ and (c) $[\mathbf{EMIM}]^+[\mathbf{BF_4}]^-$. Exp data from this work: (♦)293.15 K, (○)303.15 K, (■)313.15 K, (△)323.15 K, (●)333.15 K at p = 0.1 MPa. The solid lines represent the correlation obtained with the Redlich-Kister polynomial equation.

All the α_P^E curves are asymmetric and follow the order: $[EMIM]^+[BF_4]^-$ > $[BMIM]^+[PF_6]^-$ > $[BMIM]^+[BF_4]^-$, having the minimum values at ($\alpha_P^E \approx$ -0.0220 K^{-1} at $x_1 \approx 0.48$, $\alpha_P^E \approx$ -0.010 K^{-1} at $x_1 \approx$ 0.37 and $\alpha_P^E \approx$ -0.008 K^{-1} at $x_1 \approx 0.6$), respectively. The values of α_P^E is also used as a tool to provide useful information about the orientation and structural packing of the molecules (Pires et al., 2013).

The negative values of α_P^E implies that volumetric thermal expansion of the solution is smaller and lesser than that of pure components. Additionally, small volumetric expansion of the solution implies that there is a decrease in the average intermolecular distance between ILs and PEG200 as compared to the pure components. Thus, the solution structure of the binary mixture does not break easily (Srinivasa Rao et al., 2018). This implies that there is contraction of volume occurring upon mixing.

Additionally negative values of α_P^E reflects the association of components in the mixture. Strong association in the mixture means that there is breaking of H-bonds followed by specific ion-dipole interactions occurring upon mixing, which is observed for all the ILs and PEG200 (Rezaei-Sameti and Rakhshi, 2017). The volumetric thermal expansion decreases with increasing temperature. Thus, implying that the ion-dipole interactions becomes stronger as the temperature increases.

Comparing the effect of the anion of $[BMIM]^+[PF_6]^-$ and $[BMIM]^+[BF_4]^-$, the magnitude of α_P^E follows the order $[PF_6]^-$ > $[BF_4]^-$. This means that the decreasing volumetric thermal expansion is much greater and significant for the binary system having larger sized anion $[PF_6]^-$ as compared to the binary mixture composed of smaller molecular weight anion $[Bf_4]^-$.Thus, the decreases in volumetric thermal expansion is attributed to the formation of strong ion-dipole interactions.

Comparing the effect of the cation of $[BMIM]^+[BF_4]^-$ and $[EMIM]^+[BF_4]^-$, magnitude of α_P^E follows the order $[EMIM]^+$ > $[BMIM]^+$.The more negative values of α_P^E for $[EMIM]^+$ cation of IL serves as further evidence that the decrease in volumetric thermal expansion between ions of $[EMIM]^+$ cation and PEG200 molecules is much greater than that of $[BMIM]^+$ cation and PEG200 molecules. The decrease in volume thermal expansion suggest that the mixture is rigid thus leading to the formation of ion-dipole interactions. Thus, the ion-dipole interactions is much stronger for short alkyl cation chain length ($[EMIM]^+$) than long alkyl cation chain length ($[BMIM]^+$).

The results, therefore, indicate that the volumetric thermal expansion and the strength of intermolecular interactions between ions of ILs and molecules of PEG200 depend upon the chain length of cation and the size of the anion of ILs.

6.8.6 Excess partial molar volume ($\bar{V}_1^E$ and $\bar{V}_2^E$)

Figure 6.14 presents the variation of ($\bar{V}_1^E$ and $\bar{V}_2^E$) as a function of mole fraction of ILs. The ($\bar{V}_1^E$ and $\bar{V}_2^E$) values for $[BMIM]^+[Bf_4]^-$+ PEG200 are negative over the entire ILs composition range.

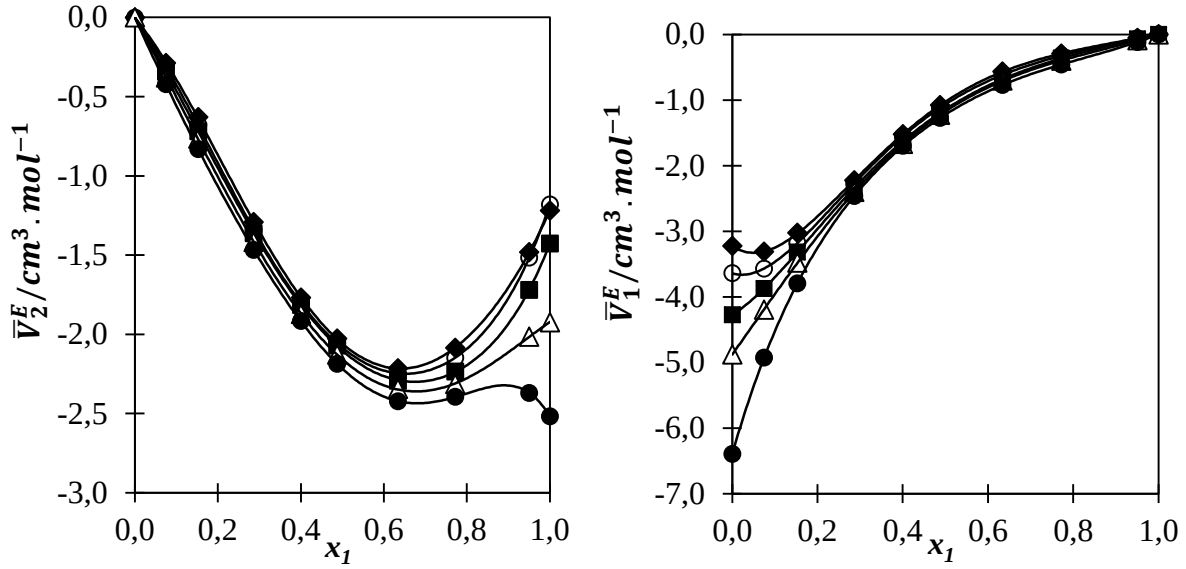

Figure 6.14: Plot of ($\bar{V}_1^E$ and $\bar{V}_2^E$) versus the IL (x_1) for the system $[BMIM]^+[BF_4]^-$+ PEG200. Exp data from this work: (♦)293.15 K, (○)303.15 K, (■)313.15 K, (△)323.15 K, (●)333.15 K at p = 0.1 MPa. The solid line is a trendline.

Figure 6.15 presents the variation of ($\bar{V}_1^E$ and $\bar{V}_2^E$) as a function of mole fraction of ILs. The ($\bar{V}_1^E$ and $\bar{V}_2^E$) values for $[BMIM]^+[PF_6]$+ PEG200 are negative over the entire ILs composition range.

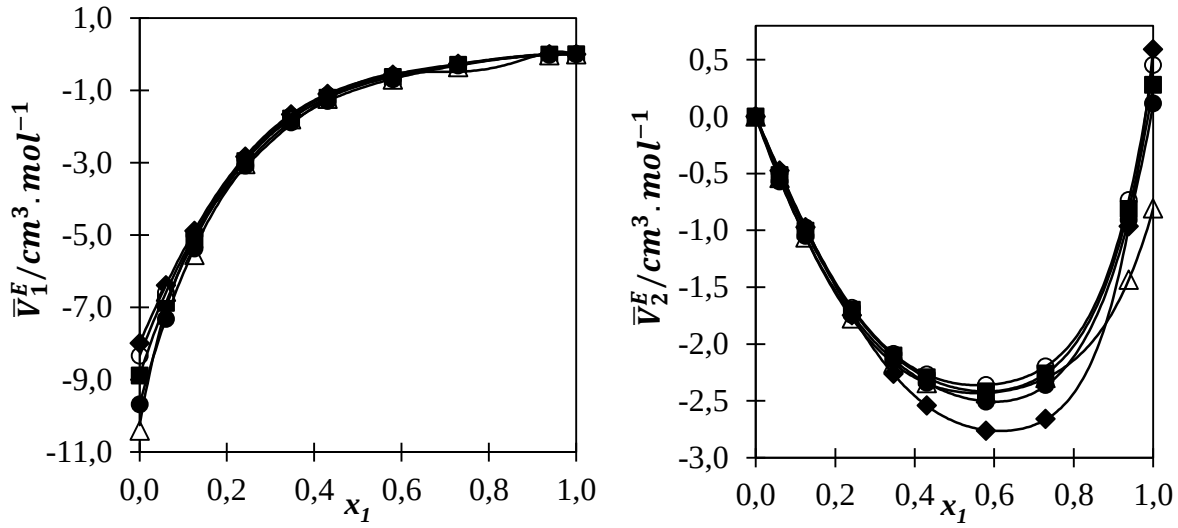

Figure 6.15: Plot of ($\bar{V}_1^E$ and $\bar{V}_2^E$) versus the IL (x_1) for the system $[\mathbf{BMIM}]^+[\mathbf{PF_6}]$+ PEG200. Exp data from this work: (♦)293.15 K, (○)303.15 K, (■)313.15 K, (△)323.15 K, (●)333.15 K at p = 0.1 MPa. The solid line is a trendline.

Figure 6.16 presents the variation of ($\bar{V}_1^E$ and $\bar{V}_2^E$) as a function of mole fraction of ILs. The ($\bar{V}_1^E$ and $\bar{V}_2^E$) values for $[EMIM]^+[BF_4]^-$ + PEG200 are negative over the entire ILs composition range.

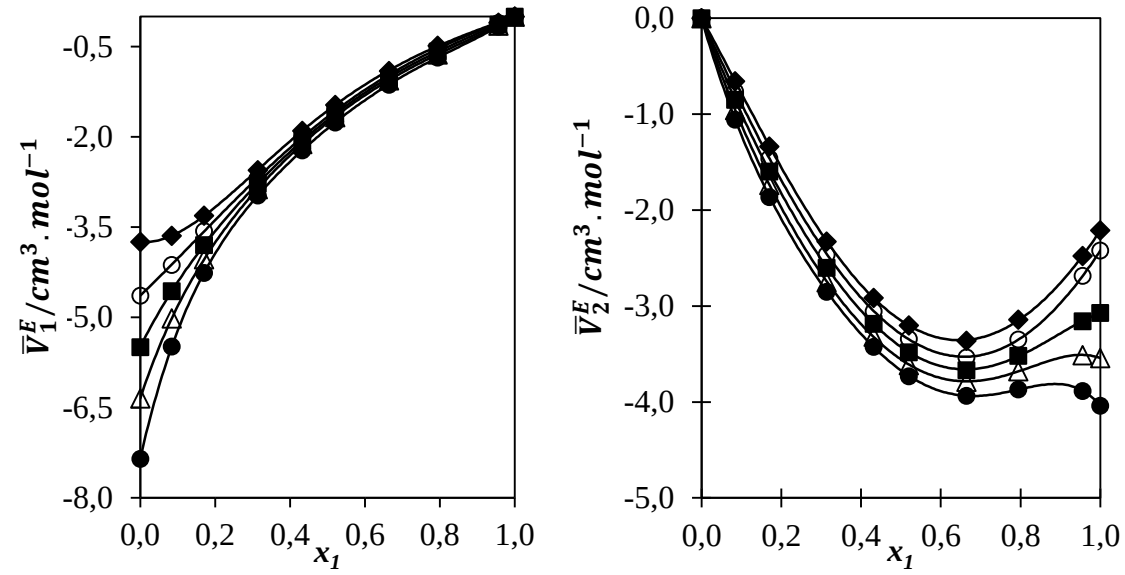

Figure 6.16: Plot of ($\bar{V}_1^E$ and $\bar{V}_2^E$) versus the IL (x_1) for the system $[\mathbf{EMIM}]^+[\mathbf{BF_4}]^-$ + PEG200. Exp data from this work: (♦)293.15 K, (○)303.15 K, (■)313.15 K, (△)323.15 K, (●)333.15 K at p = 0.1 MPa. The solid line is a trendline.

The overall excess partial molar volumes for ILs and PEG200 i,e. $\bar{V}_1^E$ and $\bar{V}_2^E$, are negative over the entire IL mole fraction range and temperatures investigated. The binary mixtures become more strongly negative with increasing temperatures.

A close examination of figures 6.14 - 6.16 indicates that $\bar{V}_1^E$ and $\bar{V}_2^E$ for ($[EMIM]^+[BF_4]^-$and $[BMIM]^+[Bf_4]^-$+ PEG200) exhibit negative deviation over the entire composition range. Binary systems with $[BMIM]^+[PF_6]^-$ possesses both negative and positive values for ($\bar{V}_1^E$ and $\bar{V}_2^E$). For $\bar{V}_1^E$, negative values are observed at almost over the entire mole fraction range, and slightly positive between the region of $x_1 \approx$ 0.97 – 1. For $\bar{V}_2^E$ values, all the binary systems exhibited negative deviation from ideal behavior, thus $\bar{V}_2^E$ values are all negative through the entire composition and slightly positive in the region of $x_1 >$ 0.98.

The negative deviation of ($\bar{V}_1^E$ and $\bar{V}_2^E$), suggest that the molar volumes ($V_{0,1}$ and $V_{0,2}$) of both IL and PEG200 in the mixtures are lower than their individual molar volumes ($V_{0,1}$ and $V_{0,2}$) in the pure state. This indicates that there is contraction/ decrease of volume upon the binary mixture at all the temperatures studied. In general, the negative of ($\bar{V}_1^E$ and $\bar{V}_2^E$) indicate the presence of significant solute-solvent interactions between unlike molecules (Desnoyers and Perron, 1997).

For systems with $[BMIM]^+[PF_6]^-$, the negative values of $\bar{V}_1^E$ suggest that there are strong solvent-solute intermolecular interactions between the molecules of PEG200 and the ions of ILs. The positive values suggest that there are weak solute-solvent interactions. However, from the results, it is clear that the negative values of $\bar{V}_1^E$ are dominant, meaning strong interactions between a solvent and a solute is dominant.

Examination of Figure 6.14 – 6.16 not only reveals the existence of strong forces between the unlike molecules but also conforms with the deductions drawn from V^E (Nayeem et al., 2014). The overall magnitude of excess partial molar volume ($\bar{V}_1^E$ and $\bar{V}_2^E$) supports the conclusions drawn from the analysis of the results of V^E, K_S^E, n_D^E, and α_P^E.

6.8.7 Excess partial molar volume at infinite dilution ($\bar{V}_i^{E,\infty}$)

The excess partial molar volume at infinite dilution ($\bar{V}_i^{E,\infty}$) is of interest because at the limit of infinite dilution the solute-solvent interaction disappears. Therefore, the values of partial molar volumes at infinite dilution provides information about solute-solvent interactions that are independent of the composition (Rezaei-Sameti and Rakhshi, 2017).

Table 6.9 presents ($\bar{V}_1^{E,\infty}$and $\bar{V}_2^{E,\infty}$) values for $[BMIM]^+[BF_4]^-$ + PEG200, over the temperature range 293.15 K to 333.15 K with 10 K intervals under *p* = 0.1 MPa.

Table 6. 10: The ($\bar{V}_1^{E,\infty}$and $\bar{V}_2^{E,\infty}$) values for $[\mathbf{BMIM}]^+[\mathbf{BF_4}]^-$ + PEG200 at *T* = (293.15 to 333.15) K intervals under and *p* = 0.1 MPa.

T/K	$\bar{V}_1^{\infty}$	$V_{0,1}$	$\bar{V}_1^{E,\infty}$	$\bar{V}_2^{\infty}$	$V_{0,2}$	$\bar{V}_2^{E,\infty}$
			$(\mathbf{cm^3.mol^{-1}})$			
293.15	184.405	187.4766	-3.0716	176.575	177.7936	-1.2190
303.15	185.113	188.7537	-3.6403	177.889	179.2501	-1.3611
313.15	185.612	189.8873	-4.2753	178.935	180.3609	-1.4263
323.15	186.139	191.0171	-4.8777	179.743	181.6662	-1.9237
333.15	185.744	192.1416	-6.3977	180.478	182.9948	-2.5168

Table 6.10 presents ($\bar{V}_1^{E,\infty}$and $\bar{V}_2^{E,\infty}$) values for $[BMIM]^+[PF_6]^{--}$ + PEG200, over the temperature range 293.15 K to 333.15 K with 10 K intervals under p = 0.1 MPa.

Table 6.11: The ($\bar{V}_1^{E,\infty}$and $\bar{V}_2^{E,\infty}$) values for $[\mathbf{BMIM}]^+[\mathbf{PF_6}]^-$ + PEG200 at *T* = (293.15 to 333.15) K intervals under and *p* = 0.1 MPa..

T/K	$\bar{V}_1^{\infty}$	$V_{0,1}$	$\bar{V}_1^{E,\infty}$	$\bar{V}_2^{\infty}$	$V_{0,2}$	$\bar{V}_2^{E,\infty}$
			$(\mathbf{cm^3.mol^{-1}})$			
293.15	199.325	207.314	-7.9900	177.793	178.3850	-0.5920
303.15	200.260	208.5890	-8.3290	179.068	179.7191	-0.6511
313.15	201.003	209.883	-8.8793	180.361	181.0890	-0.7280
323.15	200.777	211.178	-9.6796	181.666	182.4021	-0.7361
333.15	202.797	212.476	-10.4011	182.995-	183.9111	-0.9161

Table 6.11 presents ($\bar{V}_1^{E,\infty}$and $\bar{V}_2^{E,\infty}$) values for $[EMIM]^+[BF_4]^-$ + PEG200, over the temperature range 293.15 K to 333.15 K with 10 K intervals under *p* = 0.1 MPa.

Table 6.12: The ($\bar{V}_1^{E,\infty}$and $\bar{V}_2^{E,\infty}$) values for $[\mathbf{EMIM}]^+[\mathbf{BF_4}]^-$ + PEG200 at T = (293.15 to 333.15) K intervals under and p = 0.1 MPa.

T/K	$\bar{V}_1^{\infty}$	$V_{0,1}$	$\bar{V}_1^{E,\infty}$	$\bar{V}_2^{\infty}$	$V_{0,2}$	$\bar{V}_2^{E,\infty}$
			$(\mathbf{cm^3.mol^{-1}})$			
293.15	150.660	154.4063	-3.7462	175.582	177.7931	-2.2110
303.15	193.335	155.3322	-4.6370	176.6451	223.3787	-2.4230
313.15	192.479	156.2560	-5.4930	177.2901	180.3611	-3.0710
323.15	191.624	157.1836	-6.3480	178.124	181.6662	-3.5420
333.15	190.621	158.1148	-7.3510	178.958	182.9949	-4.0370

The partial molar volumes of of both ILs and PEG200 at infinite dilution ($\bar{V}_1^{E,\infty}$ and $\bar{V}_2^{E,\infty}$) are less than the corresponding pure molar volume ($V_{0,1}$ and $V_{0,2}$). This suggests that, the self-association of pure components between homogeneous molecules are removed effectively and strong ion-dipole interactions between the ions of ILs and the molecules of PEG200 are formed (Alavianmehr et al., 2017). This leads to decrease/contraction in volume and the values of excess partial molar volume at infinite dilution becomes negative as the temperature increases suggesting that the contraction of volume increases with temperature. Thus due to contraction of volume, the hydrogen bonding/ion-dipole interactions also increases with temperature.

The $\bar{V}_1^{E,\infty}$ values of ILs are more negative than $\bar{V}_2^{E,\infty}$ values of PEG200 at all studied temperatures. This is due to the fact that alkyl imidazolium ILs possess greater ability and tendencies to form hydrogen bonds than PEG200. Hence, the conclusion that the strong interactions among the unlike molecules of the mixtures increases as the temperature increases (Srinivasa Rao et al., 2018).

The given values of the excess partial molar volumes ($\bar{V}_1^{E}$ and $\bar{V}_2^{E}$) and excess partial molar volume at infinite dilution $\left(\bar{V}_1^{E,\infty}\right.$ and $\left.\bar{V}_2^{E,\infty}\right)$ should be taken with reservation and the qualitative interpretation is not necessarily representative of the general behaviour of these systems because of the limited number of experimental points for dilute solutions. Thus, this implies that the general behaviour regarding formation

or dissociation of ion-dipole interactions is interpreted by either negative or positive deviation from ideality (Domańska et al., 2006).

These observations are consistent with the V^E values obtained for the binary systems. Closer examination of these ($\bar{V}_1^{E,\infty}$ and $\bar{V}_2^{E,\infty}$) not only reveals the existence of strong solvent-solute interactions between unlike molecules but also supports the deductions drawn from the analysis of the results of $V^E, K_s^E, n_D^E, \alpha_P^E$, $\bar{V}_1^E$ and $\bar{V}_2^E$.

6.9 Calculated combined standard uncertainty for the selected binary mixtures

Table 6.12 presents the calculated experimental combined standard uncertainties for selected thermophysical properties and mixture composition $u(x_1)$ of the studied binary systems.

Table 6.13: Combined standard uncertainties for the measured variable.

Binary mixtures	x_1	$\rho/g.cm^{-3}$	$u/m.s^{-1}$	$\eta/mPa.s$	n_D
ILs + PEG200	± 0.0004	± 0.00002	± 0.02	± 0.002	± 0.00005

Standard uncertainties for temperature for the Anton Paar unit and refractometer: *u(T)* = ± 0.01 and *u(T)* = ± 0.05 K respectively.

6.10 Fitting parameters for excess thermodynamic properties using the Redlich-Kister equation

Tables 6.13, 6,14 and 6,15 presents the calculated parameters of Redlich Kister polynomial equation for the $[BMIM]^+[BF_4]^-$ + PEG200, $[BMIM]^+[PF_6]^-$ + PEG200, and $[EMIM]^+[BF_4]^-$ + PEG200 systems, respectively. As shown in the previous sections and respective figures, the Redlich Kister polynomial correlates the measured data well. The standard deviations as reported in the tables below are well within accepted errors. Slightly higher errors are observed for K_s^E.
for all systems. This is most likely due to the combined uncertainties for density (ρ) and speed of sound (u) which is used in the calculations.

Table 6.14: Redlich Kister parameters for the $[\mathbf{BMIM}]^{+}[\mathbf{BF_4}]^{-}$+ PEG200 at varying temperatures and *p* = 0.1 MPa.

Z^E	T/K	A_0	A_1	A_2	A_3	A_4	σ
$V^E/cm^3.mol^{-1}$	293.15	-3.086	2.065	0.33290	-1.0620	0.5311	0.00557
	303.15	-3.151	2.035	0.02754	-0.8052	0.7128	0.00377
	313.15	-3.246	1.916	0.00104	-0.4915	0.3942	0.00270
	323.15	-3.331	1.969	-0.11260	-0.492	0.04286	0.00459
	333.15	-3.439	1.989	-0.06146	-0.3251	-0.6802	0.00149
K_s^E/TPa^{-1}	293.15	-39.98	22.06	-13.53	26.83	-18.600	0.04406
	303.15	-43.15	25.03	-14.95	30.71	-16.450	0.05953
	313.15	-46.52	31.34	-24.74	18.98	2.635	0.17500
	323.15	-49.17	32.42	-31.56	23.26	-0.806	0.03686
	333.15	-55.26	30.59	-31.16	29.11	-4.030	0.15870
$\eta^E/mPa.s$	293.15	3.465	0.9799	-0.1515	-0.3056	-0.6146	0.01066
	303.15	3.238	0.9275	-0.2601	-0.3791	-0.8486	0.00708
	313.15	3.022	0.9013	-0.5376	-0.5987	-0.9015	0.00493
	323.15	2.814	0.9979	-0.7328	-1.064	-0.8887	0.00373
	333.15	2.606	1.0130	-0.7663	-1.168	-1.0900	0.00499
n_D^E	293.15	0.0077	-0.0047	0.0011	-0.0033	0.0038	0.00002
	303.15	0.0080	-0.0054	0.0029	-0.0035	0.0012	0.00001
	313.15	0.0084	-0.0053	0.0023	-0.0034	0.0029	0.00001
	323.15	0.0089	-0.0055	0.0013	-0.0049	0.0056	0.00003
	333.15	0.0094	-0.0062	0.0017	-0.0036	0.0052	0.00001
α_P^E/K^-	293.15	-0.0298	-0.0092	-0.0076	-0.0129	-0.0094	0.00013
	303.15	-0.0303	-0.0090	-0.0105	-0.0133	-0.0077	0.00013
	313.15	-0.0311	-0.0089	-0.0109	-0.0120	-0.0072	0.00015
	323.15	-0.0318	-0.0088	-0.0110	-0.0125	-0.0096	0.00013
	333.15	-0.0329	-0.0091	-0.0109	-0.0114	-0.0116	0.00015

Table 6.14: Redlich Kister parameters for the $[\mathbf{BMIM}]^{+}[\mathbf{PF_6}]^{-}$+ PEG200 at varying temperatures and *p* = 0.1 MPa.

Z^E	*T/K*	A_0	A_1	A_2	A_3	A_4	σ
$V^E/cm^3.mol^{-1}$	293.15	-3.096	3.029	-2.108	1.262	1.5050	0.00242
	303.15	-3.176	3.030	-2.061	1.360	1.3000	0.00167
	313.15	-3.264	3.007	-1.807	1.572	0.7707	0.00111
	323.15	-3.352	2.960	-2.570	1.837	0.3179	0.00290
	333.15	-3.411	2.978	-1.583	1.920	0.2124	0.00382
K_S^E/TPa^{-1}	293.15	-44.03	48.43	-23.500	14.28	-12.10	0.02423
	303.15	-47.96	49.33	-20.600	19.22	-19.45	0.10160
	313.15	-51.96	50.54	-16.200	22.87	-37.52	0.09773
	323.15	-56.51	49.91	-8.180	32.2	-45.99	0.09700
	333.15	-61.51	50.27	-6.806	37.27	-54.16	0.08926
$\eta^E/mPa.s$	293.15	4.138	-0.3840	-1.824	0.5086	-1.2500	0.00821
	303.15	3.961	-0.3030	-1.906	0.4375	-1.2260	0.00567
	313.15	3.768	-0.2765	-2.278	0.3912	-0.6047	0.00611
	323.15	3.556	-0.2753	-2.200	0.4379	-0.8878	0.00325
	333.15	3.369	-0.1972	-2.175	0.2251	-1.1180	0.00586
n_D^E	293.15	0.0078	-0.0072	0.0026	0.0043	-0.0041	0.00002
	303.15	0.0085	-0.0076	0.0028	0.0034	-0.0034	0.00002
	313.15	0.0095	-0.0081	0.0028	0.0025	-0.0019	0.00002
	323.15	0.0097	-0.0081	0.0038	0.0015	-0.0022	0.00002
	333.15	0.0103	-0.0082	0.0041	0.0006	-0.0009	0.00003
α_P^E/K^-	293.15	-0.0351	0.0290	-0.0138	-0.0019	0.0038	0.00011
	303.15	-0.0354	0.0293	-0.0153	-0.0025	0.0037	0.00013
	313.15	-0.0364	0.0293	-0.0131	-0.0014	0.0011	0.00015
	323.15	-0.0370	0.02970	-0.0105	-0.0001	-0.0033	0.00010
	333.15	-0.0376	0.0300	-0.0109	-0.0006	-0.0043	0.00013

Table 6.15: Redlich Kister parameters for the $[\mathbf{EMIM}]^{+}[\mathbf{BF_4}]^{-}$ + PEG200 at varying temperatures and *p* = 0.1 MPa.

Z^E	T/K	A_0	A_1	A_2	A_3	A_4	σ.
	293.15	-3.794	1.286	0.6294	-0.5183	0.1561	0.00676
	303.15	-3.970	1.266	0.4591	-0.1591	-0.0191	0.00654
$V^E/cm^3.mol^{-1}$	313.15	-4.117	1.352	0.2654	-0.1159	-0.4051	0.00601
	323.15	-4.258	1.451	0.0191	-0.0480	-0.7063	0.00536
	333.15	-4.427	1.398	-0.0467	0.2593	-1.2200	0.00293
	293.15	-69.86	40.46	-19.95	-25.06	40.81	0.10780
	303.15	-75.52	45.84	-21.04	-27.68	31.28	0.19470
K_S^E/TPa^{-1}	313.15	-80.25	49.17	-26.94	-26.36	37.78	0.33780
	323.15	-85.50	53.45	33.65	-26.44	36.85	0.39400
	333.15	-86.31	55.66	-42.09	-21.93	38.35	0.30400
	293.15	4.504	0.9594	-1.2710	0.1978	0.88910	0.01729
	303.15	4.206	0.8683	-0.9257	0.3311	-0.05723	0.01203
η^E	313.15	3.923	0.8996	-1.077	0.2822	0.00139	0.01078
	323.15	3.691	1.015	-1.164	-0.03326	-0.1383	0.00958
	333.15	3.443	1.063	-1.183	-0.2661	-0.5762	0.01332
	293.15	0.0143	-0.0079	0.0069	0.0015	-0.0069	0.00002
	303.15	0.0151	-0.0085	0.0065	0.0021	-0.0051	0.00002
n_D^E	313.15	0.0158	-0.0087	0.0062	0.0018	-0.0038	0.00002
	323.15	0.0164	-0.0088	0.0063	0.0018	-0.003	0.00002
	333.15	0.0171	-0.0091	0.0071	0.0012	-0.0024	0.00002
	293.15	-0.0854	0.0119	0.0165	-0.0021	-0.0048	0.00009
	303.15	-0.0868	0.0115	0.0154	0.0004	-0.0052	0.00011
α_P^E/K^-	313.15	-0.0883	0.0124	0.0150	0.0003	-0.0063	0.00009
	323.15	-0.0895	0.0130	0.0119	-0.0005	-0.0044	0.00010
	333.15	-0.09112	0.0129	0.01462	0.0014	-0.01086	0.00010

6.11 Fourier-transform infrared spectroscopy of three selected binary mixtures

Excess thermodynamic and thermophysical properties can only provide possible explanations of the nature of non-ideal behaviour in the mixture. However, only spectroscopic analysis can give a proper and clear insight into molecular interactions between components in the mixture and confirm assumptions made by excess thermodynamic properties. The FT-IR spectra enables one to observe the dissociation or association of any ion-dipole interactions between the ILs and PEG200.

Figures 6.17 – 6.19 presents the FT-IR spectra for the binary mixture of $[BMIM]^+[BF_4]^-$, $[BMIM]^+[PF_6]^-$, $[EMIM]^+[BF_4]$ + PEG200 respectively. These were obtained using the FT-IR spectra as discussed in section 5.4.

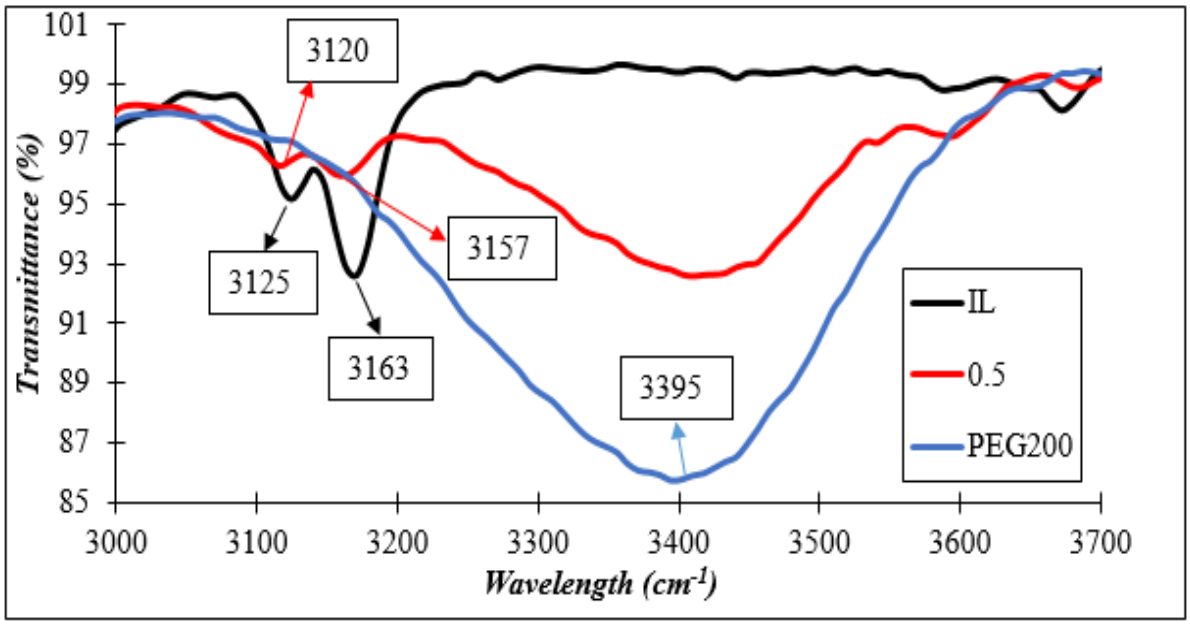

Figure 6.17: Normalized FT-IR spectra of pure (■) $[\mathbf{BMIM}]^+[\mathbf{BF_4}]^-$, (■) $[\mathbf{BMIM}]^+[\mathbf{BF_4}]^-$ + PEG200 sample ($\boldsymbol{x_1 = 0.5}$) and (■) PEG200 at temperature T = 298.15 K under atmospheric pressure of p = 0.1 MPa.

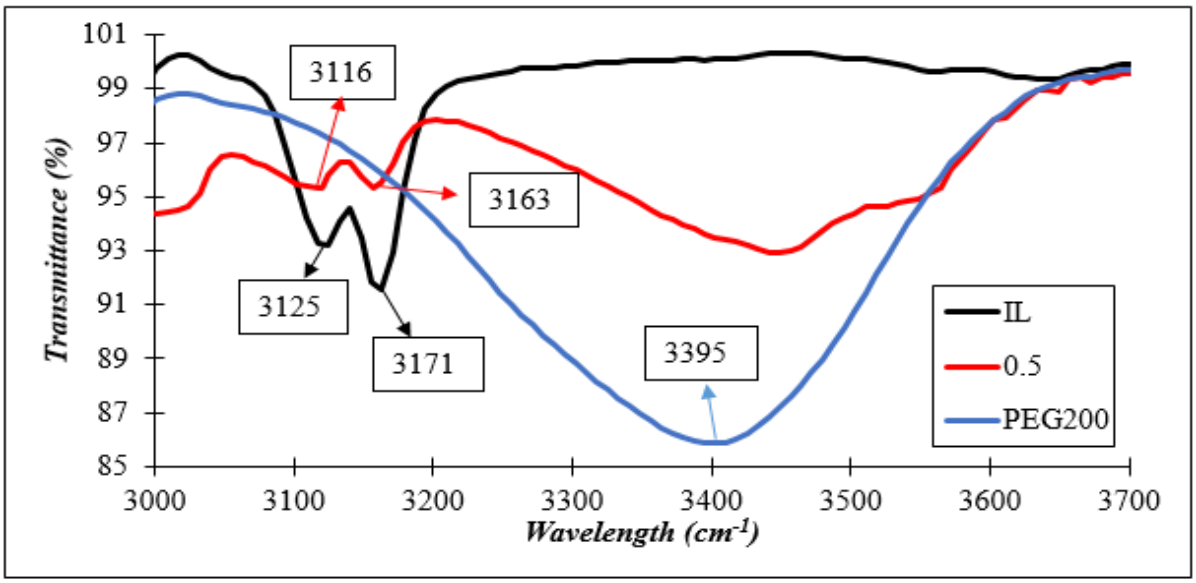

Figure 6.18: Normalized FT-IR spectra of pure (■) $[\mathbf{BMIM}]^{+}[\mathbf{PF_6}]^{-}$, (■) $[\mathbf{BMIM}]^{+}[\mathbf{PF_6}]^{-}$ + PEG200 sample ($\boldsymbol{x_1 = 0.5}$) and (■) PEG200 at temperature T = 298.15 K under atmospheric pressure of p = 0.1 MPa.

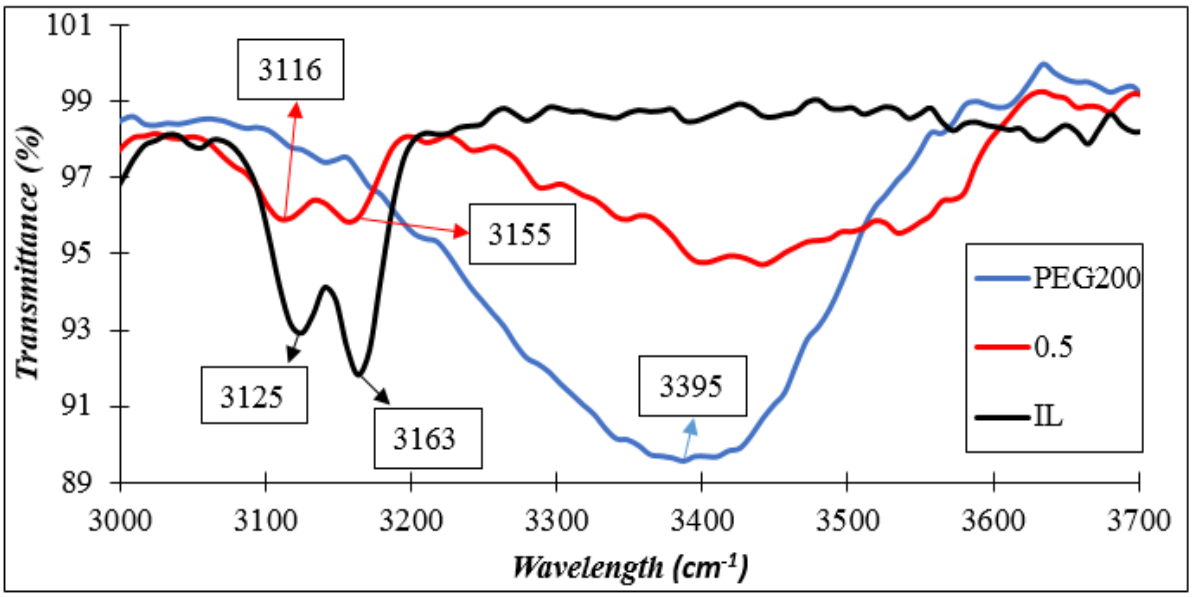

Figure 6.19: Normalized FT-IR spectra of pure (■) $[\mathbf{EMIM}]^{+}[\mathbf{BF_4}]^{-}$, (■) $[\mathbf{EMIM}]^{+}[\mathbf{BF_4}]^{-}$ + PEG200 sample ($\boldsymbol{x_1 = 0.5}$) and (■) PEG200 at temperature T = 298.15 K under atmospheric pressure of p = 0.1 MPa.

Figures 6.17 – 6.19 shows the normalized FT-IR spectra in the range 3000 - 3700 cm^{-1} recorded for ILs + PEG200 mixtures. The figures presented are for pure components and different binary mixtures at equimolar composition ($x_1 = 0.5$).

The FT-IR spectra presents four different broadband regions responsible for hydrogen bonding. These four broadband regions are 3390 – 3410 cm^{-1}, 3590 – 3650 cm^{-1}, 3550 – 3200 cm^{-1} and 3100 – 3200 cm^{-1}. These broadband regions represent the following; –OH group of pure PEG200, the stretching of the O-H due to free O–H, O–H stretching due to intermolecular hydrogen bonding and lastly the C–H stretching bond due to ion-dipole interactions (Pandey et al., 2013), respectively.

The interpretation of the formation of hydrogen bonding between the frequencies of 3400 cm^{-1} and 3100 cm^{-1} – 3200 cm^{-1} is different.

For the frequency change on 3400 cm^{-1}; a broadband is observed for pure PEG200 at 3395 cm^{-1} and there is significant change in the frequency upon the addition of ILs at (x_1 = 0.5). There is a slight shift from lower frequencies to higher frequencies, indicating the reduction in hydrogen bonds intensity of individual compounds such as ions from ILs and dipolar molecules from PEG200. The reduction of individual hydrogen bonds suggests that there are strong formation of ion-dipole interactions present upon mixing (Krishna et al., 2017).

For the frequency change on 3100 cm^{-1} – 3200 cm^{-1}; the intensity of the hydrogen bonding between the molecules on the FT-IR spectra analysis is based on the position of the shifted broad bands. The shift of the broad bands towards the lower frequency suggests that the hydrogen bonding is more extensive, and the shift in the broad band towards the higher frequency denotes less extensive hydrogen bonding (Yokozeki et al., 2007a).

The frequency region of 3100 – 3200 cm^{-1} represents the C–H bonds predominantly originating from aromatic imidazolium ring of the ILs (Dhumal et al., 2011). Two broad bands are observed in the region (3100 – 3200 cm^{-1}). These two broad bands ring may exist in two different environments, e.g in dissociated ions and ion pairs (Pandey et al., 2013). The two peaks are due to C–H stretching vibrations in the imidazolium ring. The first broadband is observed at 3125 cm^{-1} for all the investigated ILs, and the second broadbands rings are observed at 3163 cm^{-1}, 3163 cm^{-1} and 3171 cm^{-1} for $[BMIM]^+[BF_4]^-$, $[EMIM]^+[BF_4]^-$ and $[BMIM]^+[PF_6]^-$, respectively. On addition of PEG200 the two different peaks representing (C–H stretching mode) shift towards lower frequencies. This shift is due to ion-dipole

interactions/hydrogen bonding between nitrogen molecules in the imidazolium cation of ILs (Yokozeki et al., 2007b) and dipolar hydroxyl (–OH) group of PEG200 molecules. The shift is more noticeable and pronounced for the binary mixture composed of $[EMIM]^+[BF_4]^-$ (3125 cm^{-1} and 3163 cm^{-1} to 3116 cm^{-1} and 3155 cm^{-1}) followed by $[BMIM]^+[PF_6]^-$ (3125 cm^{-1} and 3171 cm^{-1} to 3116 cm^{-1} and 3163 cm^{-1}) and lastly $[BMIM]^+[Bf_4]^-$(3125 cm^{-1} and 3163 cm^{-1} to 3120 cm^{-1} and 3157 cm^{-1}). Thus the strength of the ion-dipole interactions follows the order: $[EMIM]^+[BF_4]^- > [BMIM]^+[PF_6]^- > [BMIM]^+[BF_4]^-$.

The deductions inferred from the FT-IR spectra observed for all the three binary mixtures are consistent with results and explanations drawn from the excess thermodynamic properties, as discussed in section 6.8.

CHAPTER SEVEN

CONCLUSIONS

Imidazolium based ILs ($[BMIM]^+[BF_4]^-$, $[BMIM]^+[PF_6]^-$ and $[EMIM]^+[BF_4]^-$) blended with PEG200 were selected for investigation, due to the lack of data available for thermophysical measurement and excess thermodynamic calculations in the open literature.

Thermophysical properties such as ρ, u, η and n_D were measured at five different temperatures (293.15, 303.15, 313.15, 323.15 and 333.15) K under p = 0.1 MPa. From the experimental data, excess thermodynamic data were calculated to get a deeper understanding of the intermolecular behaviour and arrangement between the ions of ILs and molecules of PEG200.

Excess thermodynamic properties such as V^E, K_s^E, η^E, n_D^E, α_P^E, $\bar{V}_1^E$, $\bar{V}_2^E$, $\bar{V}_1^{E,\infty}$ and $\bar{V}_2^{E,\infty}$ were calculated for all the binary mixtures throughout the entire composition. Excess thermodynamic properties such as V^E, K_s^E, α_P^E, $\bar{V}_1^E$, $\bar{V}_2^E$, $\bar{V}_1^{E,\infty}$ and $\bar{V}_2^{E,\infty}$ resulted in a negative deviation. This implies that there exist strong ion-dipole interactions between the ions of ILs and the molecules of PEG200. For η^E and n_D^E , results indicated positive deviations which implies that there exist strong ion-dipole interactions between the ions of ILs and the molecules of PEG200. The excess thermodynamic data apart from $\bar{V}_1^E$ and $\bar{V}_2^E$ were correlated and fitted with a Redlich-Kister polynomial model.

The magnitude of the V^E of all the binary mixtures follow the order: $[EMIM]^+[BF_4]^-$ > $[BMIM]^+[PF_6]^-$ > $[BMIM]^+[BF_4]^-$, having maximum values at ($V^E \approx$ -1.1 $cm^3 \cdot mol^{-1}$ at $x_1 \approx 0.4$), ($V^E \approx$ -1.0 $cm^3 \cdot mol^{-1}$ at $x_1 \approx 0.25$) and ($V^E \approx$ -0.88 $cm^3 \cdot mol^{-1}$ at $x_1 \approx 0.4$), respectively.

All the binary mixtures are asymmetric and the magnitude of η^E follows this order: $[EMIM]^+[BF_4]^-$ > $[BMIM]^+[PF_6]^-$ > $[BMIM]^+[BF_4]^-$. The minimum η^Epoint for $[EMIM]^+[BF_4]^-$, $[BMIM]^+[PF_6]^-$ and $[BMIM]^+[BF_4]^-$ binary systems were observed at ($\eta^E \approx$ 1.0 mPa.s at $x_1 \approx 0.57$, 0.9 mPa.s at $x_1 \approx 0.5$ and 0.75 mPa.s at $x_1 \approx 0.58$), respectively.

The fitting curves for binary systems are all symmetric and the magnitude of the K_s^E of all the binary mixtures follow the order: $[EMIM]^+[BF_4]^-$ > $[BMIM]^+[PF_6]^-$ > $[BMIM]^+[BF_4]^-$, having the maximum values at ($K_s^E \approx$ -13 TPa^{-1} at $x_1 \approx 0.30$, $K_s^E \approx$ -15 TPa^{-1} at $x_1 \approx 0.34$ and $K_s^E \approx$ -21 TPa^{-1} at $x_1 \approx 0.38$), respectively.

All the n_D^E curves are asymmetric and follow the order: $[EMIM]^+[BF_4]^-$ > $[BMIM]^+[PF_6]^-$ > $[BMIM]^+[BF_4]^-$, having the maximum values at ($n_D^E \approx 0.004$ at $x_1 \approx 0.35$, $n_D^E \approx 0.0025$ at $x_1 \approx 0.32$ and $n_D^E \approx 0.0022$ at $x_1 \approx 0.35$), respectively.
All the α_P^E curves are asymmetric and follow the order: $[EMIM]^+[BF_4]^-$ > $[BMIM]^+[PF_6]^-$ > $[BMIM]^+[BF_4]^-$, having the minimum values at ($\alpha_P^E \approx$ -0.0220 K^{-1} at $x_1 \approx 0.48$, $\alpha_P^E \approx$ -0.010 K^{-1} at $x_1 \approx$ 0.37 and $\alpha_P^E \approx$ -0.008 K^{-1} at $x_1 \approx 0.6$), respectively.

Further more, excess partial molar volumes ($\bar{V}_1^E$ and $\bar{V}_2^E$) and excess partial molar volume at infinite dilutions ($\bar{V}_1^{E,\infty}$ and $\bar{V}_2^{E,\infty}$) were obtained to further support the deduction drawn from V^E, K_s^E, n_D^E and α_P^E. The negative deviation of ($\bar{V}_1^E$ and $\bar{V}_2^E$) and the negative values of ($\bar{V}_1^{E,\infty}$ and $\bar{V}_2^{E,\infty}$) are in good agreement with the conclusion drawn from V^E, K_s^E, n_D^E and α_P^E.

The binary mixtures were also analysed using FT-IR spectroscopy and the results from FT-IR spectra supports the formation of a strong ion-dipole interactions between unlike molecules. The results from both excess thermodynamic calculations and FT-IR spectroscopy analyses indicated that the strength of ion-dipole interactions formed in these binary systems follow the order: $[EMIM]^+[BF_4]^-$ > $[BMIM]^+[PF_6]^-$ > $[BMIM]^+[BF_4]^-$.

CHAPTER EIGHT

RECOMMENDATIONS

The density (ρ) data of multicomponent solutions play an important role in industrial-scale such as process designing, liquid-liquid phase separation design, developing models, heat and mass transfer (Vercher et al., 2015).

In this study, the ρ data were utilized to calculate excess thermodynamic such as excess molar volume (V^E), excess isentropic compressibility (K_S^E), excess thermal expansion coefficient (α_P^E) excess partial molar volumes ($\overline{\mathrm{V}}_{\mathrm{i}}^{\mathrm{E}}$) and excess partial molar volume at infinite ($\bar{V}_i^{E,\infty}$). This therefore makes ρ data very important in deriving excess thermodynamic data. The Peng–Robinson equation of state has been applied for correlation and prediction of pure ILs density (ρ) and other thermophysical properties in a wide range of temperatures and pressures (Bagheri and Ghader, 2017). Thus, the Peng–Robinson equation of state was found to give the best fit for all the newly measured data sets for binary mixtures. These model are therefore recommended for the regression of the data sets for thermophysical properties should this study be extended to varying pressures.

A computational simulation known as density functional theory (DFT) model has been used to investigate the dissociation and association of hydrogen bonding (Singh et al., 2011). DFT program codes can analyse complex an enormous range of chemical, structural, vibrational, optical, spectroscopic, thermodynamic phenomena and elastic (Hasnip et al., 2014). Understanding of intermolecular interactions of compounds is challenging since it involves thousands and hundreds of molecules and atoms. The atoms and molecules are affected by various external factors, such as temperature and pressure. Therefore, the DFT simulations is able to perform routinely on systems of hundreds of atoms, with calculations for thousands of atoms being demanding, but possible (Hasnip et al., 2014). For future work, the DFT model may be used to get a deeper understanding of the mechanism of binary systems between ILs and polymers.

REFERENCES

AKBAR, M. M. & MURUGESAN, T. 2012. Thermophysical properties for the binary mixtures of 1-hexyl-3-methylimidazolium bis(trifluoromethylsulfonyl)imide [hmim][Tf_2N] + N-methyldiethanolamine (MDEA) at temperatures (303.15 to 323.15) K. *Journal of Molecular Liquids,* 169**,** 95-101.DOI 10.1016/j.molliq.2012.02.014

ALAVIANMEHR, M., HEMMATI, N. & GHODRATI, H. 2017. Excess molar volumes, excess thermal expansion coefficients and isentropic compressibility deviations for binary mixtures of benzyl alcohol+(1-butanol, 2-butanol, 2-methyl-1-butanol and tert-butanol) at T=(298.15-328.15) K and ambient pressure. *Physics and Chemistry of Liquids,* 55**,** 85-99

ALI, A., ANSARI, S. & NAIN, A. K. 2013. Densities, refractive indices and excess properties of binary mixtures of dimethylsulphoxide with some poly(ethylene glycol)s at different temperatures. *Journal of Molecular Liquids,* 178**,** 178-184.DOI 10.1016/j.molliq.2012.12.002

ALI, A. & NAIN, A. K. 2002. Ultrasonic and volumetric study of binary mixtures of benzyl alcohol with Amides. *Bulletin of the Chemical Society of Japan,* 75**,** 681-687.DOI 10.1246/bcsj.75.681

ALVAREZ, V. H., MATTEDI, S., MARTIN-PASTOR, M., AZNAR, M. & IGLESIAS, M. 2011. Thermophysical properties of binary mixtures of {ionic liquid 2-hydroxy ethylammonium acetate plus (water, methanol, or ethanol)}. *Journal of Chemical Thermodynamics,* 43**,** 997-1010.DOI 10.1016/j.jct.2011.01.014

ANDERSON, J. L., DIXON, J. K. & BRENNECKE, J. F. 2007. Solubility of CO2, CH4, C2H6, C2H4, O2, and N2 in 1-hexyl-3-methylpyridinium bis(trifluoromethylsulfonyl)imide: comparison to other ionic liquids. *Acc Chem Res,* 40**,** 1208-16.DOI 10.1021/ar7001649

ANGELL, C. & SARE, E. 1970. Glass-forming composition regions and glass transition temperatures for aqueous electrolyte solutions. *The Journal of Chemical Physics,* 52**,** 1058-1068

ANTON PAAR. 2017a. *Density and sound velocity meter: DSA 5000 M* [Online]. Available: https://www.anton-paar.com/za-en/products/details/density-and-sound-velocity-meter-dsa-5000-m/ [Accessed Septrmber 10 2017].

ANTON PAAR. 2017b. *Rolling-ball viscometer Lovis 2000 M/ME* [Online]. Available: https://www.anton-paar.com/za-en/products/details/rolling-ball-viscometer-lovis-2000-mme/ [Accessed September 22 2017].

ANURADHA, S., PREMA, S. & RAJAGOPAL, K. 2005. Ultrasonic studies on molecular interactions in binary mixtures of acetonitrile with carbonyl molecules. *Journal of Pure and Applied Ultrasonics,* 27**,** 49

ATAGO U.S.A., I. 2017. *Refractometer RX-7000α* [Online]. Available: http://prolabmas.com/wmview.php?ArtID=2036 [Accessed June 25, 2017].

BAGHERI, H. & GHADER, S. 2017. Correlating ionic liquids density over wide range of temperature and pressure by volume shift concept. *Journal of Molecular Liquids,* 236**,** 172-183.DOI 10.1016/j.molliq.2017.03.101

BAHADUR, I., KGOMOTSO, M., EBENSO, E. E. & REDHI, G. 2016. Influence of temperature on molecular interactions of imidazolium-based ionic liquids with acetophenone: thermodynamic properties and quantum chemical studies. *RSC Advances,* 6**,** 104708-104723.DOI 10.1039/c6ra15476j

BARBOSA, R. D. 2003. *High pressure and temperature dependence of thermodynamic properties of model food solutions obtained from in situ ultrasonic measurements.* PhD Dissertation. University of Florida.

BATES, E. D., MAYTON, R. D., NTAI, I. & DAVIS, J. H. 2002. CO*2* capture by a task-specific ionic liquid. *Journal of the American Chemical Society,* 124**,** 926-927.DOI 10.1021/ja017593d

BENSON, G. C. & KIYOHARA, O. 1976. Thermodynamic properties of some cycloalkane-cycloalkanol systems at 298.15 K. 4. Excess volumes. *Journal of Chemical and Engineering Data,* 21**,** 362-365

BICH, W., COX, M. G., DYBKAER, R., ELSTER, C., ESTLER, W. T., HIBBERT, B., IMAI, H., KOOL, W., MICHOTTE, C. & NIELSEN, L. 2012. Revision of the 'Guide to the expression of uncertainty in measurement'. *Metrologia,* 49**,** 702

BONHÔ, P. 1996. te, A.-P. Dias, N. Papageorgiou, K. Kalyanasundaram, M. Grä, tzel. *Inorg. Chem,* 35**,** 10.1021

BONHOTE, P., DIAS, A. P., PAPAGEORGIOU, N., KALYANASUNDARAM, K. & GRATZEL, M. 1996. Hydrophobic, Highly Conductive Ambient-Temperature Molten Salts. *Inorg Chem,* 35**,** 1168-1178.DOI 10.1021/ic951325x

BROCOS, P., PINEIRO, A., BRAVO, R. & AMIGO, A. 2003. Refractive indices, molar volumes and molar refractions of binary liquid mixtures: concepts and correlations. *Physical Chemistry Chemical Physics,* 5**,** 550-557.DOI 10.1039/b208765k

BRUCE, P. G., FREUNBERGER, S. A., HARDWICK, L. J. & TARASCON, J.-M. 2012. Li-O2 and Li-S batteries with high energy storage. *Nature Materials,* 11**,** 19

CALADO, M., IVANIS, G., VUKSANOVIC, J., KIJEVCANIN, M. L., SERBANOVIC, S. & VISAK, Z. 2013. "Green Meets Green"–Sustainable solutions of imidazolium and phosphonium ionic liquids with poly (ethylene glycol): Solubility and phase behavior. *Fluid Phase Equilibria,* 344**,** 6-12

CAPELO, S. B., MENDEZ-MORALES, T., CARRETE, J., LOPEZ LAGO, E., VILA, J., CABEZA, O., RODRIGUEZ, J. R., TURMINE, M. & VARELA, L. M. 2012. Effect of temperature and cationic

chain length on the physical properties of ammonium nitrate-based protic ionic liquids. *J Phys Chem B,* 116**,** 11302-12.DOI 10.1021/jp3066822

CARISSIMI, G. N., MONTALBÁN, M. G., DÍAZ BAÑOS, F. G. & VÍLLORA, G. 2019. Density, Refractive Index and Volumetric Properties of Water–Ionic Liquid Binary Systems with Imidazolium-Based Cations and Tetrafluoroborate, Triflate and Octylsulfate Anions at T= 293 to 343 K and p= 0.1 MPa. *Journal of Chemical & Engineering Data,*

CARMICHAEL, A. J. & SEDDON, K. R. 2000. Polarity study of some 1-alkyl-3-methylimidazolium ambient-temperature ionic liquids with the solvatochromic dye, Nile Red. *Journal of Physical Organic Chemistry,* 13**,** 591-595

ÇENGEL, Y. and GHARAJ A. 2014. *Heat and mass transfer: fundamentals and applications*, McGraw-Hill Higher Education.

CHEN, C. Y., EVEN, M. A., WANG, J. & CHEN, Z. 2002. Sum frequency generation vibrational Spectroscopy studies on molecular conformation of liquid polymers poly(ethylene glycol) and poly(propylene glycol) at different interfaces. *Macromolecules,* 35**,** 9130-9135.DOI 10.1021/ma020614j

CHEN, J., SPEAR, S. K., HUDDLESTON, J. G. & ROGERS, R. D. 2005. Polyethylene glycol and solutions of polyethylene glycol as green reaction media. *Green Chemistry,* 7**,** 64-82.10.1039/b413546f

CHIAPPE, C. & PIERACCINI, D. 2005. Ionic liquids: solvent properties and organic reactivity. *Journal of Physical Organic Chemistry,* 18**,** 275-297.DOI 10.1002/poc.863

CHUM, H. L., KOCH, V. R., MILLER, L. L. & OSTERYOUNG, R. A. 1975. Electrochemical Scrutiny of Organometallic Iron Complexes and Hexamethylbenzene in a Room-Temperature Molten-Salt. *Journal of the American Chemical Society,* 97**,** 3264-3265.DOI 10.1021/ja00844a081

CIOCIRLAN, O., CROITORU, O. & IULIAN, O. 2011. Densities and Viscosities for Binary Mixtures of 1-Butyl-3-Methylimidazolium Tetrafluoroborate Ionic Liquid with Molecular Solvents. *Journal of Chemical and Engineering Data,* 56**,** 1526-1534.DOI 10.1021/je101206u

CIOCIRLAN, O., CROITORU, O. & LULIANT, O. 2014. Density and Refractive Index of Binary Mixtures of Two 1-Alkyl-3-methylimidazolium Ionic Liquids with 1,4-Dioxane and Ethylene Glycol. *Journal of Chemical and Engineering Data,* 59**,** 1165-1174.DOI 10.1021/je400659p

COHEN, Y. 1996. Volatile organic compounds in the environment: A multimedia perspective. *Volatile organic compounds in the environment.* ASTM International.

DANESHVAR, A. & MOOSAVI, M. 2016. A Study of the Transport Properties of [Bmim] BF4 and PEG Mixtures Using Diffusion-Ordered NMR and UV–Visible Spectroscopy Techniques. *Industrial & Engineering Chemistry Research,* 55**,** 6517-6529

DÁVILA, M. A. J., APARICIO, S. & ALCALDE, R. 2009. Thermophysical properties of binary and ternary mixtures containing lactams and methanol. *Industrial & Engineering Chemistry Research,* 48**,** 10065-10076

DE AZEVEDO, R. G., SZYDLOWSKI, J., PIRES, P., ESPERANÇA, J., GUEDES, H. & REBELO, L. 2004. A novel non-intrusive microcell for sound-speed measurements in liquids. Speed of sound and thermodynamic properties of 2-propanone at pressures up to 160 MPa. *The Journal of Chemical Thermodynamics,* 36**,** 211-222

DEENADAYALU, N. & BHUJRAJH, P. 2006. Excess molar volumes and partial molar volumes for (propionitrile+ an alkanol) at T= 298.15 K and p= 0.1 MPa. *The Journal of Chemical Thermodynamics,* 38**,** 278-282

DEETLEFS, M. & SEDDON, K. R. 2003. Improved preparations of ionic liquids using microwave irradiation. *Green Chemistry,* 5**,** 181-186.DOI 10.1039/b300071k

DESNOYERS, J. E. & PERRON, G. 1997. Treatment of excess thermodynamic quantities for liquid mixtures. *Journal of Solution Chemistry,* 26**,** 749-755.DOI 10.1007/Bf02767781

DHUMAL, N. R., KIM, H. J. & KIEFER, J. 2011. Electronic structure and normal vibrations of the 1-ethyl-3-methylimidazolium ethyl sulfate ion pair. *J Phys Chem A,* 115**,** 3551-8.10.1021/jp1122322

DOMANSKA, U. & KROLIKOWSKA, M. 2010. Effect of temperature and composition on the surface tension and thermodynamic properties of binary mixtures of 1-butyl-3-methylimidazolium thiocyanate with alcohols. *Journal of Solution Chemistry,* 348**,** 661-667.DOI 10.1016/j.jcis.2010.04.060

DOMAŃSKA, U., POBUDKOWSKA, A. & WIŚNIEWSKA, A. 2006. Solubility and excess molar properties of 1, 3-dimethylimidazolium methylsulfate, or 1-butyl-3-methylimidazolium methylsulfate, or 1-butyl-3-methylimidazolium octylsulfate ionic liquids with n-alkanes and alcohols: Analysis in terms of the PFP and FBT models. *Journal of Solution Chemistry,* 35**,** 311-334

DOUHÉRET, G., DAVIS, M. I., REIS, J. C. R. & BLANDAMER, M. J. 2001. Isentropic compressibilities—experimental origin and the quest for their rigorous estimation in thermodynamically ideal liquid mixtures. *Chem. Phys. Chem,* 2**,** 148-161

DUPONT, J. 2004. On the solid, liquid and solution structural organization of imidazolium ionic liquids. *Journal of the Brazilian Chemical Society,* 15**,** 341-350.Doi 10.1590/S0103-50532004000300002

ENDRES, F. & ZEIN EL ABEDIN, S. 2006. Air and water stable ionic liquids in physical chemistry. *Phys Chem Chem Phys,* 8**,** 2101-16.DOI 10.1039/b600519p

FICKE, L. E., NOVAK, R. R. & BRENNECKE, J. F. 2010. Thermodynamic and Thermophysical Properties of Ionic Liquid plus Water Systems. *Journal of Chemical and Engineering Data,* 55**,** 4946-4950.DOI 10.1021/je100522z

FORT, D. A., SWATLOSKI, R. P., MOYNA, P., ROGERS, R. D. & MOYNA, G. 2006. Use of ionic liquids in the study of fruit ripening by high-resolution 13C NMR spectroscopy:'green'solvents meet green bananas. *Chemical Communications***,** 714-716

FORTIN, T. J., LAESECKE, A., FREUND, M. & OUTCALT, S. 2013. Advanced calibration, adjustment, and operation of a density and sound speed analyzer. *Journal of Chemical Thermodynamics,* 57**,** 276-285.DOI 10.1016/j.jct.2012.09.009

FOX, D. M., GILMAN, J. W., MORGAN, A. B., SHIELDS, J. R., MAUPIN, P. H., LYON, R. E., DE LONG, H. C. & TRULOVE, P. C. 2008. Flammability and thermal analysis characterization of imidazolium-based ionic liquids. *Industrial & Engineering Chemistry Research,* 47**,** 6327-6332.10.1021/ie800665u

FRANCESCONI, R., BIGI, A., RUBINI, K. & COMELLI, F. 2007. Molar heat capacities, densities, viscosities, and refractive indices of poly(ethylene glycols)+2-methyltetrahydrofuran at (293.15, 303.15, and 313.15) K. *Journal of Chemical and Engineering Data,* 52**,** 2020-2025.DOI 10.1021/je7003066

FRÖBA, A. P., KREMER, H. & LEIPERTZ, A. 2008. Density, refractive index, interfacial tension, and viscosity of ionic liquids [EMIM][EtSO4],[EMIM][NTf2],[EMIM][N (CN) 2], and [OMA][NTf2] in dependence on temperature at atmospheric pressure. *The Journal of Physical Chemistry B,* 112**,** 12420-12430

GABRIEL, S. & WEINER, J. 1888. Ueber einige abkömmlinge des propylamins. *Berichte der deutschen chemischen Gesellschaft,* 21**,** 2669-2679

GARDAS, R. L. & COUTINHO, J. A. P. 2008. Extension of the Ye and Shreeve group contribution method for density estimation of ionic liquids in a wide range of temperatures and pressures. *Fluid Phase Equilibria,* 263**,** 26-32.DOI 10.1016/j.fluid.2007.09.016

GARDAS, R. L., FREIRE, M. G., CARVALHO, P. J., MARRUCHO, I. M., FONSECA, I. M. A., FERREIRA, A. G. M. & COUTINHO, J. A. P. 2007. High-pressure densities and derived thermodynamic properties of imidazolium-based ionic liquids. *Journal of Chemical and Engineering Data,* 52**,** 80-88.DOI 10.1021/je060247x

GHOTLI, R. A., AZIZ, A. R. A., ATADASHI, I. M., HASAN, D. B., KONG, P. S. & AROUA, M. K. 2015. Selected physical properties of binary mixtures of crude glycerol and methanol at various temperatures. *Journal of Industrial and Engineering Chemistry,* 21**,** 1039-1043.DOI 10.1016/j.jiec.2014.05.013

GIRIDHAR, P., VENKATESAN, K. A., SRINIVASAN, T. G. & RAO, P. R. V. 2007. Electrochemical behavior of uranium(VI) in 1-butyl-3-methylimidazolium chloride and thermal characterization of uranium oxide deposit. *Electrochimica Acta,* 52**,** 3006-3012.DOI 10.1016/j.electacta.2006.09.038

GONZÁLEZ, E. J., GONZÁLEZ, B., CALVAR, N. & DOMÍNGUEZ, Á. 2007. Physical properties of binary mixtures of the ionic liquid 1-ethyl-3-methylimidazolium ethyl sulfate with several alcohols at T=(298.15, 313.15, and 328.15) K and atmospheric pressure. *Journal of Chemical & Engineering Data,* 52**,** 1641-1648

GOODENOUGH, J. B. & PARK, K. S. 2013. The Li-ion rechargeable battery: a perspective. *J Am Chem Soc,* 135**,** 1167-76.DOI 10.1021/ja3091438

GOVINDA, V., REDDY, P. M., ATTRI, P., VENKATESU, P. & VENKATESWARLU, P. 2013. Influence of anion on thermophysical properties of ionic liquids with polar solvent. *Journal of Chemical Thermodynamics,* 58**,** 269-278.DOI 10.1016/j.jct.2012.11.014

GOVINDA, V., VASANTHA, T., KHAN, I. & VENKATESU, P. 2015. Effect of the Alkyl Chain Length of the Cation on the Interactions between Water and Ammonium-Based Ionic Liquids: Experimental and COSMO-RS Studies. *Industrial & Engineering Chemistry Research,* 54**,** 9013-9026.DOI 10.1021/acs.iecr.5b01796

GOVINDA, V., VENKATESU, P. & BAHADUR, I. 2016. Molecular interactions between ammonium-based ionic liquids and molecular solvents: current progress and challenges. *Physical Chemistry Chemical Physics,* 18**,** 8278-8326.DOI 10.1039/c6cp00199h

GU, Z. Y. & BRENNECKE, J. F. 2002. Volume expansivities and isothermal compressibilities of imidazolium and pyridinium-based ionic liquids. *Journal of Chemical and Engineering Data,* 47**,** 339-345.DOI 10.1021/je010242u

GUSAIN, R., PANDA, S., BAKSHI, P. S., GARDAS, R. L. & KHATRI, O. P. 2018. Thermophysical properties of trioctylalkylammonium bis(salicylato) borate ionic liquids: Effect of alkyl chain length. *Journal of Molecular Liquids,* 269**,** 540-546.10.1016/j.molliq.2018.08.083

HANDA, Y. P. & BENSON, G. C. 1979. Volume changes on mixing two liquids: A review of the experimental techniques and the literature data. *Fluid Phase Equilibria,* 3**,** 185-249

HARRIS, Z. & ZALIPSKY, S. 1997. *Poly(ethylene Glycol)*, American Chemical Society Staff.Poly (ethylene glycol). Vol. Washingtonn,DC: *American Chemical Society*, 1997.

HASIB-UR-RAHMAN, M., SIAJ, M. & LARACHI, F. 2010. Ionic liquids for CO_2 capture—development and progress. *Chemical Engineering and Processing: Process Intensification,* 49**,** 313-322

HASNIP, P. J., REFSON, K., PROBERT, M. I., YATES, J. R., CLARK, S. J. & PICKARD, C. J. 2014. Density functional theory in the solid state. *Philos Trans A Math Phys Eng Sci,* 372**,** 20130270.DOI 10.1098/rsta.2013.0270

HAYAMIZU, K., AIHARA, Y., NAKAGAWA, H., NUKUDA, T. & PRICE, W. S. 2004. Ionic conduction and ion diffusion in binary room-temperature ionic liquids composed of [emim][BF4] and LiBF4. *Journal of Physical Chemistry B,* 108**,** 19527-19532.DOI 10.1021/jp0476601

HEISEL, M. & BELLONI, A. 1991. Options available in the Solinox vent gas purification process. *Gas Separation & Purification,* 5**,** 111-113

HELDEBRANT, D. J., WITT, H. N., WALSH, S. M., ELLIS, T., RAUSCHER, J. & JESSOP, P. G. 2006. Liquid polymers as solvents for catalytic reductions. *Green Chemistry,* 8**,** 807-815.DOI 10.1039/b605405f

HEROLD, D. A., KEIL, K. & BRUNS, D. E. 1989. Oxidation of polyethylene glycols by alcohol dehydrogenase. *Biochem Pharmacol,* 38**,** 73-6.DOI 10.1016/0006-2952(89)90151-2

HESS, W. T., KURTZ, A. & STANTON, D. 1995. Kirk-Othmer encyclopedia of chemical technology. Wiley, New York.

HIRSEHFELDER, J. O., CURTISS, C. F. & BIRD, R. B. 1954. Molecular theory of gases and liquids. *New York,* J. Wiley.

HUANG, X., MARGULIS, C. J., LI, Y. & BERNE, B. J. 2005. Why is the partial molar volume of CO2 so small when dissolved in a room temperature ionic liquid? Structure and dynamics of CO2 dissolved in [Bmim+][PF6-]. *Journal of the American Chemical Society,* 127**,** 17842-17851

HUDDLESTON, J. G., VISSER, A. E., REICHERT, W. M., WILLAUER, H. D., BROKER, G. A. & ROGERS, R. D. 2001. Characterization and comparison of hydrophilic and hydrophobic room temperature ionic liquids incorporating the imidazolium cation. *Green Chemistry,* 3**,** 156-164.DOI 10.1039/b103275p

HUO, Y., XIA, S. & MA, P. 2007. Densities of ionic liquids, 1-butyl-3-methylimidazolium hexafluorophosphate and 1-butyl-3-methylimidazolium tetrafluoroborate, with benzene, acetonitrile, and 1-propanol at T=(293.15 to 343.15) K. *Journal of Chemical & Engineering Data,* 52**,** 2077-2082

IGLESIAS-OTERO, M., TRONCOSO, J., CARBALLO, E. & ROMANI, L. 2007. Density and refractive index for binary systems of the ionic liquid [Bmim][BF 4] with methanol, 1, 3-dichloropropane, and dimethyl carbonate. *Journal of Solution Chemistry,* 36**,** 1219

IGLESIAS-OTERO, M. A., TRONCOSO, J., CARBALLO, E. & ROMANI, L. 2008. Density and refractive index in mixtures of ionic liquids and organic solvents: Correlations and predictions. *Journal of Chemical Thermodynamics,* 40**,** 949-956.DOI 10.1016/j.jct.2008.01.023

JAMAL, M. A., KHOSA, M. K., NASEEM, B., ZAHEER-UD-DIN, M. & MUNEER, M. 2016. Excess molar volume and isentropic compressibility of monoethanolamine in aqueous system at temperatures from 298.15 to 318.15 K. *Physics and Chemistry of Liquids,* 54**,** 384-393.10.1080/00319104.2015.1109993

KALLIDANTHIYIL CHELLAPPAN, L. 2012. Synthesis of ionic liquids based on new cationic cores.

KAVITHA, T., ATTRI, P., VENKATESU, P., DEVI, R. S. & HOFMAN, T. 2012a. Influence of alkyl chain length and temperature on thermophysical properties of ammonium-based ionic liquids with molecular solvent. *J Phys Chem B,* 116**,** 4561-74.DOI 10.1021/jp3015386

KAVITHA, T., ATTRI, P., VENKATESU, P., DEVI, R. S. R. & HOFMAN, T. 2012b. Influence of temperature on thermophysical properties of ammonium ionic liquids with N-methyl-2-pyrrolidone. *Thermochimica Acta,* 545**,** 131-140.DOI 10.1016/j.tca.2012.07.004

KAVITHA, T., ATTRI, P., VENKATESU, P., DEVI, R. S. R. & HOFMAN, T. 2012c. Temperature dependence measurements and molecular interactions for ammonium ionic liquid with N-methyl-2-pyrrolidone. *Journal of Chemical Thermodynamics,* 54**,** 223-237.DOI10.1016/j.jct.2012.03.034

KAVITHA, T., VASANTHA, T., VENKATESU, P., DEVI, R. S. R. & HOFMAN, T. 2014. Thermophysical properties for the mixed solvents of N-methyl-2-pyrrolidone with some of the imidazolium-based ionic liquids. *Journal of Molecular Liquids,* 198**,** 11-20.DOI 10.1016/j.molliq.2014.07.002

KAWAIZUMI, F., OHNO, M. & MIYAHARA, Y. 1977. Ultrasonic and Volumetric Investigation of Aqueous-Solutions of Amides. *Bulletin of the Chemical Society of Japan,* 50**,** 2229-2233.DOI 10.1246/bcsj.50.2229

KESKIN, S., KAYRAK-TALAY, D., AKMAN, U. & HORTACSU, O. 2007. A review of ionic liquids towards supercritical fluid applications. *Journal of Supercritical Fluids,* 43**,** 150-180.DOI 10.1016/j.supflu.2007.05.013

KIM, I. W., JANG, M. D., RYU, Y. K., CHO, E. H., LEE, Y. K. & PARK, J. H. 2002. Dipolarity, hydrogen-bond basicity and hydrogen-bond acidity of aqueous poly(ethylene glycol) solutions. *Anal Sci,* 18**,** 1357-60.DOI 10.2116/analsci.18.1357

KIYOHARA, O., DARCY, P. J. & BENSON, G. C. 1979. Ultrasonic Velocities, Compressibilities, and Heat-Capacities of Water + Tetrahydrofuran Mixtures at 298.15 K. *Canadian Journal of Chemistry-Revue Canadienne De Chimie,* 57**,** 1006-1010.DOI 10.1139/v79-167

KOLBECK, C., LEHMANN, J., LOVELOCK, K. R., CREMER, T., PAAPE, N., WASSERSCHEID, P., FROBA, A. P., MAIER, F. & STEINRUCK, H. P. 2010. Density and surface tension of ionic liquids. *J Phys Chem B,* 114**,** 17025-36.DOI 10.1021/jp1068413

KOOHYAR, F. 2013. Refractive index and its applications. *J. Thermodyn Catal.,* 4**,** 117

KRESTOV, G. A. 1991. *Thermodynamics of solvation*, Ellis Horwood.

KRISHNA, T. S., NARENDRA, K., GOWRISANKAR, M., NAIN, A. K. & MUNIBHADRAYYA, B. 2017. Physicochemical and spectroscopic studies of molecular interactions of 1-butyl-3-methylimidazolium hexafluorophosphate+2-methoxyethanol or 2-ethoxyethanol binary mixtures at temperatures from 298.15 to 323.15 K. *Journal of Molecular Liquids,* 227**,** 333-350.DOI 10.1016/j.molliq.2016.11.066

KRISHNA, T. S., RAJU, K. T. S. S., GOWRISANKAR, M., NAIN, A. K. & MUNIBHADRAYYA, B. 2016. Volumetric, ultrasonic and spectroscopic studies of molecular interactions in binary mixtures of 1-butyl-3-methylimidazolium hexafluorophosphate with 2-propoxyethanol at temperatures from 298.15 to 323.15 K. *Journal of Molecular Liquids,* 216**,** 484-495.DOI 10.1016/j.molliq.2016.01.085

KUMAR, P. K., GOVINDA, V., SREENUVASULU, K., VENKATESU, P., BAHADUR, I. & EBENSO, E. E. 2016. A study of the molecular interactions between ammonium-based ionic liquids and N,N-dimethylacetamide. *Journal of Molecular Liquids,* 223**,** 687-698.DOI 10.1016/j.molliq.2016.08.069

LAPKIN, A. A., PLUCINSKI, P. K. & CUTLER, M. 2006. Comparative assessment of technologies for extraction of artemisinin. *J Nat Prod,* 69**,** 1653-64.DOI 10.1021/np060375j

LAUS, G., BENTIVOGLIO, G., SCHOTTENBERGER, H., KAHLENBERG, V., KOPACKA, H., RÖDER, T. & SIXTA, H. 2005. Ionic liquids: current developments, potential and drawbacks for industrial applications. *Lenzinger Berichte,* 84**,** 71-85

LODGE, T. P. 2008. Materials science. A unique platform for materials design. *Science,* 321**,** 50-1.DOI 10.1126/science.1159652

LÓPEZ, N. & ILLAS, F. 1998. Ab initio modeling of the metal− support interface: The interaction of Ni, Pd, and Pt on MgO (100). *The Journal of Physical Chemistry B,* 102**,** 1430-1436

MANOJ, D., THEYAGARAJAN, K., SARAVANAKUMAR, D., SENTHILKUMAR, S. & THENMOZHI, K. 2018. Aldehyde functionalized ionic liquid on electrochemically reduced graphene oxide as a versatile platform for covalent immobilization of biomolecules and biosensing. *Biosensors & Bioelectronics,* 103**,** 104-112.DOI 10.1016/j.bios.2017.12.030

MARSH, K., BOXALL, J. & LICHTENTHALER, R. 2004. Room temperature ionic liquids and their mixtures—a review. *Fluid Phase Equilibria,* 219**,** 93-98

MASAKI, T., NISHIKAWA, K. & SHIROTA, H. 2010. Microscopic study of ionic liquid-H2O systems: alkyl-group dependence of 1-alkyl-3-methylimidazolium cation. *J Phys Chem B,* 114**,** 6323-31.DOI 10.1021/jp1017967

MATKOWSKA, D. & HOFMAN, T. 2013. Volumetric properties of the ionic liquids: [C(6)mim][MeSO4], [C(6)mim][EtSO4], [C(4)mim][EtSO4] and their mixtures with methanol or ethanol. *Journal of Molecular Liquids,* 177**,** 301-305.10.1016/j.molliq.2012.09.024

MCCRARY, P. D. & ROGERS, R. D. 2013. 1-Ethyl-3-methylimidazolium hexafluorophosphate: from ionic liquid prototype to antitype. *Chem Commun (Camb),* 49**,** 6011-4.DOI 10.1039/c3cc42175a

MERRITT, H. E. 1967. *Hydraulic control systems*, John Wiley & Sons.

MICHELSON, A. A. 1891. XXXVIII. On the application of interference-methods to spectroscopic measurements.—I. *The London, Edinburgh, and Dublin Philosophical Magazine and Journal of Science,* 31**,** 338-346

MIKKOLA, J.-P. T., VIRTANEN, P. P., KORDÁS, K., KARHU, H. & SALMI, T. O. 2007. SILCA—supported ionic liquid catalysts for fine chemicals. *Applied Catalysis A: General,* 328**,** 68-76

MIRGANE, S. S. P. S. R. 2011. Thermodyanmic Properties of Binary Liquid Mixtures of Industrially important Acrylic Esters with Octane-1-Ol at Different Temperatures. *Pharmaceutical Research,* 2**,** 72-82

MOHAMMADI, L. & OMRANI, A. 2018. Density, refractive index, and excess properties of sulfolane and alkanediols binary mixtures at different temperatures. *Journal of Thermal Analysis and Calorimetry,* 131**,** 1527-1543.DOI 10.1007/s10973-017-6702-9

MOHAMMED, M. 2016. Viscosity and density of asymmetric hydrocarbon mixtures. Semantic Scholar. Corpus ID: 99957628

MONTALBAN, M. G., BOLIVAR, C. L., BANOS, F. G. D. & VILLORA, G. 2015. Effect of Temperature, Anion, and Alkyl Chain Length on the Density and Refractive Index of 1-Alkyl-3-methylimidazolium-Based Ionic Liquids. *Journal of Chemical and Engineering Data,* 60**,** 1986-1996.10.1021/je501091q

MOOSAVI, M., DANESHVAR, A. & SEDGHAMIZ, E. 2015. Rheological properties of {[bmim]PF6 + methanol} mixtures at different temperatures, shear rates and compositions. *Journal of Molecular Liquids,* 209**,** 693-705.DOI 10.1016/j.molliq.2015.05.029

MRAD, S., LAFUENTE, C., HICHRI, M. & KHATTECH, I. 2016. Density, Speed of Sound, Refractive Index, and Viscosity of the Binary Mixtures of N,N-dimethylacetamide with Methanol and Ethanol. *Journal of Chemical and Engineering Data,* 61**,** 2946-2953.10.1021/acs.jced.5b01000

MULDOON, M. J., AKI, S. N., ANDERSON, J. L., DIXON, J. K. & BRENNECKE, J. F. 2007. Improving carbon dioxide solubility in ionic liquids. *J Phys Chem B,* 111**,** 9001-9.DOI 10.1021/jp071897q

NAVIA, P., TRONCOSO, J. & ROMANI, L. 2008. Viscosities for ionic liquid binary mixtures with a common ion. *Journal of Solution Chemistry,* 37**,** 677-688.10.1007/s10953-008-9260-8

NAYEEM, M., KONDAIAH, M., SREEKANTH, K. & KRISHNA RAO, D. 2014. Thermoacoustic, volumetric, and viscometric investigations in binary liquid system of cyclohexanone with benzyl benzoate at T= 308.15, 313.15, and 318.15 K. *Journal of Thermodynamics,* 2014

NEUKERMANS, S. 2015. *Thermophysical properties of mixtures of imidazolium-based ionic liquids with alcohols.* Masters in Science Dissertation. Universitat de València.

PAL, A., GABA, R., SINGH, T. & KUMAR, A. 2010. Excess thermodynamic properties of binary mixtures of ionic liquid (1-butyl-3-methylimidazolium hexafluorophosphate) with alkoxyalkanols at several temperatures. *Journal of Molecular Liquids,* 154**,** 41-46.DOI 10.1016/j.molliq.2010.03.018

PAL, A. & KUMAR, B. 2011. Volumetric, acoustic and spectroscopic studies for binary mixtures of ionic liquid (1-butyl-3-methylimidazolium hexafluorophosphate) with alkoxyalkanols at T=(288.15 to 318.15) K. *Journal of Molecular Liquids,* 163**,** 128-134

PAL, A. & KUMAR, B. 2012. Volumetric and Acoustic Properties of Binary Mixtures of the Ionic Liquid 1-Butyl-3-methylimidazolium Tetrafluoroborate [bmim][BF4] with Alkoxyalkanols at Different Temperatures. *Journal of Chemical and Engineering Data,* 57**,** 688-695.DOI 10.1021/je2010209

PAL, A., SAINI, M. & KUMAR, B. 2016. Volumetric, ultrasonic and spectroscopic (FT-IR) studies for the binary mixtures of imidazolium based ILs with 1,2-propanediol. *Fluid Phase Equilibria,* 411**,** 66-73.DOI 10.1016/j.fluid.2015.12.007

PANDEY, P. K. 2012. *Acoustic and Spectroscopic studies of multicomponent liquid mixtures.* PhD Dissertation. University of Lucknow Lucknow.

PANDEY, P. K., AWASTHI, A. & AWASTHI, A. 2013. Intermolecular interactions in binary mixtures of 2-Chloroethanol with 2-Dimethylaminoethanol and 2-Diethylaminoethanol at different temperatures. *Chemical Physics,* 423**,** 119-126.DOI 10.1016/j.chemphys.2013.06.025

PAPARI, M., GHODRATI, H., FADAEI, F., SADEGHI, R., BEHROUZ, S., RAD, M. S. & MOGHADASI, J. 2013. Volumetric and ultrasonic study of mixtures of 2-phenylethanol with 1-butanol, 2-butanol, and 2-methyl-1-butanol at T=(298.15–323.15) K and atmospheric pressure: measurement and prediction. *Journal of Molecular Liquids,* 180**,** 121-128

PEREIRO, A., TOJO, E., RODRıGUEZ, A., CANOSA, J. & TOJO, J. 2006. Properties of ionic liquid HMIMPF 6 with carbonates, ketones and alkyl acetates. *The Journal of Chemical Thermodynamics,* 38**,** 651-661

PHILIPPOVA, O. E., KUCHANOV, S. I., TOPCHIEVA, I. N. & KABANOV, V. A. 1985. Hydrogen-Bonds in Dilute-Solutions of Poly(Ethylene Glycol). *Macromolecules,* 18**,** 1628-1633.DOI 10.1021/ma00150a018

PIRES, J., TIMPERMAN, L., JACQUEMIN, J., BALDUCCI, A. & ANOUTI, M. 2013. Density, conductivity, viscosity, and excess properties of (pyrrolidinium nitrate-based Protic Ionic Liquid plus propylene carbonate) binary mixture. *Journal of Chemical Thermodynamics,* 59**,** 10-19.10.1016/j.jct.2012.11.020

PLECHKOVA, N. V., ROGERS, R. D. & SEDDON, K. R. 2010. *Ionic liquids: from knowledge to application,* ACS Publications.

PLECHKOVA, N. V. & SEDDON, K. R. 2008. Applications of ionic liquids in the chemical industry. *Chem Soc Rev,* 37**,** 123-50.DOI 10.1039/b006677j

RAJPUT, D. S., YAMADA, K. & SEKHON, S. S. 2013. Study of ion diffusional motion in ionic liquid-based polymer electrolytes by simultaneous solid state NMR and DTA. *J Phys Chem B,* 117**,** 2475-81.DOI 10.1021/jp3116512

RAO, G. V. R., SARMA, A. V. & RAMBABU, C. 2004. Evaluation of excess thermodynamic properties in some binary mixtures of o-chlorophenol. *Indian Journal of Chemistry Section a-Inorganic Bio-Inorganic Physical Theoretical & Analytical Chemistry,* 43**,** 2518-2528

REDDY, M. S., NAYEEM, S. M., SOUMINI, C., RAJU, K. T. S. & BABU, B. H. 2016a. Study of molecular interactions in binary liquid mixtures of [Emim][BF4] with 2-methoxyethanol using thermo acoustic, volumetric and optical properties. *Thermochimica Acta,* 630**,** 37-49

REDDY, M. S., NAYEEM, S. M., SOUMINI, C., RAJU, K. T. S. & BABU, B. H. 2016b. Study of molecular interactions in binary liquid mixtures of [Emim][BF 4] with 2-methoxyethanol using thermo acoustic, volumetric and optical properties. *Thermochimica Acta,* 630**,** 37-49

REDLICH, O. & KISTER, A. 1948. Algebraic representation of thermodynamic properties and the classification of solutions. *Industrial & Engineering Chemistry,* 40**,** 345-348

REIS, J. C., LAMPREIA, I. M., SANTOS, A. F., MOITA, M. L. & DOUHERET, G. 2010. Refractive index of liquid mixtures: theory and experiment. *Chem. Phys. Chem,* 11**,** 3722-33.DOI 10.1002/cphc.201000566

REZAEI-SAMETI, M. & RAKHSHI, M. 2017. Excess thermodynamic parameters for binary and ternary mixtures of {1-butanol (1) + cyclohexylamine (2) + n-heptane (3)} at different temperatures: A theoretical study. *Arabian Journal of Chemistry,* 10**,** S691-S699.DOI 10.1016/j.arabjc.2012.11.010

RODRIGUEZ, H., FRANCISCO, M., RAHMAN, M., SUN, N. & ROGERS, R. D. 2009. Biphasic liquid mixtures of ionic liquids and polyethylene glycols. *Physical Chemistry Chemical Physics,* 11**,** 10916-10922.DOI 10.1039/b916990c

ROY, M. N., EKKA, D. & DEWAN, R. 2011. Physico-Chemical Studies of Some Bio-active Solutes in Pure Methanoic Acid. *Acta Chimica Slovenica,* 58**,** 792-796

ROY, M. N., SAH, R. S. & PRADHAN, P. 2010. Densities, Viscosities, Sound Speeds, Refractive Indices, and Excess Properties of Binary Mixtures of Isoamyl Alcohol with Some Alkoxyethanols. *International Journal of Thermophysics,* 31**,** 316-326.DOI 10.1007/s10765-010-0719-7

ROY, M. N., SINHA, B. & DAKUA, V. K. 2006. Excess molar volumes and viscosity deviations of binary liquid mixtures of 1,3-dioxolane and 1,4-dioxane with butyl acetate, butyric acid, butylamine, and 2-butanone at 298.15 K. *Journal of Chemical and Engineering Data,* 51**,** 590-594.DOI 10.1021/je0504109

SALINAS, R., PLA-FRANCO, J., LLADOSA, E. & MONTON, J. B. 2015. Density, Speed of Sound, Viscosity, and Excess Properties of Binary Mixtures Formed by Ethanol and Bis(trifluorosulfonyl)imide-Based Ionic Liquids. *Journal of Chemical and Engineering Data,* 60**,** 525-540.DOI 10.1021/je500594z

SCHRÖDER, U., WADHAWAN, J. D., COMPTON, R. G., MARKEN, F., SUAREZ, P. A., CONSORTI, C. S., DE SOUZA, R. F. & DUPONT, J. 2000. Water-induced accelerated ion diffusion: voltammetric studies in 1-methyl-3-[2, 6-(S)-dimethylocten-2-yl] imidazolium tetrafluoroborate, 1-butyl-3-methylimidazolium tetrafluoroborate and hexafluorophosphate ionic liquids. *New Journal of Chemistry,* 24**,** 1009-1015

SHAFAATI, S. & ALMASI, M. 2017. Influence of Temperature and Carbon Chain on Thermophysical Properties of Benzaldehyde/Alkan-2-ol Binary Mixtures. *Journal of Chemical and Engineering Data,* 62**,** 2406-2412.DOI 10.1021/acs.jced.7b00335

SHARRNA, M., RANA, S. & SHARMA, A. 2010. Excess Viscosity and Compressibility of Binary Mixtures of Methanol with Acetonitrile and Dimethyl Formamide at Different Temperatures. *Iranica Journal of Energy & Environment,* 50**,** 280-286

SIMONE, P. M. & LODGE, T. P. 2009. Phase behavior and ionic conductivity of concentrated solutions of polystyrene-poly(ethylene oxide) diblock copolymers in an ionic liquid. *ACS Appl Mater Interfaces,* 1**,** 2812-20.DOI 10.1021/am900555f

SINGH, D. K., SRIVASTAVA, S. K., SCHLÜCKER, S., SINGH, R. K. & ASTHANA, B. 2011. Self-association and hydrogen bonding of propionaldehyde in binary mixtures with water and methanol investigated by concentration-dependent polarized Raman study and DFT calculations. *Journal of Raman Spectroscopy,* 42**,** 851-858

SMIGLAK, M., METLEN, A. & ROGERS, R. D. 2007. The second evolution of ionic liquids: from solvents and separations to advanced materials--energetic examples from the ionic liquid cookbook. *Acc Chem Res,* 40**,** 1182-92.DOI 10.1021/ar7001304

SMITH, J., VAN NESS, H. & ABBOTT, M. 2005. Vapor/Liquid Equilibrium: Introduction. Introduction to Chemical Engineering Thermodynamics. Singapore: McGraw Hill. p.

SOLDATOVIC, D. A., VUKSANOVIC, J. M., RADOVIC, I. R. & KIJEVCANIN, M. L. 2016. Thermodynamic and spectroscopic interpretation of molecular interactions of nicotine plus alcohol binary mixtures. *Journal of Chemical Thermodynamics,* 102**,** 105-129.DOI 10.1016/j.jct.2016.07.005

SORIANO, A. N., DOMA, B. T. & LI, M. H. 2009. Measurements of the density and refractive index for 1-n-butyl-3-methylimidazolium-based ionic liquids. *Journal of Chemical Thermodynamics,* 41**,** 301-307.DOI 10.1016/j.jct.2008.08.010

SRINIVASA RAO, V., SRINIVASA REDDY, M., SRINIVASA RAO, A., PUSHPA RAJU, G., RAJU, K. T. S. & HARI BABU, B. 2018. Volumetric, acoustic, optical and spectroscopic studies of binary mixtures of the ionic liquid, 1-butyl-3-methyl imidazolium bis (trifluoromethylsulfonyl) imide and diethyl carbonate. *Physics and Chemistry of Liquids,* 56**,** 332-352

STEC, M., TATARCZUK, A., SPIEWAK, D. & WILK, A. 2014. Densities, Excess Molar Volumes, and Thermal Expansion Coefficients of Aqueous Aminoethylethanolamine Solutions at Temperatures from 283.15 to 343.15 K. *Journal of Solution Chemistry,* 43**,** 959-971.DOI 10.1007/s10953-014-0175-2

STOIMENOVSKI, J., MACFARLANE, D. R., BICA, K. & ROGERS, R. D. 2010. Crystalline vs. ionic liquid salt forms of active pharmaceutical ingredients: a position paper. *Pharm Res,* 27**,** 521-6.DOI 10.1007/s11095-009-0030-0

TAMURA, K., NAKAMURA, M. & MURAKAMI, S. 1997. Excess volumes of water plus acetonitrile and water plus dimethylsulfoxide at 30 degrees C and the effect of the excess thermal expansivity coefficients on derived thermodynamic properties. *Journal of Solution Chemistry,* 26**,** 1199-1207.DOI 10.1023/A:1022985208144

TANAKA, K. & WILEY-VCH, W. 2003. Search PubMed;(b) Ionic Liquids in Synthesis, ed. P. Wasserscheid, and T. Welton. Wiley-VCH, Weinheim.

TARIQ, M., FORTE, P. A. S., GOMES, M. F. C., LOPES, J. N. C. & REBELO, L. P. N. 2009. Densities and refractive indices of imidazolium- and phosphonium-based ionic liquids: Effect of temperature, alkyl chain length, and anion. *Journal of Chemical Thermodynamics,* 41**,** 790-798.DOI 10.1016/j.jct.2009.01.012

TAYLOR, B. N. & KUYATT, C. E. 1994. Guidelines for evaluating and expressing the uncertainty of NIST measurement results. NIST Technical Note 1297. National INstitute of Standards and Technolohy. USA.

TORABI, K. 2001. *Fourier transform infrared spectroscopy in size exclusion chromatography.* National Library of Canada, Bibliothèque nationale du Canada.

TRIVEDI, S. & PANDEY, S. 2011. Interactions within a [Ionic Liquid plus Poly(ethylene glycol)] Mixture Revealed by Temperature-Dependent Synergistic Dynamic Viscosity and Probe-Reported Microviscosity. *Journal of Physical Chemistry B,* 115**,** 7405-7416.DOI 10.1021/jp203079p

TRONCOSO, J., CERDEIRINA, C. A., SANMAMED, Y. A., ROMANI, L. & REBELO, L. P. N. 2006. Thermodynamic properties of imidazolium-based ionic liquids: Densities, heat capacities, and enthalpies of fusion of [bmim][PF6] and [bmim][NTf2]. *Journal of Chemical and Engineering Data,* 51**,** 1856-1859.DOI 10.1021/je060222y

UMAPATHI, R., ATTRI, P. & VENKATESU, P. 2014. Thermophysical properties of aqueous solution of ammonium-based ionic liquids. *J Phys Chem B,* 118**,** 5971-82.DOI 10.1021/jp502400z

UMAPATHI, R., RAMJUGERNATH, D. & VENKATESU, P. 2017. Influence of temperature on thermophysical properties of tri(butyl)methylphosphonium methyl sulfate plus N-methyl-2-pyrrolidone. *Journal of Molecular Liquids,* 242**,** 375-381.10.1016/j.molliq.2017.07.014

URZHUMOV, Y. A. 2007. *Sub-wavelength electromagnetic phenomena in plasmonic and polaritonic nanostructures: from optical magnetism to super-resolution*, The University of Texas at Austin.

VAKILI-NEZHAAD, G., VATANI, M., ASGHARI, M. & ASHOUR, I. 2012. Effect of temperature on the physical properties of 1-butyl-3-methylimidazolium based ionic liquids with thiocyanate and tetrafluoroborate anions, and 1-hexyl-3-methylimidazolium with tetrafluoroborate and hexafluorophosphate anions. *Journal of Chemical Thermodynamics,* 54**,** 148-154.10.1016/j.jct.2012.03.024

VAN VALKENBURG, M. E., VAUGHN, R. L., WILLIAMS, M. & WILKES, J. S. 2005. Thermochemistry of ionic liquid heat-transfer fluids. *Thermochimica Acta,* 425**,** 181-188

VERCHER, E., LLOPIS, F. J., GONZALEZ-ALFARO, V., MIGUEL, P. J., ORCHILLES, V. & MARTINEZ-ANDREU, A. 2015. Volumetric properties, viscosities and refractive indices of binary liquid mixtures of tetrafluoroborate-based ionic liquids with methanol at several temperatures. *Journal of Chemical Thermodynamics,* 90**,** 174-184.DOI 10.1016/j.jct.2015.06.036

VILA, J., GINES, P., PICO, J., FRANJO, C., JIMENEZ, E., VARELA, L. & CABEZA, O. 2006. Temperature dependence of the electrical conductivity in EMIM-based ionic liquids: evidence of Vogel–Tamman–Fulcher behavior. *Fluid Phase Equilibria,* 242**,** 141-146

VISAK, Z. P., ILHARCO, L. M., GARCIA, A. R., NAJDANOVIC-VISAK, V., FARELEIRA, J. M., CAETANO, F. J., KIJEVCANIN, M. L. & SERBANOVIC, S. P. 2011. Volumetric properties

and spectroscopic studies of pyridine or nicotine solutions in liquid polyethylene glycols. *J Phys Chem B,* 115**,** 8481-92.DOI 10.1021/jp202464h

VOGEL, H. 1926. Phys 1921, 22, 645–646;(b) Fulcher, GS J Am Ceram Soc 1925, 8, 339,340;(c) Tamman, G.; Hesse, W. *Z Anorg Allg Chem,* 156**,** 245-247

VUKSANOVIC, J. M., CALADO, M. S., IVANIS, G. R., KIJEVCANIN, M. L., SERBANOVIC, S. P. & VISAK, Z. P. 2013. Environmentally friendly solutions of liquid poly(ethylene glycol) and imidazolium based ionic liquids with bistriflamide and triflate anions: Volumetric and viscosity studies. *Fluid Phase Equilibria,* 352**,** 100-109.DOI 10.1016/j.fluid.2013.05.013

WALISZEWSKI, D., STEPNIAK, I., PIEKARSKI, H. & LEWANDOWSKI, A. 2005. Heat capacities of ionic liquids and their heats of solution in molecular liquids. *Thermochimica Acta,* 433**,** 149-152.DOI DOI 10.1016/j.tca.2005.03.001

WANG, J. J., ZHU, A. L., ZHAO, Y. & ZHUO, K. L. 2005. Excess molar volumes and excess logarithm viscosities for binary mixtures of the ionic liquid 1-butyl-3-methylimidazolium hexaflurophosphate with some organic compounds. *Journal of Solution Chemistry,* 34**,** 585-596.DOI 10.1007/s10953-005-5594-7

WASSERSCHEID, P., VAN HAL, R. & BÖSMANN, A. 2002. 1-n-Butyl-3-methylimidazolium ([bmim]) octylsulfate—an even 'greener'ionic liquid. *Green Chemistry,* 4**,** 400-404

WASSERSCHEID, P. & WELTON, T. 2008. *Ionic liquids in synthesis*, John Wiley & Sons.

WATANABE, M., YAMADA, S.-I., SANUI, K. & OGATA, N. 1993. High ionic conductivity of new polymer electrolytes consisting of polypyridinium, pyridinium and aluminium chloride. *Journal of the Chemical Society, Chemical Communications***,** 929-931

WELTON, T. 1999. Room-Temperature Ionic Liquids. Solvents for Synthesis and Catalysis. *Chem Rev,* 99**,** 2071-2084.DOI 10.1021/cr980032t

WILKES, J. S. 2002. A short history of ionic liquids—from molten salts to neoteric solvents. *Green Chemistry,* 4**,** 73-80

WILKES, J. S. & ZAWOROTKO, M. J. 1992. Air and Water Stable 1-Ethyl-3-Methylimidazolium Based Ionic Liquids. *Journal of the Chemical Society-Chemical Communications***,** 965-967.DOI 10.1039/c39920000965

WOOD, S. E. & BATTINO, R. 1990. *Thermodynamics of chemical systems*, Cambridge University Press.

WU, J. Y., CHEN, Y. P. & SU, C. S. 2015. Density and Viscosity of Ionic Liquid Binary Mixtures of 1-n-Butyl-3-methylimidazolium Tetrafluoroborate with Acetonitrile, N,N-Dimethylacetamide, Methanol, and N-Methyl-2-pyrrolidone. *Journal of Solution Chemistry,* 44**,** 395-412.DOI 10.1007/s10953-014-0273-1

WU, T. Y., HAO, L., CHEN, P. R. & LIAO, J. W. 2013. Ionic Conductivity and Thermophysical Properties of 1-Butyl-1-Methylpyrrolidinium Butyl Sulfate and its Binary Mixtures with Poly(ethylene glycol) at Various Temperatures. *International Journal of Electrochemical Science,* 8**,** 5067-5085

YANG, Z. & PAN, W. B. 2005. Ionic liquids: Green solvents for nonaqueous biocatalysis. *Enzyme and Microbial Technology,* 37**,** 19-28.DOI 10.1016/j.enzmictec.2005.02.014

YAO, H., ZHANG, S., WANG, J., ZHOU, Q., DONG, H. & ZHANG, X. 2012. Densities and Viscosities of the Binary Mixtures of 1-Ethyl-3-methylimidazolium Bis (trifluoromethylsulfonyl) imide with N-Methyl-2-pyrrolidone or Ethanol at T=(293.15 to 323.15) K. *Journal of Chemical & Engineering Data,* 57**,** 875-881

YOKE III, J. T., WEISS, J. F. & TOLLIN, G. 1963. Reactions of triethylamine with copper (I) and copper (II) halides. *Inorganic Chemistry,* 2**,** 1210-1216

YOKOZEKI, A., KASPRZAK, D. J. & SHIFLETT, M. B. 2007a. Thermal effect on C–H stretching vibrations of the imidazolium ring in ionic liquids. *Physical Chemistry Chemical Physics,* 9**,** 5018-5026

YOKOZEKI, A., KASPRZAK, D. J. & SHIFLETT, M. B. 2007b. Thermal effect on C-H stretching vibrations of the imidazolium ring in ionic liquids. *Physical Chemistry Chemical Physics*, 9(36), pp. 5018-5026.

ZAFARANI-MOATTAR, M. T. & SHEKAARI, H. 2005. Volumetric and speed of sound of ionic liquid, 1-butyl-3-methylimidazolium hexafluorophosphate with acetonitrile and methanol at T=(298.15 to 318.15) K. *Journal of Chemical & Engineering Data,* 50**,** 1694-1699

ZAFARANI-MOATTAR, M. T. & SHEKAARI, H. 2006. Application of Prigogine–Flory–Patterson theory to excess molar volume and speed of sound of 1-n-butyl-3-methylimidazolium hexafluorophosphate or 1-n-butyl-3-methylimidazolium tetrafluoroborate in methanol and acetonitrile. *The Journal of Chemical Thermodynamics,* 38**,** 1377-1384

ZHANG, Z., SUN, L., TAN, Z., XU, F., LV, X., ZENG, J. & SAWADA, Y. 2006. Thermodynamic investigation of room temperature ionic liquid: heat capacity and thermodynamic functions of BPBF4. *Journal of thermal analysis and calorimetry,* 89**,** 289-294

ZHAO, S. F., HORNE, M., BOND, A. M. & ZHANG, J. 2015. Electrochemical reduction of aromatic ketones in 1-butyl-3-methylimidazolium-based ionic liquids in the presence of carbon dioxide: the influence of the ketone substituent and the ionic liquid anion on bulk electrolysis product distribution. *Phys Chem Chem Phys,* 17**,** 19247-54.10.1039/c5cp00095e

ZHOU, T., XIAO, X. H., LI, G. K. & CAI, Z. W. 2011. Study of polyethylene glycol as a green solvent in the microwave-assisted extraction of flavone and coumarin compounds from medicinal plants. *Journal of Chromatography A,* 1218**,** 3608-3615.DOI 10.1016/j.chroma.2011.04.031

ŽIVKOVIĆ, N. V., ŠERBANOVIĆ, S. S., KIJEVČANIN, M. L. & ZIVKOVIC, E. 2013. Volumetric and viscometric behavior of binary systems 2-butanol+ PEG 200,+ PEG 400,+ tetraethylene glycol dimethyl ether, and+ N-methyl-2-pyrrolidone. *Journal of Chemical & Engineering Data,* 58**,** 3332-3341

Appendices

Appendix A

This appendix section presents all the calibration data and all the calibration plots performed prior to the main measurements. The calculated standard uncertainty for calibration data of ρ, η and n_D is presented in table 6.2 from section 6.3 of chapter 6.

Appendix A.1: Calibration

A.1 Densimeter and viscometer calibration

Calibration for ρ and η were carried under the following condition: T = (298.15, 313.15, 323.15 and 333.15) K at atmospheric pressure of p = 0.1 MPa. The Standard solutions for ρ and η used for calibration were provided by the manufacturer. Samples were analyzed three times and an average deviation for the ρ and η were obtained within a tolerance of 0.00001 and 0.002 respectively.

Table A.1: Density ($\boldsymbol{\rho}$) calibration data perfomed at T = (298.15, 313.15, 323.15 and 333.15) K under atmospheric pressure of p = 0.1 MPa.

T/K	$\boldsymbol{\rho/g.cm^{-3}}$ *(Standard solution)*	$\boldsymbol{\rho/g.cm^{-3}}$ *(exp)*
298.15	0.81529	0.81523
313.15	0.80496	0.80490
323.15	0.79809	0.79799
333.15	0.79116	0.79107

Table A.2: Viscosity ($\boldsymbol{\eta}$) calibration data perfomed at T = (298.15, 313.15, 323.15 and 333.15) K under atmospheric pressure of p = 0.1 MPa.

T/K	$\boldsymbol{\eta/mPa.s}$ *(Standard solution)*	$\boldsymbol{\eta/mPa.s}$ *(exp)*
298.15	4.014	4.014
313.15	2.894	2.894
323.15	2.397	2.413
333.15	2.025	2.041

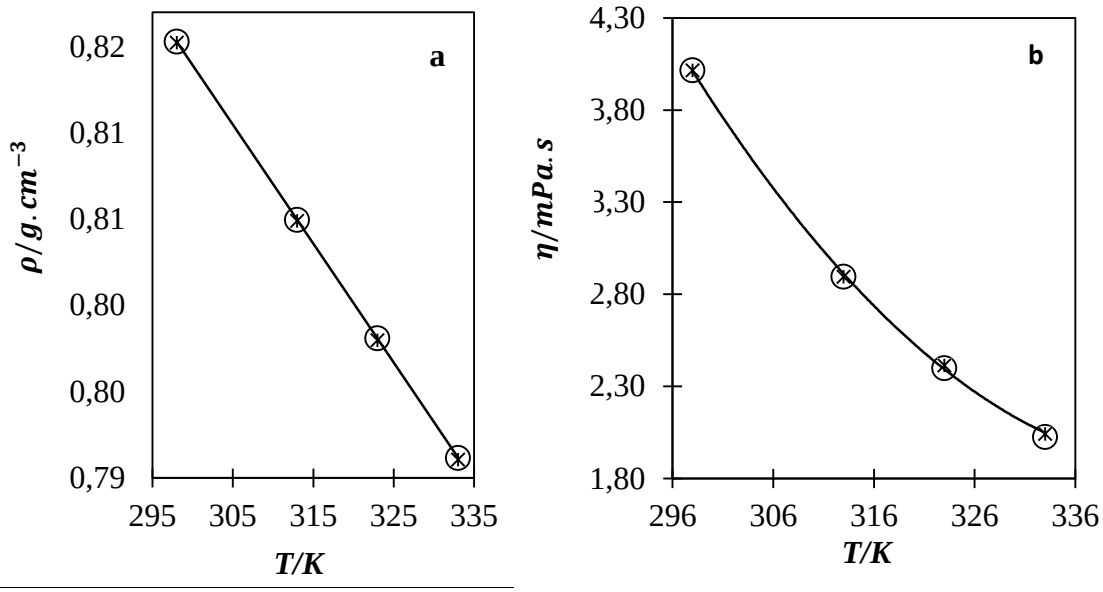

Figure A.1: Calibration plot of $\boldsymbol{\rho}$ and η; Comparison between $(\circ)$ standard solution and the $(*)$ experimental value. The ρ and η plots are represented by a and b respectively. The solid lines for $\boldsymbol{\rho}$ and η represent the least squares and Vogel–Fulcher–Tammann (VFT) model respectively.

Table A.3: The trendline equations for the calibration data of density and viscosity. Where x represent the temperature.

Thermophysical data	***Trendline equation***	$\boldsymbol{R^2}$	***Std uncertainty***
Density (g/cm^3)	$y = -0.0007x + 1.021$	1.000	± 0.00001
Viscosity (mPa.s)	$y = 1265e^{-0.019x}$	0.9958	± 0.0023

Temperature standard uncertainties for calibration of density (ρ) and viscosity (η) is $u(T)$ = ± 0.01 K and $u(T)$ = ± 0.01 K respectively.

A.2 Refractometer calibration

Calibration for n_D were carried under this condition: T = (298.15, 308.15, 318.15 and 328.15) K at atmospheric pressure of p = 0.1 MPa. Standard solution was not available, thus a literature data was used for calibration. Samples were analyzed three times and an average deviation was obtained within a tolerance of 0.00001.

Table A.4: Refractive index ($\boldsymbol{n_D}$) calibration data perfomed at T = (298.15, 308.15, 318.15, 328.15 and 333.15) K under atmospheric pressure of p = 0.1 MPa

T/K	$\boldsymbol{n_D}$ *(Lit)*	$\boldsymbol{n_D}$ *(exp)*
298.15	1.3280	1.3281
308.15	1.3238	1.3238
318.15	1.3197	1.3199
328.15.	1.3157	1.3157

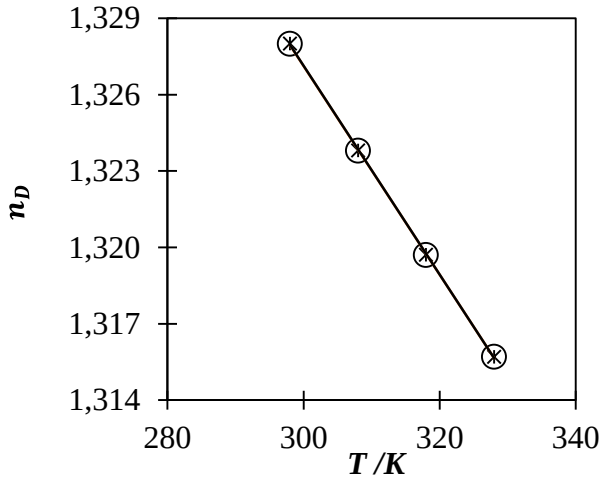

Figure A.2: Calibration plot of $\boldsymbol{n_D}$; Comparison between (○) lit (Ghotli et al., 2015) and the (∗) experimental value. The solid lines represent the least-squares model.

Table A.5: The trendline equations for the calibration data of refractive index. Where *x* represent temperature.

Thermophysical data	*Trendline equation*	R^2	*Std uncertainty*
Refractive index	$y = -0.0004x + 1.4501$	0.9999	± 0.00005

Temperature standard uncertainties for calibration of refractive index (n_D) is $u(T)$ = 0.05 K.

Appendix B

This appendix section present the excess thermodynamic data for the three selected test systems i.e. excess molar volume (V^E), excess partial molar volumes ($\bar{V}_1^E$ and $\bar{V}_2^E$) and excess thermal expansion coefficients (α_P^E). This section only presents the excess thermodynamic data and section 6.4 of chapter 6 present all the graphs for test systems that is figure 6.1 - 6.3

Appendix B.1: Test systems

B.1 Test system of (V^E)

The binary mixture of a binary mixture test system of ($[\mathrm{BMIM}]^+[\mathrm{BF_4}]^-$(1) + methanol (2)) performed at 298.15 K under atmospheric pressure of p = 0.1 MPa (Vercher et al., 2015). The test system was performed prior to the main measurements.

Table B.1: Excess molar volume $(\boldsymbol{V^E})$ test system of ($[\mathbf{BMIM}]^+[\mathbf{BF_4}]^-(\mathbf{1})$ + methanol (2)) performed at 298.15 K under atmospheric pressure of p = 0.1 MPa

x_1 *(lit)*	V^E*(lit)*	x_1 *(exp)*	V^E*(cal)*
0.0000	0.0000	0.0000	0.0000
0.0499	-0.4000	0.0145	-0.1422
0.0998	-0.5700	0.0281	-0.2529
0.1498	-0.6500	0.0449	-0.3496
0.1998	-0.6900	0.0649	-0.4745
0.3002	-0.7100	0.0880	-0.5253
0.4004	-0.6200	0.1165	-0.5910
0.5001	-0.5200	0.1519	-0.6513
0.6004	-0.4300	0.2116	-0.6899
0.6987	-0.3100	0.2504	-0.7166
0.8005	-0.2200	0.2755	-0.7158
0.8486	-0.1500	0.3259	-0.6848
0.8987	-0.1200	0.4345	-0.5918
0.9476	-0.0400	0.5313	-0.4822
1.0000	0.0000	0.6576	-0.3536
-	-	0.8508	-0.1660
-	-	1.0000	0.0000

B.2 Test system of ($\bar{V}_1^E$ and $\bar{V}_2^E$)

A binary mixture test system of (nicotine (1) + 1-butanol (2)) performed at 303.15 K under atmospheric pressure of p = 0.1 MPa (Soldatovic et al., 2016). This test system is the second test system performed prior to the main measurements.

Table B.2: Excess partial molar volumes ($\bar{V}_1^E$ and $\bar{V}_2^E$) test system of of (nicotine (1) + 1-butanol (2)) performed at 303.15 K under atmospheric pressure of p = 0.1 MPa.

x_1*(lit)*	$x_1\ (exp)$	$\bar{V}_1^E$ *(lit)*	$\bar{V}_1^E$ *(cal)*	$\bar{V}_2^E$ *(lit)*	$\bar{V}_2^E$ *(cal)*
0.0000	0.00000	-3.2728	-3.3118	0.0000	0.0000
0.1000	0.04861	-2.5933	-2.9620	-0.1343	-0.0087
0.1960	0.10293	-2.0241	-2.5978	-0.1343	-0.0386
0.3000	0.16391	-1.4959	-2.22149	-0.3082	-0.0966
0.3931	0.23418	-1.0979	-1.8294	-0.5191	-0.1941
0.5000	0.31385	-0.7240	-1.4369	-0.8204	-0.3423
0.5930	0.40687	-0.4671	-1.0456	-1.1296	-0.5626
0.7000	0.51680	-0.2457	-0.6661	-1.5337	-0.8832
0.7931	0.64634	-0.1135	-0.3431	-1.9227	-1.3352
0.9000	0.80345	-0.0256	0.0274	-2.4058	-1.9746
1.0000	1.00000	0.0000	0.0000	-2.8870	-2.8820

B.3 Test system of (α_P^E)

A binary mixture test system of (nicotine (1) + 1-butanol (2)) were performed at 303.15 K under atmospheric pressure of p = 0.1 MPa (Soldatovic et al., 2016).

Table B.3: Excess thermal expansion coefficients (α_P^E) test system of of (nicotine (1) + 1-butanol (2)) performed at 303.15 K under atmospheric pressure of p = 0.1 MPa.

$x_1(lit)$	$x_1\ (exp)$	α_P^E *(lit)*	α_P^E*(cal)*
0.0000	0.0000	0.0000	0.0000
0.1000	0.0486	4.7928	4.5928
0.1960	0.1029	7.2622	7.3536
0.3000	0.1639	8.3409	8.3709
0.3931	0.2342	8.2415	8.3003
0.5000	0.3139	7.3389	7.5820

Table B.4: Excess thermal expansion coefficients (α_P^E) test system of of (nicotine (1) + 1-butanol (2)) performed at 303.15 K under atmospheric pressure of p = 0.1 MPa. (Continued)

$x_1(lit)$	$x_1\ (exp)$	α_P^E *(lit)*	α_P^E *(cal)*
0.5930	0.4069	5.0378	5.3612
0.7931	0.6463	2.9051	2.7931
0.9000	0.8035	1.2710	1.3538
1.0000	1.0000	0.0000	0.0000

Appendix C

This section present estimated fitting parameters of PEG200

Appendix C.1: Molar isobaric heat capacity .

C.1 calculated parameters for molar heat capacity values

This appendix section presents the estimated fitting parameters which are C_0, C_1, C_2 and their estimated standard deviation (σ). The C_P values for all the ILs and PEG200 for this study are provided in section 6.5 of chapter 6 (table 6.6).

Table C.1: Estimated fitting parameters for $\boldsymbol{C_P}$ of PEG200 from (293.15 to 333.15) K with 10 K interval under atmospheric pressure of 0.1 MPa. The below table is taken from (Francesconi et al., 2007).

Component	$\boldsymbol{C_0}$	$\boldsymbol{C_1}$	$\boldsymbol{C_2}$	$\boldsymbol{\sigma}$
PEG200	579.1381	-1.4716	0.0031	0.45

Appendix D

This appendix section presents all the thermophysical measured data performed for the binary mixtures of ILs and PEG200. The selected thermophysical properties are ρ, η u and n_D. This section only present thermophysical data and chapter 6 present all the plotted curves.

Appendix D.1: Thermophysical properties of ILs + PEG200

D.1 Thermophysical properties of $[\mathbf{BMIM}]^+[\mathbf{BF_4}]^- + \mathbf{PEG200}$.

The below table D.1 present all the measured thermophysical properties of $[BMIM]^+[BF_4]^-$ + PEG200.

Table D.1: Thermophysical properties of $[BMIM]^+[BF_4]^-$ + PEG200 at (293.15 to 333.15) K with 10 K interval under atmospheric pressure of p = 0.1 MPa.

x_1	$\rho/g.cm^{-3}$	$u/m.s^{-1}$	$\eta/mPa.s$	n_D
		T/K = 293.15		
0.0000	1.12490	1617.26	62.600	1.46074
0.0748	1.13282	1628.76	64.483	1.45880
0.1528	1.14079	1631.92	66.144	1.45640
0.2865	1.15362	1628.73	69.002	1.45197
0.4001	1.16318	1623.22	71.144	1.44780
0.4873	1.16982	1618.12	73.014	1.44429
0.6341	1.18018	1608.15	75.011	1.43849
0.7719	1.18943	1597.20	83.074	1.43282
0.9504	1.20126	1582.20	111.544	1.42530
1.0000	1.20460	1578.14	128.226	1.42300
		T/K = 303.15		
0.0000	1.11689	1584.63	38.439	1.45726
0.0748	1.12497	1596.82	39.005	1.45549
0.1528	1.13306	1601.23	39.499	1.45320
0.2865	1.14592	1599.06	40.734	1.44893
0.4001	1.15552	1594.72	41.895	1.44485

Table D.1: Thermophysical properties of $[BMIM]^+[BF_4]^-$ + PEG200 at (293.15 to 333.15) K with 10 K interval under atmospheric pressure of p = 0.1 MPa. (Continued)

x_1	$\rho/g.cm^{-3}$	$u/m.s^{-1}$	$\eta/mPa.s$	n_D
0.4873	1.16225	1590.20	42.902	1.44142
0.6341	1.17278	1581.09	45.175	1.43574
0.7719	1.18215	1571.96	50.104	1.43019
0.9504	1.19405	1557.26	68.000	1.42280
1.0000	1.19743	1554.03	77.203	1.42054
		T/K = 313.15		
0.0000	1.10889	1553.03	25.043	1.45381
0.0748	1.11715	1564.19	25.485	1.45220
0.1528	1.12531	1570.98	25.954	1.44998
0.2865	1.13819	1571.12	26.592	1.44581
0.4001	1.14789	1567.58	27.257	1.44184
0.4873	1.15473	1563.24	27.913	1.43847
0.6341	1.16545	1555.69	30.674	1.43292
0.7719	1.17493	1546.23	35.157	1.42745
0.9504	1.18692	1534.23	44.581	1.42018
1.0000	1.19029	1531.16	48.654	1.41794
		T/K = 323.15		
0.0000	1.10092	1522.04	17.339	1.45038
0.0748	1.10941	1534.88	18.682	1.44892
0.1528	1.11763	1541.60	20.089	1.44681
0.2865	1.13057	1542.86	22.515	1.44277
0.4001	1.14037	1539.68	24.532	1.43889
0.4873	1.14728	1536.22	26.032	1.43561
0.6341	1.15809	1529.81	28.446	1.43014
0.7719	1.16779	1522.31	30.522	1.42476
0.9504	1.17992	1511.24	33.025	1.41759
1.0000	1.18325	1508.27	33.755	1.41541

Table D.1: Thermophysical properties of $[BMIM]^+[BF_4]^-$ + PEG200 at (293.15 to 333.15) K with 10 K interval under atmospheric pressure of p = 0.1 MPa. (Continued)

x_1	$\rho/g.cm^{-3}$	$u/m.s^{-1}$	$\eta/mPa.s$	n_D
		T/K = 333.15		
0.0000	1.09293	1491.47	12.617	1.44702
0.1528	1.11002	1512.71	12.953	1.44369
0.2865	1.12298	1514.83	13.236	1.43979
0.4001	1.13286	1513.14	13.463	1.43602
0.4873	1.13989	1511.10	13.961	1.43281
0.6341	1.15089	1505.98	15.498	1.42741
0.7719	1.16068	1499.20	17.695	1.42210
0.9504	1.17307	1488.50	22.156	1.41507
1.0000	1.17632	1485.61	24.082	1.41289.

Standard uncertainties: $x_1 = \pm 0.0004$, ρ = ± 0.00002, u = ± 0.02, η = ± 0.002 and n_D = ± 0.00002.

D.2 Themophysical properties of $[\mathbf{BMIM}]^+[\mathbf{PF_6}]^- + \mathbf{PEG200}$

The below table D.2 present all the measured thermophysical properties of $[\mathrm{BMIM}]^+[\mathrm{PF_6}]^- + \mathrm{PEG200}$.

Table D.2: Thermophysical properties of $[\mathbf{BMIM}]^+[\mathbf{PF_6}]^- + \mathbf{PEG200}$ at (293.15 to 333.15) K with 10 K interval under atmospheric pressure of p = 0.1 MPa.

x_1	$\rho/g.cm^{-3}$	$u/m.s^{-1}$	$\eta/mPa.s$	n_D
		T/K = 293.15		
0.0000	1.1250	1617.26	62.600	1.46074
0.0604	1.14469	1618.86	71.254	1.45835
0.1254	1.16480	1614.78	80.086	1.45558
0.2420	1.19791	1597.84	95.586	1.45075
0.3466	1.22514	1577.88	103.922	1.44574
0.4305	1.24582	1560.29	108.002	1.44125
0.5795	1.28078	1528.86	115.002	1.43343
0.7291	1.31395	1499.21	137.215	1.42549
0.9384	1.35785	1463.85	239.399	1.41434
1.0000	1.37082	1454.26	293.440	1.41077
		T/K = 303.15		
0.0000	1.11689	1584.63	38.439	1.45726
0.0604	1.13670	1587.43	42.174	1.45508
0.1254	1.15672	1583.22	45.211	1.45242
0.2420	1.18978	1567.55	49.954	1.44772
0.3466	1.21697	1548.88	51.121	1.44282
0.4305	1.23762	1532.12	51.752	1.43842
0.5795	1.27254	1502.15	52.001	1.43070
0.7291	1.30568	1473.55	61.112	1.42288
0.9384	1.34951	1439.10	124.002	1.41188
1.0000	1.37082	1454.26	293.440	1.41077
		T/K = 313.15		
0.0000	1.10889	1553.03	25.043	1.45381
0.0604	1.12874	1556.65	26.001	1.45181

Table D.2: Thermophysical properties of $[BMIM]^+[PF_6]^- + PEG200$ at (293.15 to 333.15) K with 10 K interval under atmospheric pressure of p = 0.1 MPa. (Continued)

x_1	$\rho/g.cm^{-3}$	$u/m.s^{-1}$	$\eta/mPa.s$	n_D
0.1254	1.14870	1553.15	30.102	1.44928
0.2420	1.18162	1538.27	30.011	1.44466
0.3466	1.20878	1520.89	31.211	1.43988
0.4305	1.22942	1505.01	32.211	1.43551
0.5795	1.26431	1476.79	33.244	1.42787
0.7291	1.29736	1448.98	38.233	1.42015
0.9384	1.34115	1416.04	82.386	1.40925
1.0000	1.35404	1406.85	109.970	1.40577
		T/K = 323.15		
0.0000	1.10092	1522.04	17.339	1.45038
0.0604	1.12078	1526.38	19.222	1.44855
0.1254	1.14072	1523.85	20.005	1.44612
0.2420	1.17351	1509.15	20.125	1.44162
0.3466	1.20061	1493.09	21.423	1.43691
0.4305	1.22127	1478.88	21.453	1.43260
0.5795	1.25617	1451.87	20.215	1.42511
0.7291	1.28911	1425.10	24.245	1.41748
0.9384	1.33286	1393.15	57.321	1.40669
1.0000	1.34574	1384.41	78.829	1.40323
		T/K = 333.15		
0.0000	1.09293	1491.47	10.001	1.44702
0.0604	1.11281	1496.53	10.888	1.44530
0.1254	1.13266	1494.88	12.003	1.44310
0.2420	1.16543	1481.21	12.111	1.43856
0.3466	1.19248	1466.23	12.164	1.43392
0.4305	1.21311	1452.95	12.452	1.42969
0.5795	1.24800	1427.88	12.501	1.42227
0.7291	1.28092	1401.98	13.456	1.41471
0.9384	1.32466	1371.22	39.003	1.40399
1.0000	1.33752	1362.50	52.776	1.40052

Standard uncertainties: $x_1 = \pm 0.0004$, ρ = ± 0.00002, u = ± 0.02, η = ± 0.002 and n_D = ± 0.00002.

D.3 Thermophysical properties of $[\mathbf{EMIM}]^{+}[\mathbf{BF_4}]^{-} + \mathbf{PEG200}$

The below table D.3 present all the measured thermophysical properties of $[\mathrm{EMIM}]^{+}[\mathrm{BF_4}]^{-} + \mathrm{PEG200}$.

Table D.3: Thermophysical properties of $[\mathbf{EMIM}]^{+}[\mathbf{BF_4}]^{-} + \mathbf{PEG200}$ at (293.15 to 333.15) K with 10 K interval under atmospheric pressure of p = 0.1 MPa**.**

x_1	$\rho/g.cm^{-3}$	$u/m.s^{-1}$	$\eta/mPa.s$	n_D
		T/K =293.15		
0.0000	1.12490	1617.26	62.600	1.46074
0.0845	1.13860	1631.89	61.110	1.45867
0.1707	1.15268	1647.89	59.555	1.45598
0.3143	1.17589	1663.85	57.000	1.45014
0.4323	1.19438	1666.85	54.755	1.44457
0.5204	1.20799	1664.98	53.000	1.44014
0.6643	1.22999	1660.55	49.985	1.43270
0.7944	1.24972	1653.55	47.000	1.42569
0.9563	1.27515	1643.22	43.122	1.41660
1.0000	1.28215	1640.75	42.000	1.41420
		T/K =303.15		
0.0000	1.11689	1584.63	38.422	1.45726
0.0845	1.13088	1600.85	37.758	1.45538
0.1707	1.14495	1618.22	37.070	1.45281
0.3143	1.16818	1634.36	35.969	1.44720
0.4323	1.18673	1637.55	34.921	1.44177
0.5204	1.20030	1637.22	34.055	1.43742
0.6643	1.22239	1632.99	32.495	1.43010
0.7944	1.24219	1627.33	30.881	1.42323
0.9563	1.26750	1619.38	28.653	1.41435
1.0000	1.27451	1616.43	28.014	1.41189
		T/K =313.15		
0.0000	1.10889	1553.03	25.044	1.45381
0.0845	1.12311	1569.22	24.839	1.45192
0.1707	1.13733	1587.32	24.630	1.44945
0.3143	1.16048	1603.72	24.329	1.44402

Table D.3: Thermophysical properties of $[\mathbf{EMIM}]^+[\mathbf{BF_4}]^- + \mathbf{PEG200}$ at (293.15 to 333.15) K with 10 K interval under atmospheric pressure of p = 0.1 MPa**.** (Continued)

x_1	$\rho/g.cm^{-3}$	$u/m.s^{-1}$	$\eta/mPa.s$	n_D
0.4323	1.17901	1607.95	23.969	1.43869
0.5204	1.19268	1607.55	23.609	1.43443
0.6643	1.21481	1605.96	22.871	1.42720
0.7944	1.23469	1600.55	22.037	1.42042
0.9563	1.26011	1595.12	20.765	1.41163
1.0000	1.26697	1592.84	20.399	1.40918
		T/K =323.15		
0.0000	1.10092	1522.04	17.339	1.45038
0.0845	1.11542	1540.00	17.319	1.44865
0.1707	1.12968	1559.55	17.311	1.44634
0.3143	1.15285	1576.02	17.321	1.44101
0.4323	1.17134	1580.85	17.236	1.43582
0.5204	1.18508	1581.35	17.081	1.43163
0.6643	1.20722	1580.41	16.652	1.42449
0.7944	1.22728	1576.55	16.098	1.41780
0.9563	1.25270	1572.11	15.161	1.40908
1.0000	1.25950	1569.65	14.901	1.40662
		T/K =333.15		
0.0000	1.09293	1491.47	12.617	1.44691
0.0845	1.10768	1512.33	12.598	1.44542
0.1707	1.12201	1532.85	12.614	1.44319
0.3143	1.14512	1549.50	12.658	1.43801
0.4323	1.16372	1554.89	12.623	1.43288
0.5204	1.17751	1556.01	12.508	1.42874
0.6643	1.19975	1556.13	12.135	1.42172
0.7944	1.21992	1554.11	11.655	1.41510
0.9563	1.24535	1549.11	10.808	1.40645
1.0000	1.25208	1546.82	10.602	1.40398

Standard uncertainties: $x_1 = \pm 0.0004$, ρ = ± 0.00002, u = $\pm$0.02, η = $\pm$0.002 and n_D = ± 0.00002.

Appendix E

The first section of this appendix presents all the calculated excess thermodynamic data that is excess molar volume (V^E), excess isentropic compressibility (K_s^E), excess viscosity (η^E), excess refractive index (n_D^E) and excess thermal expansion coefficients (α_P^E). The second present the excess partial molar volumes (V_1^E and V_2^E) thermodynamic data. The third section of this appendix present infinite excess partial molar volume ($\bar{V}_1^{E,\infty}$ and $\bar{V}_2^{E,\infty}$).

Appendix E.1: Excess thermodynamic properties of ILs + PEG200

Table E.1, E,2 and E.3 present all the calculated excess thermodynamic properties of $[BMIM]^+[BF_4]^-$, $[BMIM]^+[PF_6]^-$ and $[EMIM]^+[BF_4]^-$ + PEG, respectively.

Table E.1: Excess thermodynamic properties of $[\mathbf{BMIM}]^+[\mathbf{BF_4}]^- + \mathbf{PEG200}$ at (293.15 to 333.15) K with 10 K interval under atmospheric pressure of p = 0.1 MPa. .

x_1	φ_1	$V_m^E/cm^3.mol^{-1}$	K_s^E/TPa^{-1}	$\eta^E/mPa.s$	n_D^E	α_P^E/K^{-1}
			T/K = 293.15			
0.0000	0.0000	-0.0005	0.0026	-0.0075	0.0000	0.0000
0.0748	0.0786	-0.2610	-6.6073	0.1562	0.0009	-0.0016
0.1528	0.1599	-0.4937	-9.6741	0.3575	0.0016	-0.0033
0.2865	0.2976	-0.7820	-11.1582	0.6060	0.0020	-0.0055
0.4001	0.4131	-0.8359	-10.8827	0.7870	0.0021	-0.0066
0.4873	0.5008	-0.7817	-10.1144	0.8662	0.0020	-0.0074
0.6341	0.6465	-0.5848	-8.0016	0.8520	0.0017	-0.0078
0.7719	0.7813	-0.3523	-5.1923	0.6822	0.0011	-0.0069
0.9504	0.9529	-0.0634	-1.0947	0.1665	0.0003	-0.0029
1.0000	1.0000	0.0000	0.0000	-0.0012	0.0000	0.0000
			T/K = 303.15			
0.0000	0.0000	-0.0013	0.0000	-0.0022	0.0000	0.0000
0.0748	0.0786	-0.2808	-7.0992	0.1383	0.0010	-0.0017
0.1528	0.1599	-0.5269	-10.6230	0.3171	0.0017	-0.0035
0.2865	0.2976	-0.8067	-12.0831	0.5640	0.0022	-0.0057
0.4001	0.4131	-0.8512	-11.8306	0.7335	0.0023	-0.0068

Table E.1: Excess thermodynamic properties of $[\mathbf{BMIM}]^{+}[\mathbf{BF_4}]^{-} + \mathbf{PEG200}$ at (293.15 to 333.15) K with 10 K interval under atmospheric pressure of p = 0.1 MPa. (Continued)

x_1	φ_1	$V_m^E/cm^3.mol^{-1}$	K_s^E/TPa^{-1}	$\eta^E/mPa.s$	n_D^E	α_P^E/K^{-1}
0.4873	0.5008	-0.7991	-10.9326	0.8086	0.0022	-0.0075
0.6341	0.6465	-0.6066	-8.5221	0.7942	0.0018	-0.0080
0.7719	0.7813	-0.3710	-5.4021	0.6267	0.0012	-0.0071
0.9504	0.9529	-0.0660	-0.9661	0.1400	0.0003	-0.0030
1.0000	1.0000	-0.0002	0.0000	0.0000	0.0000	0.0000
			T/K = 313.15			
0.0000	0.0000	0.0001	0.0000	-0.0007	0.0000	0.0000
0.0748	0.0786	-0.3051	-6.8229	0.1199	0.0010	-0.0018
0.1528	0.1599	-0.5552	-11.3502	0.2797	0.0017	-0.0037
0.2865	0.2976	-0.8230	-13.3491	0.5169	0.0022	-0.0059
0.4001	0.4131	-0.8699	-12.9697	0.6806	0.0023	-0.0070
0.4873	0.5008	-0.8215	-11.7462	0.7524	0.0022	-0.0077
0.6341	0.6465	-0.6368	-9.3233	0.7390	0.0018	-0.0082
0.7719	0.7813	-0.3957	-5.7679	0.5633	0.0012	-0.0072
0.9504	0.9529	-0.0763	-1.1591	0.1095	0.0003	-0.0030
1.0000	1.0000	0.0000	0.0000	0.0008	0.0000	0.0000
			T/K = 323.15			
0.0000	0.0000	0.0000	0.0000	0.0012	0.0000	0.0000
0.0748	0.0786	-0.3348	-7.8714	0.1167	0.0012	-0.0019
0.1528	0.1599	-0.5869	-12.3255	0.2431	0.0019	-0.0039
0.2865	0.2976	-0.8499	-14.4137	0.4734	0.0024	-0.0060
0.4001	0.4131	-0.8962	-13.7106	0.6248	0.0025	-0.0072
0.4873	0.5008	-0.8449	-12.4739	0.6936	0.0024	-0.0079
0.6341	0.6465	-0.6502	-9.8504	0.6969	0.0019	-0.0083
0.7719	0.7813	-0.4210	-6.5202	0.5100	0.0013	-0.0074
0.9504	0.9529	-0.0907	-1.3911	0.0818	0.0003	-0.0031
1.0000	1.0000	0.0000	0.0000	-0.0020	0.0000	0.0000
			T/K = 333.15			
0.0000	0.0000	0.0001	0.0000	-0.0003	0.0000	0.0000
0.0748	0.0786	-0.3684	-8.3689	0.0973	0.0012	-0.0021

Table E.1: Excess thermodynamic properties of $[\mathbf{BMIM}]^{+}[\mathbf{BF_4}]^{-} + \mathbf{PEG200}$ at (293.15 to 333.15) K with 10 K interval under atmospheric pressure of p = 0.1 MPa. (Continued)

x_1	φ_1	$V_m^E/cm^3.mol^{-1}$	K_s^E/TPa^{-1}	$\eta^E/mPa.s$	n_D^E	α_P^E/K^{-1}
0.1528	0.1599	-0.6343	-13.4727	0.2110	0.0020	-0.0041
0.2865	0.2976	-0.8798	-15.5145	0.4279	0.0025	-0.0063
0.4001	0.4131	-0.9191	-15.0243	0.5771	0.0026	-0.0074
0.4873	0.5008	-0.8722	-14.0814	0.6384	0.0025	-0.0082
0.6341	0.6465	-0.6790	-11.3451	0.6501	0.0020	-0.0086
0.7719	0.7813	-0.4367	-7.6008	0.4664	0.0014	-0.0076
0.9504	0.9529	-0.1132	-1.6708	0.0618	0.0004	-0.0032
1.0000	1.0000	0.0000	0.0000	0.0000	0.0000	0.0000

Table E.2: Excess thermodynamic properties of $[\mathbf{BMIM}]^{+}[\mathbf{PF_6}]^{-} + \mathbf{PEG200}$ at (293.15 to 333.15) K with 10 K interval under atmospheric pressure of p = 0.1 MPa.

x_1	φ_1	$V_m^E/cm^3.mol^{-1}$	K_s^E/TPa^{-1}	$\eta^E/mPa.s$	n_D^E	α_P^E/K^{-1}
			T/K = 293.15			
0.0000	0.0000	-0.0005	0.0000	-0.0075	0.0000	0.0000
0.0604	0.0697	-0.4143	-6.8912	0.1166	0.0006	-0.0040
0.1254	0.1433	-0.7261	-11.3641	0.3005	0.0013	-0.0067
0.2420	0.2713	-0.9716	-14.2952	0.6842	0.0021	-0.0098
0.3466	0.3822	-0.9593	-13.9817	0.9100	0.0023	-0.0103
0.4305	0.4685	-0.8726	-12.5540	1.0268	0.0022	-0.0096
0.5795	0.6165	-0.6511	-8.9770	0.9783	0.0017	-0.0075
0.7291	0.7584	-0.3861	-5.1206	0.7070	0.0011	-0.0049
0.9384	0.9467	-0.0194	-0.9888	0.1148	0.0002	-0.0011
1.0000	1.0000	0.0000	0.0000	0.0003	0.0000	0.0000
			T/K = 303.15			
0.0000	0.0000	-0.0013	0.0000	0.0000	0.0000	0.0000
0.0604	0.0697	-0.4316	-7.6264	0.0994	0.0008	-0.0041
0.1254	0.1433	-0.7399	-12.0247	0.2750	0.0015	-0.0068
0.2420	0.2713	-0.9892	-15.1856	0.6437	0.0023	-0.0100
0.3466	0.3822	-0.9796	-14.9936	0.8661	0.0025	-0.0104
0.4305	0.4685	-0.8914	-13.5119	0.9716	0.0024	-0.0097
0.5795	0.6165	-0.6687	-9.8280	0.9461	0.0018	-0.0076
0.7291	0.7584	-0.4008	-5.7049	0.6704	0.0012	-0.0050
0.9384	0.9467	-0.0244	-1.0769	0.1051	0.0003	-0.0012
1.0000	1.0000	0.0004	0.0000	0.0000	0.0000	0.0000
			T/K = 313.15			
0.0000	0.0000	0.0001	0.0000	-0.0007	0.0000	0.0000
0.0604	0.0697	-0.4500	-8.2320	0.0918	0.0008	-0.0042
0.1254	0.1433	-0.7607	-12.9131	0.2538	0.0015	-0.0069
0.2420	0.2713	-1.0021	-16.0535	0.5963	0.0023	-0.0101
0.3466	0.3822	-0.9955	-15.9742	0.8160	0.0025	-0.0106
0.4305	0.4685	-0.9110	-14.4563	0.9179	0.0024	-0.0099
0.5795	0.6165	-0.6891	-10.7786	0.9008	0.0018	-0.0078

Table E.2: Excess thermodynamic properties of $[\mathrm{BMIM}]^{+}[\mathrm{PF}_6]^{-} + \mathrm{PEG200}$ at (293.15 to 333.15) K with 10 K interval under atmospheric pressure of p = 0.1 MPa. (Continued)

x_1	φ_1	$V_m^E/cm^3.mol^{-1}$	K_s^E/TPa^{-1}	$\eta^E/mPa.s$	n_D^E	α_P^E/K^{-1}
0.7291	0.7584	-0.4104	-6.2112	0.6220	0.0012	-0.0051
0.9384	0.9467	-0.0291	-1.3338	0.0989	0.0003	-0.0012
1.0000	1.0000	0.0000	0.0000	0.0000	0.0000	0.0000
			T/K = 323.15			
0.0000	0.0000	0.0000	0.0000	0.0012	0.0000	0.0000
0.0604	0.0697	-0.4643	-8.8353	0.0727	0.0010	-0.0043
0.1254	0.1433	-0.7825	-13.9590	0.2241	0.0018	-0.0071
0.2420	0.2713	-1.0162	-16.7676	0.5528	0.0027	-0.0102
0.3466	0.3822	-1.0076	-16.8172	0.7710	0.0029	-0.0107
0.4305	0.4685	-0.9294	-15.6697	0.8684	0.0027	-0.0101
0.5795	0.6165	-0.7137	-11.7551	0.8459	0.0021	-0.0079
0.7291	0.7584	-0.4193	-6.8242	0.5843	0.0014	-0.0051
0.9384	0.9467	-0.0322	-1.3881	0.0813	0.0003	-0.0012
1.0000	1.0000	0.0000	0.0000	0.0000	0.0000	0.0000
			T/K = 333.15			
0.0000	0.0000	0.0001	0.0000	0.0003	0.0000	0.0000
0.0604	0.0697	-0.4804	-9.4806	0.0003	0.0010	-0.0043
0.1254	0.1433	-0.7936	-15.0162	0.0676	0.0018	-0.0071
0.2420	0.2713	-1.0353	-17.9122	0.1950	0.0027	-0.0102
0.3466	0.3822	-1.0237	-17.9859	0.5178	0.0029	-0.0107
0.4305	0.4685	-0.9435	-16.8382	0.7304	0.0027	-0.0101
0.5795	0.6165	-0.7275	-13.0403	0.8219	0.0021	-0.0079
0.7291	0.7584	-0.4294	-7.6419	0.7963	0.0014	-0.0051
0.9384	0.9467	-0.0354	-1.7054	0.5541	0.0003	-0.0012
1.0000	1.0000	0.0000	0.0000	0.0571	0.0000	0.0000

Table E.3: Excess thermodynamic properties of $[\mathbf{EMIM}]^{+}[\mathbf{BF_4}]^{-} + \mathbf{PEG200}$ at (293.15 to 333.15) K with 10 K interval under atmospheric pressure of p = 0.1 MPa.

x_1	φ_1	$V_m^E/cm^3.mol^{-1}$	K_s^E/TPa^{-1}	$\eta^E/mPa.s$	n_D^E	α_P^E/K^{-1}
			T/K = 293.15			
0.0000	0.0000	-0.0005	0.0000	0.0000	0.0000	0.0000
0.0845	0.0741	-0.3133	-6.3625	0.2502	0.0016	-0.0066
0.1707	0.1515	-0.5922	-12.8028	0.4722	0.0030	-0.0122
0.3143	0.2845	-0.9007	-18.4217	0.8746	0.0039	-0.0189
0.4323	0.3978	-0.9656	-18.5790	1.0608	0.0038	-0.0212
0.5204	0.4849	-0.9312	-16.9399	1.1205	0.0035	-0.0213
0.6643	0.6319	-0.7494	-13.3414	1.0692	0.0028	-0.0177
0.7944	0.7702	-0.4669	-8.5917	0.7651	0.0019	-0.0121
0.9563	0.9500	-0.1049	-1.7967	0.2217	0.0004	-0.0027
1.0000	1.0000	0.0000	0.0000	0.0000	0.0000	0.0000
			T/K = 303.15			
0.0000	0.0000	-0.0013	0.0000	0.0000	0.0000	0.0000
0.0845	0.0741	-0.3623	-7.3468	0.2155	0.0018	-0.0069
0.1707	0.1515	-0.6389	-14.5165	0.4253	0.0031	-0.0125
0.3143	0.2845	-0.9472	-20.1004	0.8185	0.0041	-0.0192
0.4323	0.3978	-1.0155	-19.9623	0.9988	0.0040	-0.0216
0.5204	0.4849	-0.9705	-18.4951	1.0496	0.0037	-0.0216
0.6643	0.6319	-0.7893	-14.2562	0.9870	0.0029	-0.0180
0.7944	0.7702	-0.5030	-9.2515	0.7274	0.0020	-0.0124
0.9563	0.9500	-0.1087	-2.2616	0.1842	0.0005	-0.0027
1.0000	1.0000	0.0000	-0.0012	0.0003	0.0000	0.0000
			T/K = 313.15			
0.0000	0.0000	0.0001	0.0016	0.0000	0.0000	0.0000
0.0845	0.0741	-0.3994	-7.9601	0.1874	0.0019	-0.0071
0.1707	0.1515	-0.6993	-15.8639	0.3791	0.0033	-0.0129
0.3143	0.2845	-0.9915	-21.4810	0.7449	0.0042	-0.0196
0.4323	0.3978	-1.0493	-21.3560	0.9331	0.0042	-0.0220
0.5204	0.4849	-1.0121	-19.4634	0.9823	0.0038	-0.0220
0.6643	0.6319	-0.8225	-15.4249	0.9126	0.0030	-0.0183

Table E.3: Excess thermodynamic properties of $[\mathbf{EMIM}]^+[\mathbf{BF_4}]^- + \mathbf{PEG200}$ at (293.15 to 333.15) K with 10 K interval under atmospheric pressure of p = 0.1 MPa. (Continued)

x_1	φ_1	$V_m^E/cm^3.mol^{-1}$	K_s^E/TPa^{-1}	$\eta^E/mPa.s$	n_D^E	α_P^E/K^{-1}
0.7944	0.7702	-0.5320	-9.6751	0.6831	0.0021	-0.0126
0.9563	0.9500	-0.1318	-2.4420	0.1630	0.0005	-0.0028
1.0000	1.0000	0.0000	0.0013	-0.0003	0.0000	0.0000
			T/K = 323.15			
0.0000	0.0000	0.0000	0.0000	0.0000	0.0000	0.0000
0.0845	0.0741	-0.4462	-8.9158	0.1626	0.0020	-0.0073
0.1707	0.1515	-0.7513	-17.5974	0.3448	0.0034	-0.0132
0.3143	0.2845	-1.0415	-23.0623	0.6807	0.0044	-0.0200
0.4323	0.3978	-1.0851	-22.7637	0.8727	0.0044	-0.0223
0.5204	0.4849	-1.0508	-20.8629	0.9302	0.0040	-0.0223
0.6643	0.6319	-0.8482	-16.3839	0.8591	0.0032	-0.0186
0.7944	0.7702	-0.5668	-10.5305	0.6411	0.0022	-0.0129
0.9563	0.9500	-0.1466	-2.7758	0.1391	0.0006	-0.0029
1.0000	1.0000	0.0000	-0.0014	0.0000	0.0000	0.0000
			T/K = 333.15			
0.0000	0.0000	0.0001	0.0000	0.0000	0.0000	0.0000
0.0845	0.0741	-0.4901	-8.9158	0.1320	0.0021	-0.0076
0.1707	0.1515	-0.8039	-17.5974	0.3052	0.0036	-0.0135
0.3143	0.2845	-1.0770	-23.0623	0.6185	0.0046	-0.0203
0.4323	0.3978	-1.1289	-22.7637	0.8125	0.0045	-0.0227
0.5204	0.4849	-1.0933	-20.8629	0.8731	0.0042	-0.0227
0.6643	0.6319	-0.8885	-16.3839	0.7959	0.0033	-0.0189
0.7944	0.7702	-0.6044	-10.5305	0.5935	0.0023	-0.0131
0.9563	0.9500	-0.1623	-2.7758	0.1061	0.0006	-0.0030
1.0000	1.0000	0.0000	-0.0014	0.0000	0.0000	0.0000

Appendix F

This appendix presents all the calculated excess partial molar volumes (V_1^E and V_2^E) thermodynamic data and excess partial molar volume at infinite dilusions ($\bar{V}_1^{E,\infty}$ and $\bar{V}_2^{E,\infty}$).

Appendix F.1: Excess partial molar volume ($\bar{V}_i^E$) properties of Ils + PEG200

Table F.1, F,2 and F.3 present all the calculated excess partial molar volume ($\bar{V}_i^E$) properties of $[BMIM]^+[BF_4]^-$, $[BMIM]^+[PF_6]^-$ and $[EMIM]^+[BF_4]^-$ + PEG, respectively.

Table F.1: Excess partial molar volumes ($\bar{V}_1^E$ and $\bar{V}_2^E$) of $[\mathbf{BMIM}]^+[\mathbf{BF_4}]^- + \mathbf{PEG200}$ from the temperature range of (293.15 to 333.15) K with 10 K interval under atmospheric pressure of p = 0.1 MPa.

x_1	$\bar{V}_1$	$V_1^\star$	$\bar{V}_1^E$	$\bar{V}_2$	$V_2^\star$	$\bar{V}_2^E$
			($\mathbf{cm^3.mol^{-1}}$)			
			T/K=293.15			
0.0000	184.5014	187.6304	-3.2250	177.7936	177.7936	0.0000
0.0748	184.7388	187.6304	-2.8916	177.7691	177.7936	-0.0245
0.1528	185.2052	187.6304	-2.4252	177.6726	177.7936	-0.1210
0.2865	186.2023	187.6304	-1.4280	177.3124	177.7936	-0.4812
0.4001	186.9648	187.6304	-0.6655	176.8691	177.7936	-0.9245
0.4873	187.3852	187.6304	-0.2451	176.5237	177.7936	-1.2699
0.6341	187.7190	187.6304	0.0887	176.1283	177.7936	-1.6652
0.7719	187.7198	187.6304	0.0894	176.1081	177.7936	-1.6855
0.9504	187.6336	187.6304	0.0033	176.1832	177.7936	-1.6104
1.0000	187.6304	187.6304	0.0000	175.9906	177.7936	-1.2190
			T/K=303.15			
0.0000	185.0287	188.7539	-3.6403	179.0695	179.0695	0.0000
0.0748	185.5114	188.7539	-3.2423	179.0380	179.0695	-0.0315
0.1528	186.1507	188.7539	-2.6030	178.9264	179.0695	-0.1431
0.2865	187.2839	188.7539	-1.4698	178.5478	179.0695	-0.5216
0.4001	188.0675	188.7539	-0.6862	178.1067	179.0695	-0.9628
0.4873	188.4844	188.7539	-0.2693	177.7677	179.0695	-1.3018
0.6341	188.8207	188.7539	0.0670	177.3652	179.0695	-1.7042
0.7719	188.8399	188.7539	0.0862	177.3185	179.0695	-1.7509
0.9504	188.7588	188.7539	0.0051	177.5835	179.0695	-1.4860

Table F.1 Excess partial molar volumes ($\bar{V}_1^E$ and $\bar{V}_2^E$) of $[\mathbf{BMIM}]^+[\mathbf{BF_4}]^- + \mathbf{PEG200}$ from the temperature range of (293.15 to 333.15) K with 10 K interval under atmospheric pressure of p = 0.1 MPa. (Continued)

x_1	$\bar{V}_1$	$V_1^\star$	$\bar{V}_1^E$	$\bar{V}_2$	$V_2^\star$	$\bar{V}_2^E$
			($\mathbf{cm^3.mol^{-1}}$)			
1.0000	188.7537	188.7539	0.0000	177.5985	179.0695	-1.1809
			T/K=313.15			
0.0000	185.2533	189.8873	-4.2753	180.3609	180.3609	0.0000
0.0748	186.1960	189.8873	-3.6913	180.3193	180.3609	-0.0416
0.1528	187.0969	189.8873	-2.7904	180.1893	180.3609	-0.1716
0.2865	188.3999	189.8873	-1.4874	179.7922	180.3609	-0.5688
0.4001	189.2015	189.8873	-0.6858	179.3583	180.3609	-1.0027
0.4873	189.6027	189.8873	-0.2846	179.0375	180.3609	-1.3235
0.6341	189.9031	189.8873	0.0158	178.6644	180.3609	-1.6965
0.7719	189.9161	189.8873	0.0288	178.5401	180.3609	-1.8208
0.9504	189.8848	189.8873	-0.0025	178.0240	180.3609	-1.7207
1.0000	189.8873	189.8873	0.0000	177.5129	180.3609	-1.4263
			T/K=323.15			
0.0000	186.0871	191.0171	-4.8777	181.6662	181.6662	0.0000
0.0748	187.1533	191.0171	-3.8637	181.6218	181.6662	-0.0444
0.1528	188.1325	191.0171	-2.8846	181.4877	181.6662	-0.1786
0.2865	189.4772	191.0171	-1.5398	181.0935	181.6662	-0.5728
0.4001	190.2746	191.0171	-0.7425	180.6696	181.6662	-0.9967
0.4873	190.6764	191.0171	-0.3407	180.3493	181.6662	-1.3169
0.6341	191.0059	191.0171	-0.0111	179.9423	181.6662	-1.7240
0.7719	191.0550	191.0171	0.0379	179.7933	181.6662	-1.8730
0.9504	191.0189	191.0171	0.0019	179.7246	181.6662	-1.9417
1.0000	191.0171	191.0171	0.0000	181.6662	181.6662	-1.9237
			T/K=333.15			
0.0000	186.2886	192.1416	-6.3977	182.9948	182.9948	0.0000
0.0748	187.8595	192.1416	-4.2821	182.9418	182.9948	-0.0529
0.1528	189.0853	192.1416	-3.0563	182.7970	182.9948	-0.1978
0.2865	190.5401	192.1416	-1.6015	182.4066	182.9948	-0.5881
0.4001	191.3351	192.1416	-0.8065	181.9973	182.9948	-0.9974

Table F.1: Excess partial molar volumes ($\bar{V}_1^E$ and $\bar{V}_2^E$) of $[\mathbf{BMIM}]^+[\mathbf{BF_4}]^- + \mathbf{PEG200}$ from the temperature range of (293.15 to 333.15) K with 10 K interval under atmospheric pressure of p = 0.1 MPa. (Continued)

x_1	$\bar{V}_1$	$V_1^\star$	$\bar{V}_1^E$	$\bar{V}_2$	$V_2^\star$	$\bar{V}_2^E$
			($\mathbf{cm^3.mol^{-1}}$)			
0.4873	191.7342	192.1416	-0.4074	181.6815	182.9948	-1.3133
0.6341	192.0794	192.1416	-0.0622	181.2511	182.9948	-1.7436
0.7719	192.1527	192.1416	0.0111	181.0370	182.9948	-1.9578
0.9504	192.1412	192.1416	-0.0004	180.7363	182.9948	-2.2585
1.0000	192.1416	192.1416	0.0000	180.4758	182.9948	-2.5168

Table F.2: Excess partial molar volumes ($\bar{V}_1^E$ and $\bar{V}_2^E$) of $[BMIM]^+[PF_6]^- + PEG200$ from the temperature range of (293.15 to 333.15) K with 10 K interval under atmospheric pressure of p = 0.1 MPa.

x_1	$\bar{V}_1$	$V_1^\star$	$\bar{V}_1^E$	$\bar{V}_2$	$V_2^\star$	$\bar{V}_2^E$
			($\mathbf{cm^3.mol^{-1}}$)			
			T/K=293.15			
0.0000	199.3246	207.3146	-7.9905	177.7931	177.7936	0.0000
0.0604	201.3431	207.3146	-6.3843	177.7311	177.7936	-0.4758
0.1254	203.1610	207.3146	-4.8783	177.5441	177.7936	-0.9746
0.2420	205.4574	207.3146	-2.8273	177.0151	177.7936	-1.7490
0.3466	206.6111	207.3146	-1.6614	176.4898	177.7936	-2.2621
0.4305	207.0924	207.3146	-1.0933	176.1239	177.7936	-2.5412
0.5795	207.4031	207.3146	-0.5611	175.6805	177.7936	-2.7632
0.7291	207.4344	207.3146	-0.2648	175.5181	177.7936	-2.6605
0.9384	207.3352	207.3146	0.0027	176.8457	177.7936	-0.9662
1.0000	207.3139	207.3146	0.0008	178.3851	177.7936	0.5925
			T/K=303.15			
0.0000	200.2630	208.5890	-8.3303	179.0681	179.0695	0.0000
0.0604	202.4309	208.5890	-6.5911	179.0061	179.0695	-0.4922
0.1254	204.3341	208.5890	-4.9953	178.8298	179.0695	-0.9769
0.2420	206.6859	208.5890	-2.8923	178.3730	179.0695	-1.6831
0.3466	207.8524	208.5890	-1.7162	177.9590	179.0695	-2.0875
0.4305	208.3409	208.5890	-1.1395	177.6886	179.0695	-2.2696
0.5795	208.6664	208.5890	-0.5913	177.3736	179.0695	-2.3619
0.7291	208.7069	208.5890	-0.2830	177.2689	179.0695	-2.1987
0.9384	208.6098	208.5890	-0.0036	178.3580	179.0695	-0.7336
1.0000	208.5890	208.5890	0.0004	179.5201	179.0695	0.4527
			T/K=313.15			
0.0000	201.0036	209.8826	-8.8792	180.3611	180.3609	0.0000
0.0604	203.4610	209.8826	-6.8718	180.2960	180.3609	-0.5153
0.1254	205.5116	209.8826	-5.1318	180.1164	180.3609	-1.0056
0.2420	207.9295	209.8826	-2.9553	179.6638	180.3609	-1.6995
0.3466	209.0976	209.8826	-1.7806	179.2542	180.3609	-2.1025
0.4305	209.5936	209.8826	-1.2001	178.9778	180.3609	-2.2945

Table F.2: Excess partial molar volumes ($\bar{V}_1^E$ and $\bar{V}_2^E$) of $[BMIM]^+[PF_6]^- + PEG200$ from the temperature range of (293.15 to 333.15) K with 10 K interval under atmospheric pressure of p = 0.1 MPa. (Continued)

x_1	$\bar{V}_1$	$V_1^\star$	$\bar{V}_1^E$	$\bar{V}_2$	$V_2^\star$	$\bar{V}_2^E$
			($cm^3.mol^{-1}$)			
0.5795	209.9493	209.8826	-0.6224	178.6322	180.3609	-2.4182
0.7291	210.0064	209.8826	-0.2867	178.5112	180.3609	-2.2604
0.9384	209.9031	209.8826	-0.0086	179.5783	180.3609	-0.8122
1.0000	209.8826	209.8826	0.0000	180.6401	180.3609	0.2786
			T/K=323.15			
0.0000	202.7773	211.17828	-10.4011	181.6662	181.6662	0.0000
0.0604	204.9617	211.17828	-6.5598	181.6051	181.6662	-0.5412
0.1254	206.8565	211.17828	-5.5500	181.4322	181.6662	-1.0625
0.2420	209.1778	211.17828	-3.0286	180.9845	181.6662	-1.7756
0.3466	210.3374	211.17828	-1.7932	180.5702	181.6662	-2.1688
0.4305	210.8428	211.17828	-1.2317	180.2847	181.6662	-2.3445
0.5795	211.2293	211.17828	-0.7006	179.9079	181.6662	-2.4347
0.7291	211.3195	211.17828	-0.3561	179.7620	181.6662	-2.2989
0.9384	211.2061	211.17828	-0.0206	181.2928	181.6662	-1.4354
1.0000	211.1783	211.17828	0.0000	182.8592	181.6662	-0.8071
			T/K=333.15			
0.0000	202.8091	212.4761	-9.6795	182.9949	182.9948	0.0000
0.0604	205.6492	212.4761	-7.3149	182.9051	182.9948	-0.5707
0.1254	207.9074	212.4761	-5.3660	182.7391	182.9948	-1.0500
0.2420	210.4382	212.4761	-3.0733	182.2869	182.9948	-1.7442
0.3466	211.6196	212.4761	-1.8796	181.8806	182.9948	-2.1390
0.4305	212.1268	212.4761	-1.2924	181.5971	182.9948	-2.3419
0.5795	212.5204	212.4761	-0.6837	181.2131	182.9948	-2.5089
0.7291	212.6030	212.4761	-0.3033	181.0625	182.9948	-2.3617
0.9384	212.4968	212.4761	-0.0148	182.1288	182.9948	-0.9090
1.0000	212.4761	212.4761	0.0000	183.1239	182.9948	0.1163

Table F.3: Excess partial molar volumes ($\bar{V}_1^E$ and $\bar{V}_2^E$) of $[EMIM]^+[BF_4]^- + PEG200$ from the temperature range of (293.15 to 333.15) K with 10 K interval under atmospheric pressure of p = 0.1 MPa.

x_1	$\bar{V}_1$	$V_1^\star$	$\bar{V}_1^E$	$\bar{V}_2$	$V_2^\star$	$\bar{V}_2^E$
			($\mathbf{cm^3.mol^{-1}}$)			
			T/K=293.15			
0.0000	150.6593	154.4063	-3.7467	177.7931	177.7936	0.0000
0.0845	151.0760	154.4063	-3.6432	177.4488	177.7936	-0.6570
0.1707	151.6865	154.4063	-3.3119	177.0484	177.7936	-1.3363
0.3143	152.7542	154.4063	-2.5528	176.3646	177.7936	-2.3285
0.4323	153.4732	154.4063	-1.8987	175.8434	177.7936	-2.9148
0.5204	153.8666	154.4063	-1.4709	175.5216	177.7936	-3.2022
0.6643	154.2514	154.4063	-0.9043	175.1802	177.7936	-3.3618
0.7944	154.3860	154.4063	-0.4871	175.1171	177.7936	-3.1423
0.9563	154.4074	154.4063	-0.1038	175.4201	177.7936	-2.4773
1.0000	154.4063	154.4063	0.0000	175.5821	177.7936	-2.2105
			T/K=303.15			
0.0000	150.6952	155.3322	-4.6383	223.3787	179.0695	0.0000
0.0845	151.5686	155.3322	-4.1259	222.9779	179.0695	-0.7617
0.1707	152.4058	155.3322	-3.5652	222.5561	179.0695	-1.4601
0.3143	153.5955	155.3322	-2.6839	221.8599	179.0695	-2.4646
0.4323	154.3350	155.3322	-2.0126	221.3372	179.0695	-3.0556
0.5204	154.7386	155.3322	-1.5641	221.0062	179.0695	-3.3416
0.6643	155.1460	155.3322	-0.9755	220.6323	179.0695	-3.5344
0.7944	155.3003	155.3322	-0.5349	220.5325	179.0695	-3.3478
0.9563	155.3329	155.3322	-0.1080	220.8015	179.0695	-2.6845
1.0000	155.3322	155.3322	0.0000	220.9557	179.0695	-2.4217
			T/K=313.15			
0.0000	150.7630	156.2560	-5.4929	180.3611	180.3609	0.0000
0.0845	152.0925	156.2560	-4.5629	179.9092	180.3609	-0.8514
0.1707	153.1538	156.2560	-3.8014	179.4618	180.3609	-1.5987
0.3143	154.4724	156.2560	-2.7750	178.7515	180.3609	-2.6012
0.4323	155.2383	156.2560	-2.0670	178.2255	180.3609	-3.1851
0.5204	155.6480	156.2560	-1.6200	177.8935	180.3609	-3.4798

Table F.3: Excess partial molar volumes ($\bar{V}_1^E$ and $\bar{V}_2^E$) of $[EMIM]^+[BF_4]^- + PEG200$ from the temperature range of (293.15 to 333.15) K with 10 K interval under atmospheric pressure of p = 0.1 MPa. (Continued)

x_1	$\bar{V}_1$	$V_1^\star$	$\bar{V}_1^E$	$\bar{V}_2$	$V_2^\star$	$\bar{V}_2^E$
			($\mathbf{cm^3.mol^{-1}}$)			
0.6643	156.0557	156.2560	-1.0228	177.5165	180.3609	-3.6673
0.7944	156.2094	156.2560	-0.5785	177.3754	180.3609	-3.5178
0.9563	156.2545	156.2560	-0.1333	177.3339	180.3609	-3.1591
1.0000	156.2560	156.2560	0.0000	177.2901	180.3609	-3.0711
			T/K=323.15			
0.0000	150.8356	157.1836	-6.3480	181.6662	181.6662	0.0000
0.0845	152.6117	157.1836	-5.0181	181.1560	181.6662	-0.9564
0.1707	153.9025	157.1836	-4.0325	180.6789	181.6662	-1.7387
0.3143	155.3598	157.1836	-2.8653	179.9563	181.6662	-2.7514
0.4323	156.1521	157.1836	-2.1167	179.4331	181.6662	-3.3183
0.5204	156.5654	157.1836	-1.6690	179.1041	181.6662	-3.6130
0.6643	156.9703	157.1836	-1.0616	178.7264	181.6662	-3.7881
0.7944	157.1235	157.1836	-0.6270	178.5547	181.6662	-3.6784
0.9563	157.1803	157.1836	-0.1499	178.3013	181.6662	-3.5115
1.0000	157.1836	157.1836	-6.3480	178.1242	181.6662	-3.5420
			T/K=333.15			
0.0000	150.8356	158.1148	-7.3509	182.9949	182.9948	0.0000
0.0845	152.6117	158.1148	-5.4861	182.4280	182.9948	-1.0571
0.1707	153.9025	158.1148	-4.2602	181.9352	182.9948	-1.8637
0.3143	155.3598	158.1148	-2.9754	181.2217	182.9948	-2.8503
0.4323	156.1521	158.1148	-2.2237	180.6987	182.9948	-3.4252
0.5204	156.5654	158.1148	-1.7641	180.3560	182.9948	-3.7324
0.6643	156.9703	158.1148	-1.1321	179.9474	182.9948	-3.9361
0.7944	157.1235	158.1148	-0.6800	179.7303	182.9948	-3.8692
0.9563	157.1803	158.1148	-0.1673	179.2716	182.9948	-3.8858
1.0000	157.1836	158.1148	0.0000	178.9579	182.9948	-4.0371

Appendix G

This first section of this appendix gives full details on the uncertainty in experimental quantities. The second section of this appendix gives full details on the combined standard uncertainty of the mole fraction (x_1).

Appendix G.1: Standard uncertainty

F.1: Experimental uncertainty

In any experimental measurements, Type A and B are the only methods used to calculate the standard uncertainty of measured values (Bich et al., 2012).

Type A method is based on the statistical approach technique (Taylor and Kuyatt, 1994). In which the mean values and the experimental standard deviation value should be calculated first. The mean and standard deviation values are calculated using equation F.1 and F.2, respectively.

$$\bar{x} = \frac{1}{n}\sum_{i=1}^{n} x_i \qquad \text{G.1}$$

$$s(x_i) = \sqrt{\frac{1}{n-1}\sum_{i=1}^{n}(x_i - \bar{x})} \qquad \text{G.2}$$

Where $\bar{x}$, x_i, n and $s(x_i)$ represent mean value, each thermophysical measured value, number of all the measured values and standard deviation value.

The calculations of standard uncertainty using type A is evaluated using equation G.3 (Taylor and Kuyatt, 1994).

$$u(x_i) = \frac{s(x_i)}{\sqrt{n}} \qquad \text{G.3}$$

Type B uncertainty is evaluated by several methods and information related to the measurements. Information such as manufacturer information, literature, and previous experience values and in this study calibrations data provided by the manufacturer of different instruments are needed in order to evaluate the standard uncertainty. The uncertainty can lie anywhere between the distribution and such distributions are known as rectangular.

The overall standard uncertainty is represented by:

$$u(x_i) = \frac{\Delta a}{\sqrt{3}} \quad \text{F.4}$$

where Δa is the half the width of the interval. The rectangular distribution model is always the default model in the absence of any other information (Taylor and Kuyatt, 1994). The rectangular type B standard uncertainty, the change between lower (minimum) and upper (maximum) limits is represented by a_+ for upper limit and a_- being the lower limit. The change between to lower and upper limit represented as $\Delta a = \frac{a_+ - a_-}{2}$, thus the uncertainty can lie anywhere between the distribution.

The combined standard uncertainty for measured thermophysical properties for this study was calculated using equation G.5

$$u(x) = \pm\sqrt{u_a(x)^2 + u_{rep}(x)^2 + u_b(x)^2} \quad \text{G.5}$$

Where x is measured properties such as ρ, η, u and n_D . Where u_{rep} is the measurement repeatability values for thermophysical properties, u_a and u_b is the accuracy and reproducibility of the instrument respectively.

F.2: The combined standard uncertainty of the mixture composition mole fraction (x_1)

The standard uncertainty of the mole fraction contributes highly to the overall standard uncertainty of ρ, η, u and n_D. For homogeneous mixture composition mole fraction (x_1) is constant throughout irrespective of the change in temperature and pressure, therefore mass is the only quantity that determine the mole fraction and the mole fraction is determined using the following equation:

$$x_i = \frac{n_i}{\sum_{i=1}^{2} n_i} \quad \text{G.6}$$

where, n_i is the number of mole the *i*-th component is defined as:

$$n_i = \frac{m_i}{M_i} \quad \text{G.7}$$

where m_i and M_i are the mass and molecular weight of the *i*-th component respectively.

For a binary mixture component, equation G.6 can be re-written as follows:

$$x_i = \frac{n_1}{n_1 + n_2} \quad \text{G.8}$$

Substituting equation G.7 into G.8 gives:

$$x_i = \frac{n_1}{n_1 + n_2} = \quad x_i = \frac{m_1/M_2}{m_1/M_2 + m_2/M_1} \tag{G.9}$$

By taking L.C.M equation to further simplify to

$$x_i = \frac{m_1 M_2}{m_1 M_2 + m_2 M_1} \tag{G.10}$$

The quotient rule is applied to equation G.10, this is done in order to obtain the partial derivative of x_i with respect to m_1. Equation G.11 represents the derivation of equation G.10

$$\frac{\partial x_1}{\partial m_1} = \frac{(m_1 M_2 + m_2 M_1) \times \left[\partial(m_1 M_2)/\partial m_1\right] - (m_1 M_2) \times \left[\partial(m_1 M_2 + m_2 M_1)/\partial m_1\right]}{(m_1 M_2 + m_2 M_1)^2} \tag{G.11}$$

Evaluating the partial derivatives in the square-blankets in equation G.11 yields:

$$\frac{\partial x_1}{\partial m_2} = \frac{m_1 M_2^2 + M_2 M_1 m_2 - m_1 M_2^2}{(m_1 M_2 + m_2 M_1)^2} \tag{G.12}$$

Equation G.12 reduces to:

$$\frac{\partial x_1}{\partial m_1} = \frac{M_2 M_1 m_2}{(m_1 M_2 + m_2 M_1)^2} \tag{G.13}$$

Similarly, the partial derivatives of x_1 with respect to m_2 can be obtained by differentiating equation G.12 with respect to m_2 using quotient rule as follows:

$$\frac{\partial x_1}{\partial m_2} = \frac{(m_1 M_2 + m_2 M_1) \times \left[\partial(m_1 M_2)/\partial m_2\right] - (m_1 M_2) \times \left[\partial(m_1 M_2 + m_2 M_1)/\partial m_2\right]}{(m_1 M_2 + m_2 M_1)^2} \tag{G.14}$$

Evaluating the partial derivatives in the square-blankets in equation G.14 yields:

$$\frac{\partial x_1}{\partial m_2} = \frac{-M_2 M_1 m_1}{(m_1 M_2 + m_2 M_1)^2} \tag{G.15}$$

Thus, in this case, equations G.13 and G.15 provide the partial derivatives of the mole fraction of ionic liquids (x_1) with respect to both mass of ILs (m_1), and that of PEG200 (m_2) and by substituting the values of the two masses and molar masses, the partial derivatives can be evaluated.

The relative uncertainties of m_1 and m_2 influences the uncertainty of x_1 through the partial derivatives are given by:

$$\frac{\partial x_1}{\partial m_2} = \frac{-M_2 M_1 m_1}{(m_1 M_2 + m_2 M_1)^2} \tag{G.16}$$

Simplifying expression G.15 and G.16 separately yields equation G.17:

$$m_2\left(\frac{\partial x_1}{\partial m_2}\right) = -x_1(1-x_1) \text{ and } \left(\frac{\partial x_1}{\partial m_1}\right) = x_1(1-x_1) \quad \text{G.17}$$

Hence, the standard uncertainty $u(x_1)$ is given in terms of the relative standard uncertainties $u_r(m_1)$ and $u_r(m_2)$ of the two mass measurements as follows:

$$u(x_1) = (1-x_1)[u_r^2(m_1) + u_r^2(m_2)]^{1/2} \quad \text{G.18}$$